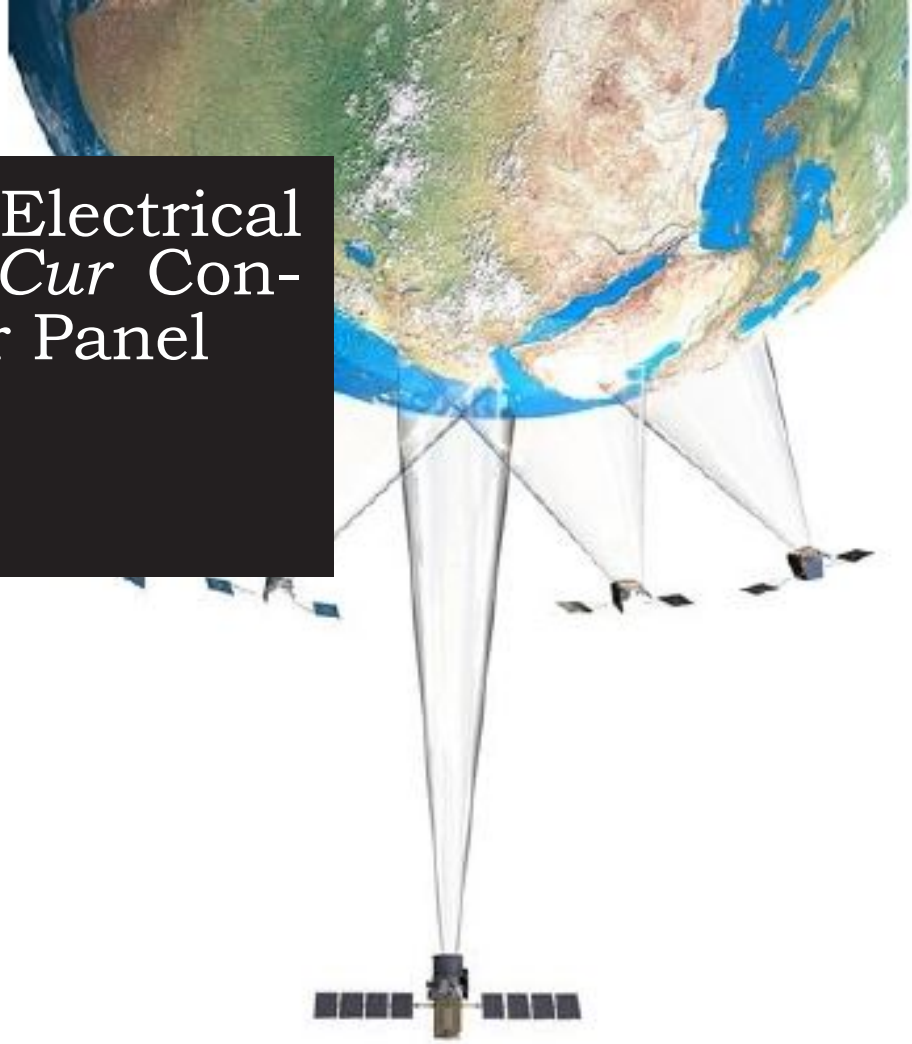

Thermal and Electrical Design of *ConCur* Concentrator Solar Panel

MSc Thesis Report

A. Gorbatenko

Delft University of Technology

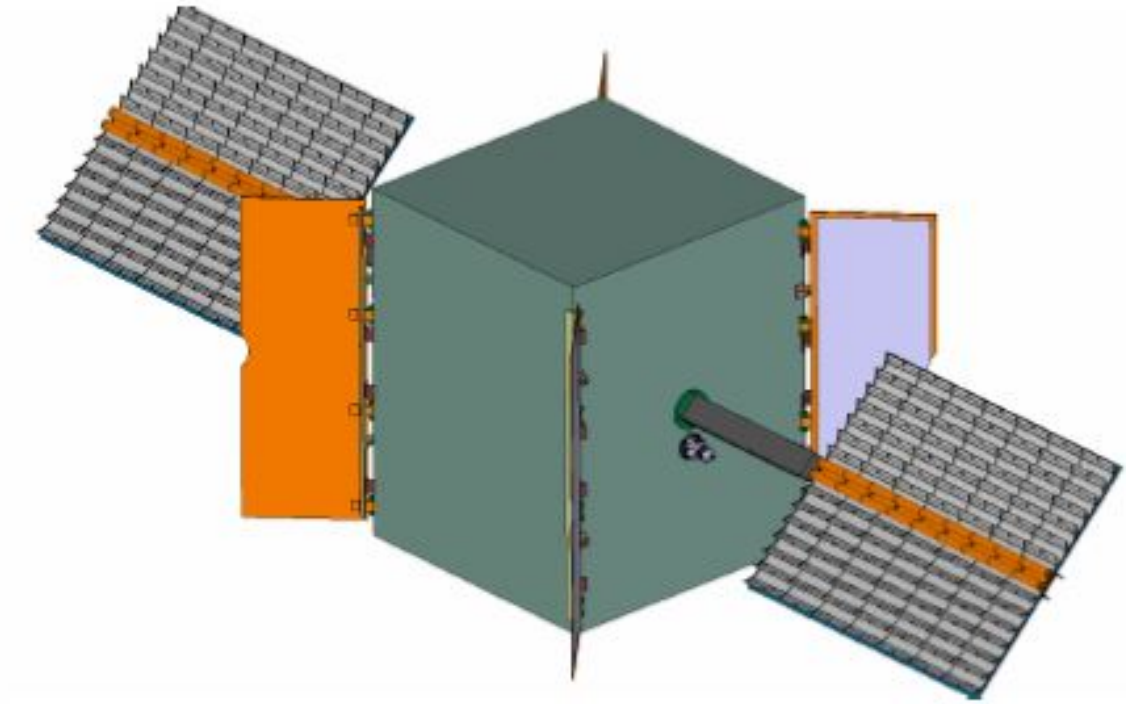

AIRBUS

TU Delft Delft University of Technology

Challenge the future

Thermal and Electrical Design of *ConCur* Concentrator Solar Panel

MSc Thesis Report

by

A. Gorbatenko

in partial fulfillment of the requirements for the degree of

Master of Science
in Sustainable Energy Technologies

at the Delft University of Technology,
to be defended publicly on Wednesday, June 27th, 2018 at 2:00 PM.

Supervisor at the TU Delft:	Prof. dr. ir. A.H.M. (Arno) Smets
Supervisors at Airbus D&S:	Ir. H. (Henk) Cruijssen
	Ir. N. (Niels) van der Pas
Thesis committee:	Prof. dr. ir. A.H.M. (Arno) Smets
	Dr. R.A.C.M.M. (Rene) van Swaaij
	Dr. S.H. (Simon) Tindemans
	Ir. N. (Niels) van der Pas

Preface

This thesis is the product of a *TU Delft's* collaboration with the company *Airbus Defence and Space* in Leiden. I am very happy that I had an opportunity to combine the knowledge I gained in my BSc program (in Aerospace Engineering) with a different field - Solar energy (as part of the SET program of Electrical Engineering faculty). I enjoyed working on this project very much despite some personal problems that I was facing by the end of it. This experience has taught me how to handle some very difficult situations in life using the power of determination and prioritizing some things over the others. Moreover, I deeply hope that the results from this study are going to be used in the future, and that the development of this concentrator solar array will progress and one day it will be operating in Space.

I am very grateful to my daily supervisor **Henk Cruijssen** for trusting me this research topic at *Airbus*. Having been our "client" in the BSc Endproject at the TU Delft in 2014, he kindly suggested a topic for me that would combine the knowledge of both the faculties. Thank you, Henk, for guiding me throughout this project, always being very cheerful and coming up with new innovative solutions. I spent nearly a year working on it in Leiden surrounded by many experts with backgrounds in aerospace, thermal, electrical engineering and other fields. Their huge amount of experience and readiness to always help inspired me a lot during my work there. Special thanks to **Niels v.d. Pas** with his help modelling in *ESATAN*, helping me with any questions regarding thermal analysis and supporting me with valuable feedback despite the study delay. I also very much appreciate the help I got from **Remco v.d. Heijden** in personal assistance regarding electrical part of the thesis, and **Peter Datema** for helping me with electrical hardware schematics. I would also like to thank **Guus Borst** very much for involving himself and helping me with the thermal design part. Also thanks to other interns at *Airbus* for keeping a very lively working atmosphere. I want to thank my TU Delft supervisor **Arno Smets** as well for guiding me and being very supportive. Finally, this would never have been possible without my family's and friends' emotional and financial support, all the way from my homeland Latvia and within the Netherlands.

A. Gorbatenko
Delft, June 2018

Summary

With the rapidly advancing technology in the field of concentrator photovoltaics for terrestrial applications, the aerospace industry is eager to innovate and incorporate this idea. Concentrated solar light offers a cheaper but more complex solution to extract more power without increasing the number of solar cells. For extraterrestrial applications generally the photovoltaic elements account for nearly half of the costs on solar array, this decreasing the number of solar cells significantly contributes to lowering the cost of electric power in space.

The solar array studied in this thesis provides a technologically innovative solution to reduce the cost of electrical energy for LEO satellites, in particular, to suit, for instance, the *OneWeb* satellite constellation mission at 1200 km altitude. Apart from being a structurally challenging design, another very important consideration is thermal feasibility. Concentrated solar light introduces hot spots of high temperatures, and heat dissipation at those locations is crucial. Hence, this thesis focuses on investigating the thermal performance of *ConCur* baseline design in orbit using thermal software *ESATAN*, and optimizing the design according to the thermal requirements, as well as performing electrical power calculations.

To broaden the knowledge regarding concentrator photovoltaics on Earth and in outer space, a literature study was first performed and the main findings are summarized in this document. Also, heat transfer in space is briefly explained as part of the methodology for modelling the solar panel in *ESATAN*, including a step-by-step guide. After modelling the panel it was put into the Low Earth Orbit simulated by *ESATAN* which provide outputs on temperature and absorbed flux results. The panel was optimized and it was found that the maximum cell temperature reaches +122°C when nonoperational, and +70°C when producing electrical energy. These and more results were post-processed and summarized and relevant conclusions were drawn. Knowing the panel temperature in orbit and slightly altering its dimensions, the amount of electrical power produced was calculated to match the required 300 W. Also a schematic of the hardware was made and the most probably cell layout designed. In addition, this report includes a brief cost estimation and comparison to the conventional solar panel of the same dimensions and that is capable of producing the same amount of power. It was estimated that the *ConCur* solar panel would cost 65-70% less than the conventional solar panel. Finally, relevant recommendations are listed for further increasing the technology readiness level (TRL) of the concept.

List of Abbreviations

Abbreviation	Description
Airbus D&S	Airbus Defence and Space
AM0	Air Mass Zero
AM1	Air Mass One
AR	Anti-reflective
ATOX	Atomic Oxygen
BOL	Beginning of Life
CFRP	Carbon Fiber Reinforced Polymer
CR	Concentration Ratio
CPV	Concentrator Photovoltaics
EEMCS	Electrical Engineering, Mathematics and Computer Science
EOL	End of Life
ESA	European Space Agency
ESATAN	European Space Agency's Thermal Analysis Network
ESTEC	European Space Research and Technology Centre
FF	Fill Factor
GCR	Geometric Concentration Ratio
HDRM	Hold Down Release Mechanism
IR	Infrared
ISS	International Space Station
LEO	Low Earth Orbit
MPPT	Maximum Power Point Tracking
NASA	National Aeronautics and Space Administration
PG	Pyrolytic Graphite
PV	Photovoltaic
SADM	Solar Array Drive Mechanism
S/C	Spacecraft
SET	Sustainable Energy Technology
SLA	Stretched Lens Array
SS	Summer Solstice
STC	Standard Test Conditions
TJ	Triple Junction
TRL	Technology Readiness Level
TU Delft	Delft University of Technology
UV	Ultraviolet
WS	Winter Solstice

List of Symbols

Symbol	Definition	SI Unit
A	Area	m^2
FF	Fill factor	$-$
h	Planck's constant	$J \cdot s$
I_{MP}	Maximum power current	mA
I_{SC}	Short circuit current	mA
J_{SC}	Short circuit current density	mA/cm^2
k	Boltzmann constant	$m^2 kg s^{-2} K^{-1}$
n	Ideality factor	$-$
P	Power	W
q	Elementary charge	C
R_S	Sheet resistance	Ω/sq
S	Surface recombination velocity	cm/s
T	Temperature	K
t	Thickness	mm
V_{MP}	Maximum power voltage	mV
V_{OC}	Open circuit voltage	mV
W	Wafer thickness	cm
α	Absorptivity	$-$
η	Efficiency	$\%$
ϵ	Emissivity	$-$
λ	Wavelength	nm
ρ	Reflectivity	$-$
ρ	Resistivity	$\Omega \cdot cm$
σ	Thermal conductivity	W/mK
τ	Transmissivity	$-$

Contents

1

Introduction

This document is the final version of the MSc Thesis report as an obligatory part of MSc Sustainable Energy Technology track, PVMD department, faculty of EEMCS at the TU Delft. The purpose of this report is to demonstrate the research problem/goal, methodology, results, relevant conclusions and recommendations for future work.

The topic of this project is proposed and commissioned by the company *Airbus Defence and Space* situated in Leiden, Netherlands. It involves research and development of the novel concentrator solar array which is currently patented by Mr. Henk Cruijssen at *Airbus* [1]. The assignment is to develop **thermal and electrical designs of panel substrate and concentrator reflectors for *ConCur* solar array wing** over a period of ~9 months full-time work, amounting to 45 ECTS according to the requirements at the TU Delft.

This chapter further briefly (1) summarizes the research topic (providing the research objective and research questions), (2) explains the general working principles of the solar cells (the photovoltaic effect), (3) introduces the concept of concentrating solar energy, (4) describes the patent analyzed in this thesis and (5) briefly summarizes the methodology followed in this research.

1.1. Research Topic

Any spacecraft uses the power derived from some particular power source depending on it's mission. For Earth-orbiting (LEO or GEO) or other near-Sun space missions the spacecraft is usually equipped with a pair of decently sized solar arrays to use the energy of the Sun by converting it into usable electricity for that particular mission's purpose. For deep space operations such an option is redundant, since the solar intensity is too low to get meaningful amount of power from the Sun, hence, in that case usually RTGs (Radioisotope Thermoelectric Generators) are used. Since in this thesis the thermal and electrical designs of the concentrator solar array for Earth-orbiting communications satellite are being developed, the RTG's are not discussed any further.

It is common to use **Gallium Arsenide** based solar cells for power production in extraterrestrial missions. They have a higher efficiency and lower degradation rate than silicon-based solar cells. The driving force for innovation in the field of solar energy for space applications is, in this case, reducing the cost of power. Typically nearly half of the solar array cost is attributed to the cost of photovoltaic elements (solar cells) see Fig. 1.1 [2]. One way to minimize the amount of solar cells used without cutting on the amount of electrical power is by light concentration technique. That way not only the energy yield per price reduces (because of using less cells), but also the energy yield per kg (smaller solar array), which is very beneficial especially for space applications, since each kg sent to space costs around 20 000 euros.

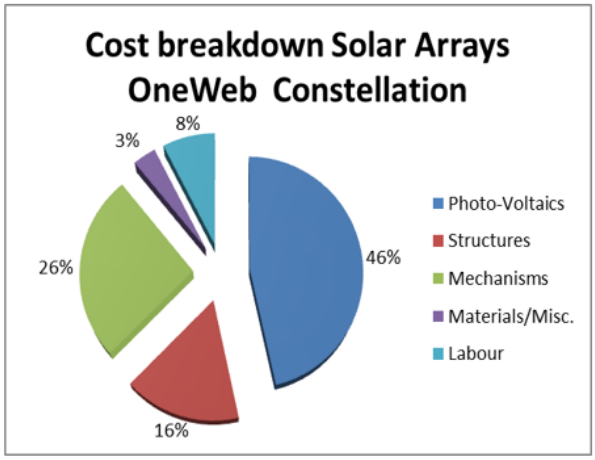

Figure 1.1: The typical solar array cost breakdown [3].

1.1.1. Research Objective

The **main goal** of this project is *to assess thermally and make necessary changes to the concentrator solar array, as well as demonstrate electrical performance of the solar cells at the achieved worst case extreme and operating temperature limits.*

1.1.2. Research Questions

The research questions that are studied in this document were drawn based on the requirements set by *Airbus* upon proposing the thesis subject (see App. A):

1. What are the thermal operating conditions in orbit?
2. Can a concentrator solar panel withstand the thermal loads during its operation in orbit for the specified lifetime of 5 years?
3. Can a concentrator solar panel of 1.11 x 1.224 m dimensions produce 300 W power in the specified orbit at an altitude of 1200 km?
4. Can a concentrator solar panel be cheaper than a planar solar array of the same size, in terms of $Euros/W$? What is the approximate cost and savings?

1.2. Photovoltaic Effect

In photovoltaics the performance of the solar cell is largely determined by measuring its current - voltage relationship, so-called I-V curve. Fig. 1.2 shows the most important parameters that can be read/calculated from the I-V curve; those are:

- Open circuit voltage V_{OC} - the voltage across the solar cell at zero net-current through the device; maximum voltage available from a solar cell,
- Short circuit current I_{SC} - the amount of charge through the solar cell when the voltage across the solar cell is zero; maximum current from a solar cell,
- Maximum power point MPP - the point at which the amount of power produced is maximum; the voltage and current at that point are V_{MPP} and I_{MPP}; the operating point of the solar cell,
- Fill factor FF - the ratio of the maximum power to the product of I_{SC} and V_{OC}, determines the maximum power from the solar cell; graphically it is a measure of ”squareness” of the I-V curve,
- Efficiency - the ratio between the output power to the input power.

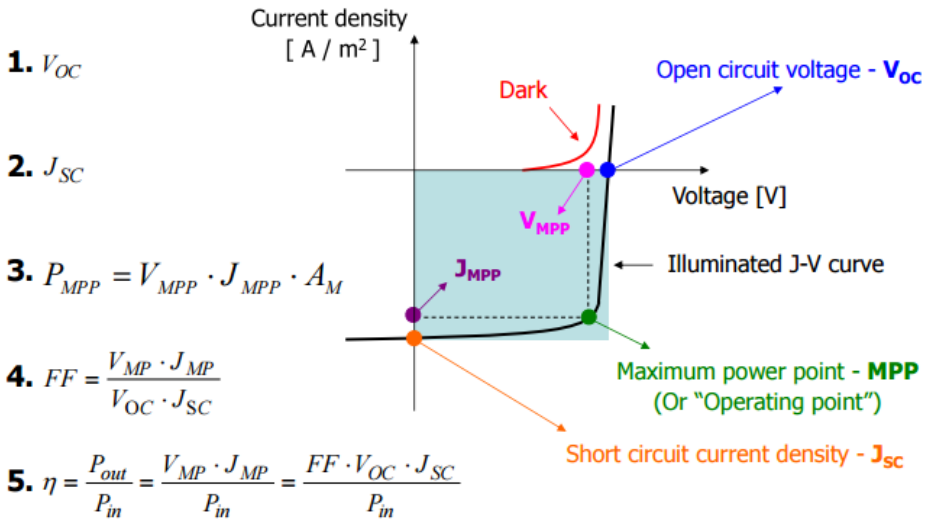

Figure 1.2: The typical I-V curve of a solar cell [4].

Solar cells being capable of generating electrical energy due to the photovoltaic effect can be regarded as the generation of a voltage difference at the junction of two different materials in response to visible or other radiation [5]. This effect can be summarized in three steps:

1. **Absorption** of light (and subsequent generation of charge carriers),
2. **Separation** of charge carriers,
3. **Collection** of the charge carriers at the electrodes.

When designing solar cell interconnections it is important to take into account the **shading** effects that will most likely cause current mismatching. Since all cells connected in series experience the same current, what happens when a single cell is shaded, is that it affects the total voltage of the string. This is why it is important to have **by-pass diodes** across the cells or strings to ensure that in shading situation the total current flow by-passes the affected string and goes through the by-pass diode which conducts current. In the normal situation the cells are forward biased and the by-pass diodes - reserve biased (in an open circuit), but when shading occurs the shaded cell can go into reverse bias allowing the by-pass diode to change its bias and take charge of the current across the cell or shaded string of cells. The by-pass diodes can be either integrated within the solar cell itself as in Fig. 1.4, or put across multiple cells as in Fig. 1.3. The same analogy can be made to cells in parallel experiencing current drop due to some cells in the circuit being shaded. The **blocking diodes** are used to prevent the total current drop, as in Fig. 1.5.

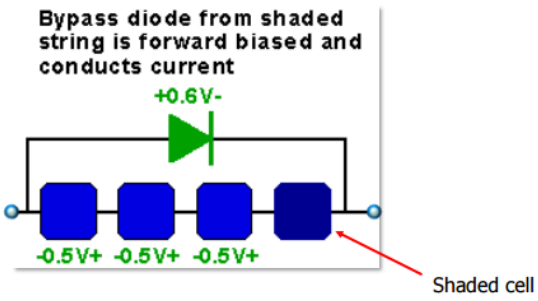

Figure 1.3: The by-pass diode across four solar cells for preventing current mismatch during shading [6].

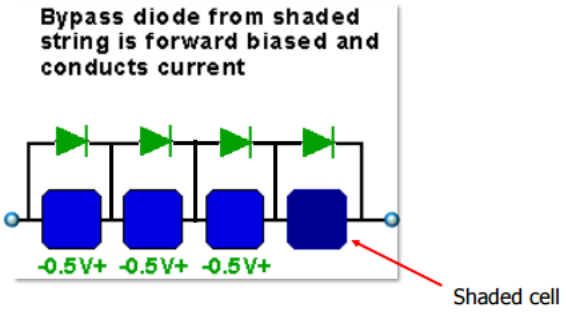

Figure 1.4: The by-pass diode across each of the solar cells for preventing current mismatch during shading [6].

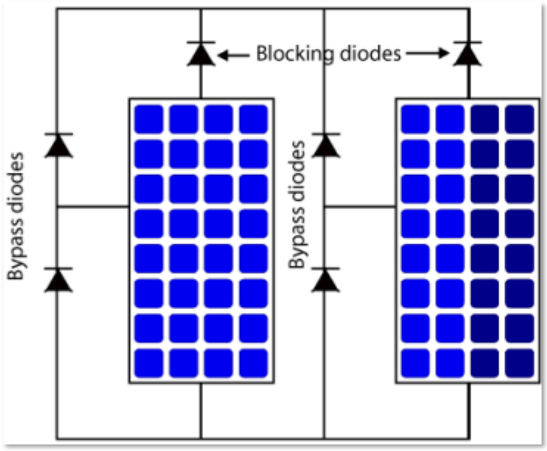

Figure 1.5: The blocking diodes across the solar modules for preventing voltage drop due to shading [6].

1.3. Concentrated Photovoltaics (CPV)

By shining the light onto a solar cell it produces certain amount of electrical charges which generate electricity. Intuitively it can be deduced that by shining more light onto a cell more power will be produced. Since 2010 the technology of concentrating solar light has advanced very rapidly and many projects have been commissioned all over the world [7]. The two basic ways of concentrating incoming light onto a solar cell is through reflection of refraction principles. The first principle requires mirror-like concentrators that are positioned and shaped in such a way that the incoming light bouncing off their surface hits the solar cell. The second principle is less common but, as turns out, more reliable [8]: using stretched lens array (Fresnel lens) shaped such that the incoming light passing through the lens is focused onto the solar cell. Both concepts will be discussed in more detail in the next chapter.

Utilizing the light concentration concept can be very beneficial. One of the benefits is that to generate the same amount of power as the planar array, the concentrator array will require less solar cells - if a planar array produces X amount of power using Y amount of solar cells, the concentrator solar array is capable of producing the same amount of power using Y/CR amount of solar cells, depending on the *concentration ratio (CR)**. Having to manufacture, integrate and maintain less solar cells ultimately saves cost.

*Concentration ratio is the geometric ratio between the area of the aperture and the area of the receiver (solar cell), hence:

$$CR = \frac{A_{Aperture}}{A_{SolarCell}} \tag{1.1}$$

1.4. *ConCur* Patent

ConCur solar array has been publicized under the **Solar Panel with Flexible Optical Elements** patent application by Ir. H. Cruijssen [9], see App. G. The invention uses the advantage of having a higher energy output per unit area of solar cells as compared to the conventional solar array because of the virtue of light concentration. It is desirable to be able to produce the required amount of electrical power with as little cells as possible, while still complying with various geometrical and mechanical requirements for the stowed and deployed array configurations. The purpose of this concept is to decrease the amount of solar cells needed and, consequently, lower the array cost. Figures 1.6 to 1.11 depict the main aspects for familiarizing with the *ConCur* concept.

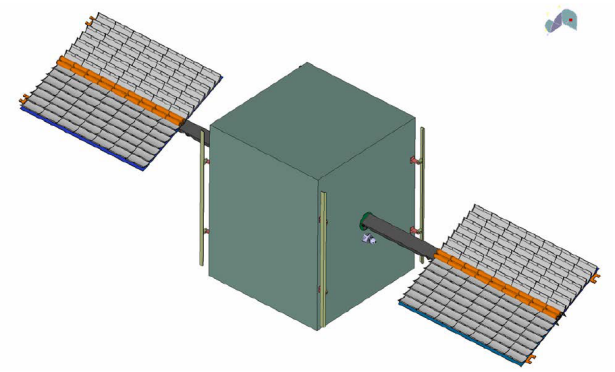

Figure 1.6: An image of a S/C with *ConCur* solar arrays [3].

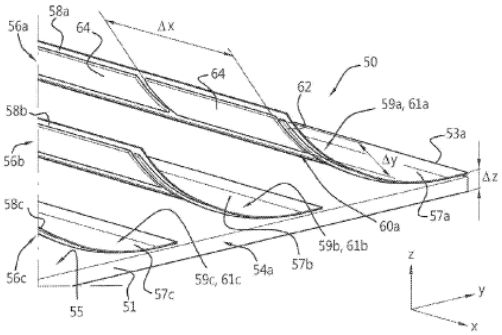

Figure 1.7: Schematic of the layout of the reflective elements and attached solar cells at their rear side [9].

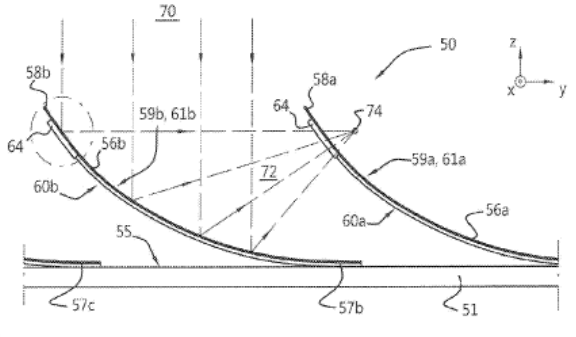

Figure 1.8: A side view of the panel: visual representation of reflecting the incoming light toward a common focal point located behind the solar cell [9].

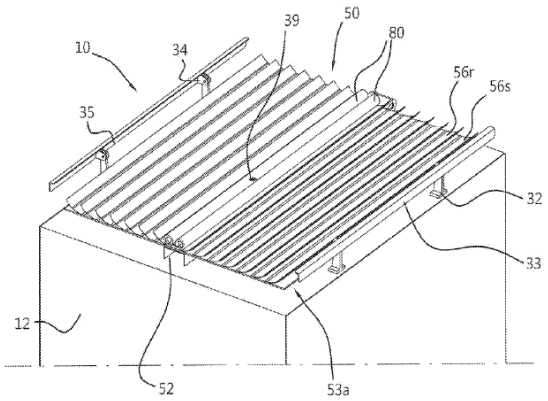

Figure 1.9: Panel in stowed configuration (being released from the hold-down mechanism and the protective foil rolled up in the middle) [9].

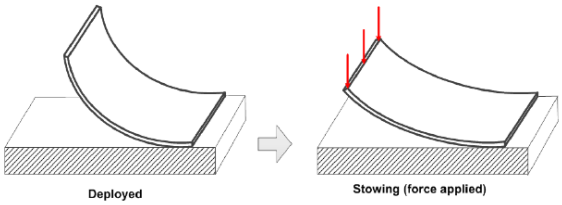

Figure 1.10: Concentrators in stowed configuration [3].

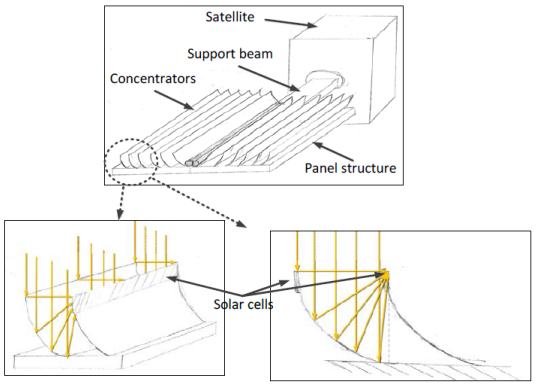

Figure 1.11: Schematic principle of light concentration [3].

1.4.1. Satellite Mission

It has been decided by *Airbus* to attempt designing the *ConCur* solar array for LEO telecommunication satellites, such as *OneWeb* or *Iridium*. The orbit altitude, therefore, is chosen based on the similar type of missions while keeping in mind that in the future the altitude may change if necessary for better solar array performance or due to other reasons (e.g. space environmental reasons).

Iridium Satellite Constellation

Iridium satellite constellation is a currently existing (in service) set of 66 active satellites (plus 6 spares) orbiting the Earth at 780 km altitude providing global mobile communications [10]. Initially the plan was to operate 77 satellites, which is where the name of the constellation comes from (element iridium has an atomic number of 77). The 66 satellites orbit in 6 different orbital planes (11 satellites per plane) spaced 30 degrees apart, and are enough to cover the whole of Earth at every instant in time. The satellites are manufactured by the company *Motorola* in the USA [10]. The required power on each satellite is produced by the two deployable solar panels and batteries.

OneWeb Satellite Constellation

OneWeb satellite constellation is a planned mission concept involving 648 satellites orbiting the Earth in 18 circular polar orbit planes at an altitude of 1200 km for providing global internet broadband service. The aim is to make the constellation operational by year 2020. The constellation is proposed by the company *WorldVu Satellites Ltd* and it chose the manufacturers to be *Airbus*. The artist's interpretation of how the OneWeb satellites would look can be seen in Fig. 1.12 [11].

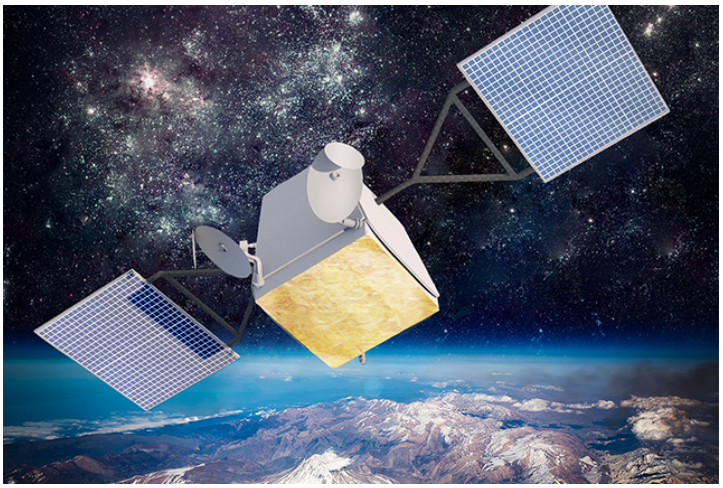

Figure 1.12: OneWeb satellite solar array position with respect to the antenna [11].

1.4.2. Solar Array Specifications

The main *ConCur* solar array structural components of the wing are:

- **Support panel** - the main support structure on which the concentrators will be mounted. Its back side acts as a heat sink collecting (some of) the waste heat from the front side concentrators and solar cells, and emitting it towards the deep space. The support panel is connected to the satellite by the support beam. The panel material is CFRP and its dimensions can be found in Table 1.1.

- **Concentrators** - parabolically shaped low thickness structure with highly reflective surface coating for a focused light reflection onto the solar cell. To ensure that most of the light gets reflected and reaches the cell the geometrical design of the concentrator needs to have a certain shape. The concentrator material is CFRP and its thickness is 0.24 mm.

- **Solar cells** - used to convert the light induced photons into charge carriers, and to generate electrical power for utilization for the satellite's mission. The ones used for this solar array design are triple junction GaAs solar cells from *Azur Space*. The amount of cells is listed in Table 1.1 and other details can be found in App. B.

- **Protection foil** - to be wrapped over the stowed concentrators for protection during the launch. Upon solar array deployment the protection foil will roll up and uncover the concentrators, and (without affecting concentrator performance) will remain attached to the support panel.

- **Support beam** (deployment yoke in Fig. 1.13) - hollow structure used to connect the solar panel to the satellite's main body. When the satellite enters the desired orbit the hollow support beam deploys the array away from the satellite's main body. During the operation of the solar array the support beam acts as the shield and protects the wiring harness which is placed along the beam on the side facing the deep space (or inside the beam). These wires connect the power conditioning unit (PCU) to the solar cells.

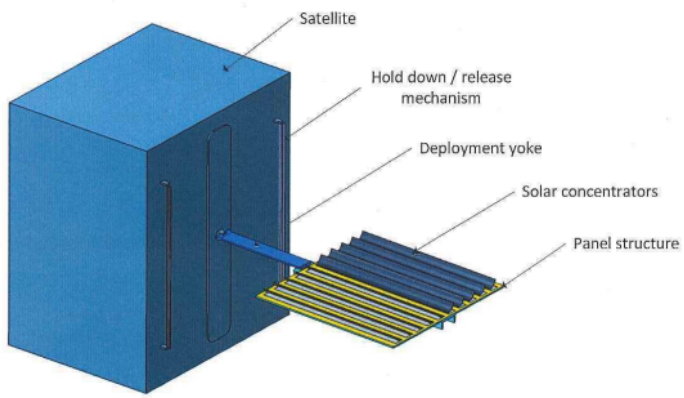

Figure 1.13: Solar concentrator array system overview (deployed configuration) [12].

Table 1.1: Concur solar array wing design parameters from the Feasibility study [13].

Parameter	**Design Feature**
Substrate panel length	1200 (1224) mm
Substrate panel width	1000 (1110) mm
Substrate panel thickness	1.5 mm
Solar cell length	80 mm
Solar cell width	15 mm
Amount of solar cells	180 (168)
Concentrator thickness	0.24 mm
Concentrator number of plies of CFRP	5 (with M55J) or 2 (with T300)
Concentrator width	90.47 mm
Concentrator height	45.74 mm
Space between concentrators	75 mm
Amount of concentrators per panel	14
Concentrator mass (single)	0.043 kg
Concentrator parabola coefficient	0.00559
Concentrator arc length	138.48 mm
Geometric concentration ratio (GCR)	5.0

Table 1.2: Concur solar array wing performance parameters from the Feasibility study [13] and [14].

Parameter	**Design Feature**
Total required voltage output per wing	50 V
Energy output per wing (required)	300 W
Energy output per solar cell	~1.55 W
Mass of one wing (estimated)	6 kg

1.5. Methodology

The following list of actions summarizes the methodology of the entire project. As in any research study, several calculations/tasks were dependent on some other, hence the tasks were executed in a specific order. Fig. 1.14 depicts the order of the main milestones in this thesis.

1. Performing the Literature Study:
   - Familiarizing with the work done on *ConCur* solar panel (feasibility study, structural and vibrations testing of the panel components),
   - Looking into the largest CPV projects for terrestrial applications,
   - Researching the CPV application in space (*Boeing* spacecraft),
   - Studying the patents of very similar concepts (Ted Stern's patents),
   - Studying the environmental impact on the panel and separate materials in orbit (concentrator reflective coating material),
   - Calculating the amount of trapped high energy particles in the solar cells at the end of the satellite's lifetime,
   - etc.
2. Narrowing down literature study to top 10 requirements,
3. Learning to use *ESATAN* (see the Midterm Report [15]):
   - Learning basic software working principles,
   - Learning the way conduction and radiation is represented and understood by *ESATAN* software,
   - Creating benchmarks: different geometries w/ and w/o boundary conditions,
   - Executing the benchmarks at specific thermal conditions.
4. Preliminary electrical design:
   - Assuming max. and min. solar cell temperatures,
   - Calculating the amount of solar cells needed to reach 50 V and 6 A (300 W in total).
5. Modelling the concentrator panel in *ESATAN*:
   - By separately modelling parts of the panel and then combining them together in one assembly,
   - Verifying the model by means of comparing some of the results to another software, and to the calculations done manually,
   - Executing the most extreme thermal case.
6. Improving the panel design to improve the heat transport by means of varying panel materials and adding thermal doublers and vertical radiator to the design,
7. Executing all thermal cases in *ESATAN*,
8. Updating electrical design with the actual thermal data,
9. Creating schematic drawings of the electrical panel design,
10. Estimating panel's total cost,
11. Drawing conclusions and recommendations.

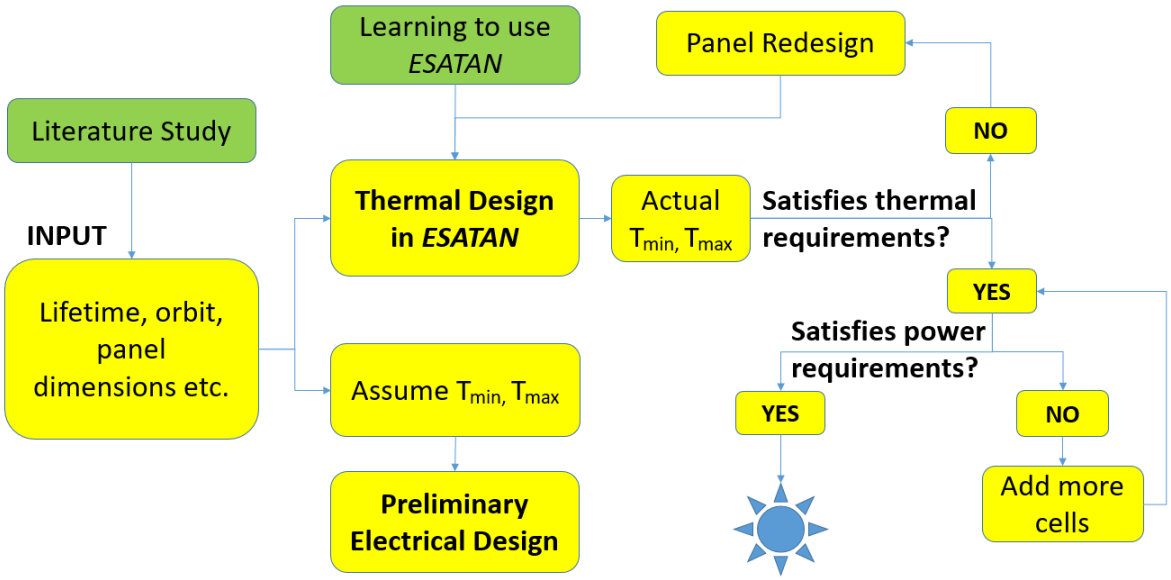

Figure 1.14: The design flow chart of this thesis.

2

Literature Study

Prior to diving into the development of thermal and electrical designs of the solar panel, the literature survey was conducted and reported in [2]. This chapter summarizes the main findings. It first briefly introduces the concept and application of solar concentrators in Section 2.1 which is followed by a summary of heat transfer processes in Section 2.2. It then describes environmental challenges to be faced in space environment in Section 2.3. The top 10 requirements derived based on the Literature Study are listed in Section 2.4. Lastly, Section 2.5 describes the material selection for separate parts of the array.

2.1. Solar Concentrators

2.1.1. Terrestrial Solar Concentrators

This section introduces a couple of the largest terrestrial power plants that incorporate the technology of concentrating the solar light. The challenges and problems that were faced by these power plants may indicate significant pitfalls that might be useful to evaluate for the space mission.

Carrisa Plains Power Plant

The Carrisa Plains solar power plant by ARCO company was the world's first ever large-scale photovoltaic power plant located in Carrisa Plains, California, US. It was built in 1983 for commercial power production and originally was rated at 5.2 MW at its peak. However due to technological reasons it began to show steady degradation in electrical performance since 1986, the capacity factor (ratio of the actual power output over a period of time, to the potential output) was decreasing. Fig. 2.1 shows the Carrisa power plant with concentrator mirrors. This power plant made use of the reflection principle concentrating solar power using mirrors.

Figure 2.1: The world's first ever large-scale photovoltaic power plant in Carrisa Plains, California [16].

The power plant routinely produced less than 3 MW as of year 1990. As the performance began to deteriorate, a certain *browning* of the modules was noticed. Detailed examination showed that it was EVA (ethylene vinyl acetate) encapsulant browning between the front cover glass and the center portion of the cell [17]. The evidence suggests that outgassing or ingassing eliminates browning of the

EVA. The recovery procedure (involves dropping an unframed module on its corner such that the front cover glass shatters but is held in place by EVA and rear tedlar cover) allows gas to escape (or perhaps to enter) and, therefore, slows or eliminates the browning [17].

PVUSA Array

Contrary to Carrisa Plains, this power plant made use of the refractive technology concentrating solar power using stretched lens. PVUSA (photovoltaics for utility scale applications) was a national cooperative research and development project dedicated to acquiring information through installation and field testing of PV technologies. It was constructed in 1986 and is still in operation in 2017 generating 650 kW which annually amounts to 1300 MWh supplying electricity to 108 homes. According to M. O'Neil the line-focus Fresnel lens array at the U.S. Department of Energy sponsored PVUSA test site in California outperformed all of the other photovoltaic technologies in an independent, side-by-side field test throughout the whole decade of the 1990's [8].

2.1.2. Concentrators in Space

In particular, two types of concentrator concepts were analyzed: *Stretched Lens Array* used by Deep Space I mission and *CellSaver* concept used by Proba 2, Boeing 702 and other missions. Both concepts are compared and the main advantages and disadvantages are summarized.

SLA Concept - Deep Space 1

The Stretched Lens Array concept involves thin, flexible stretched lens made from space qualified silicon polymer material. The lens is able to concentrate the incoming light with the concentration ratio of 8.5 Suns, thereby reducing the amount of solar cells required to reach a specific amount of electrical power as compared to an ordinary honeycomb solar panel. This concept results in 85% savings in cell area and cost compared to the planar multi-junction array, the SLA costs 50% less than planar wing of equal power. It also has a major weight advantage over a conventional panel design due to low combined weight of the lens, radiator and narrow PV cell weighing approximately half as much per m^2 as a one-sun solar cell assembly by itself.

The spacecraft designed by NASA and launched in 1998, *Deep Space 1* (DS1) demonstrated the newest technologies and tested advanced instruments while chasing the asteroid and a comet. It was operational for $\sim$ 3 years and delivered much scientific data throughout it's mission. This mission proved that the concentrator solar array can operate long term in deep space without significant degradation despite [18]:

- having abundant contamination sources in the form of organic adhesives and binders, including silicone,
- having UV impingement on contaminated surfaces (outer lens surface) to enable "photo-sticking" and cause darkening of the deposited contaminants,
- having direct line of sight from contamination sources to the Fresnel lenses.

Significant contamination darkening of the lenses was not occurring, most likely due to the following two reasons [18]:

1. Contamination sources had relatively low temperature (75°C),
2. The DS1 solar panels and lens frames were baked out (vacuum bake-out test) at high temperature prior to lens installation to minimize out-gassing in space.

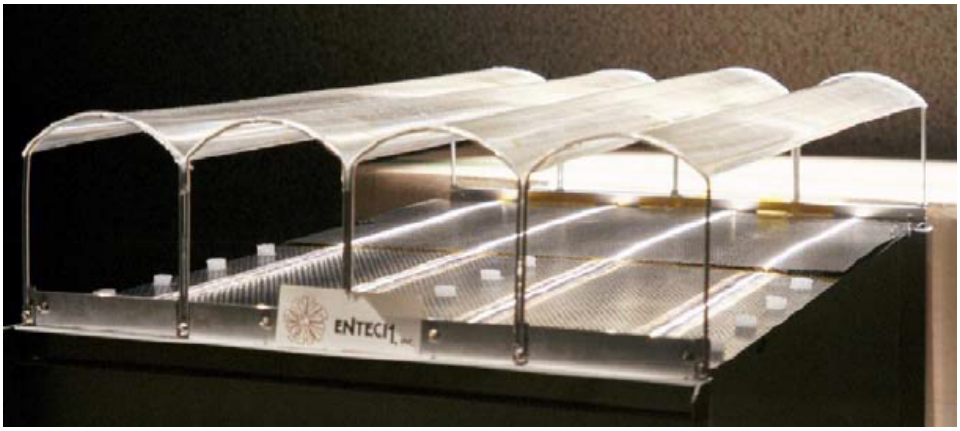

Figure 2.2: Stretched lens array with four lenses and receivers [8].

CellSaver Concept

As opposed to the SLA concept where the light transmitted through a stretched lens, the *CellSaver* concept utilizes the effect of reflecting the light. The concept was developed for the sake of minimizing the cost of the spacecraft multi-junction solar cell arrays by substituting nearly half of the number of solar cells by cheap reflectors. The *CellSaver* concept can be seen in Fig. 2.3. The reflectors are typically constructed from a single piece of thin high-strength titanium foil and coated high reflectance coating - vapour deposited silver with a protective transparent dielectric overcoat (glassy ceramic material). The ceramic material protects the silver coating from naturally occurring atomic oxygen and xenon ion erosion, the latter being caused by spacecraft ion propulsion systems. Titanium foil can be easily bent and folded to very tight radiuses without yielding, which is important in stowed configuration. Also, it is extremely stable under exposure to Space radiation and thermal cycling, which is significant for in-orbit operation. It is a light-weight material and, therefore, by saving mass it directly saves the cost [18].

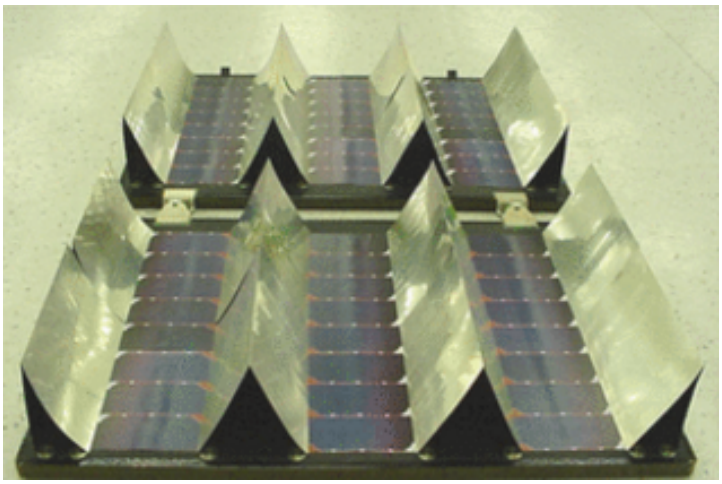

Figure 2.3: *CellSaver* solar concentrator panels [18].

- **Boeing 702** missions instead of distributed *CellSaver* reflectors used large edge reflectors, see Fig. 2.4. As a result six Boeing 702 concentrator solar arrays suffered from gaseous emission contamination [18]. The problem was that the solar panel with large edge reflectors was subjected to very high temperatures ($> 120^{\circ}$C in GEO) compared to *CellSaver* reflectors (80°C). This resulted in significantly high discharge of the panel and a large variety of gaseous contaminants. The high temperature contaminants (being able to drive off contaminants with larger molecules and higher activation energies) have been identified as the primary cause of the in-orbit dramatic power reduction [18] of Boeing 702 missions. Regarding the contamination, it is also important to note that Boeing has not officially stated whether their solar panels had been subjected to a

vacuum bake-out test prior to launch. It would be significant and as mentioned in [18] that such a test would undoubtedly minimize the outgassing in Space and contamination degradation [18].

Figure 2.4: Panel edge reflectors used on the Boeing 702 [18].

- The *CellSaver* type concentrator solar array (see Fig. 2.5) was part of the scientific payload on-board of **Proba 2** spacecraft. Experimental solar panel was sent to space in order to study the temperature effect, ageing effects due to radiation and concentrated solar flux [19]. Proba 2 was a micro satellite of $\sim$ 300 kg designed for technological purposes to be operational for 2 years in sun-synchronous LEO at 700 km altitude. The two main objectives of the mission were (1) to perform in-flight demonstration of new space technologies and (2) to support a set of scientific instruments [20]. It is recognized that contamination and ageing effects as well as thermal aspects are of major significance, but there has not been done much in-orbit testing to realistically assure full qualification of the concentrator solar array concepts.

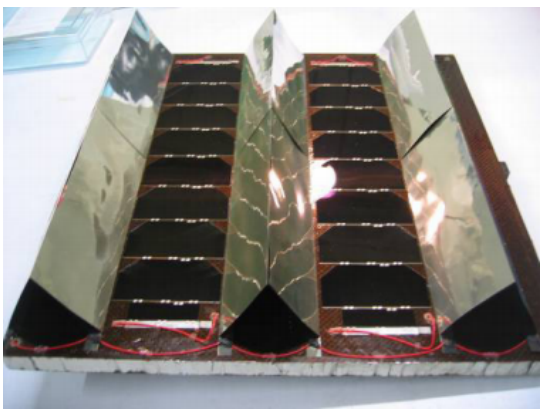

Figure 2.5: Titanium reflectors with central solar cell string [20].

Comparison

Table 2.1 compares the planar array to the *CellSaver* and *SLA* concepts.

Table 2.1: Fundamental comparison of different high-efficiency space solar arrays [8].

Item	**Planar Array**	**2X Mirror-Augmented Array**	**8.5X SLA**
Cell savings: area, mass and cost per watt	0%	50%	85%
Space flight heritage and experience	Numerous successful programs	Significant performance problems on 6 Boeing 702 Comsats; geometry is conductive to outgassing/photofixing	Extremely successful PASP+ and SCARLET on DS1; geometry discourages photofixing
Terrestrial experience for similar technology	Numerous successful programs	Significant performance problems for reflective systems (e.g. Carrisa Plains - mirrors reduced power)	Several successful programs (e.g. PVUSA arrays)
Optics - inherent shape error problems	N/A	Significant problem (efficiency and/or flux uniformity)	Negligible problem (200X advantage over mirrors)
Predictable, same, unchanging photon flux on each solar cell in each source circuit	Yes	No - reflective optics are inherently sensitive to shape errors (e.g. Hubble telescope primary)	Yes - ENTECH's error-tolerant refractive optics [18]
Cell operating temperature on GEO	50 - 60°C	120 - 130°C	75 - 80°C
Super-encapsulation of cells for high-voltage and/or high-radiation missions	Difficult and heavy	Relatively difficult and heavy	Simple and lightweight - Auburn micrometeoroid tests with cells at 1,000 V

Concur Concentrator Concept: Early US Patents

The same but slightly different variation of the same concept of a concentrator solar array as *ConCur* has been previously researched and patented in 1993, and in 2005 for a deep-space mission. Table 2.2 provides an overview of the available data regarding used materials on the two patents found in the literature.

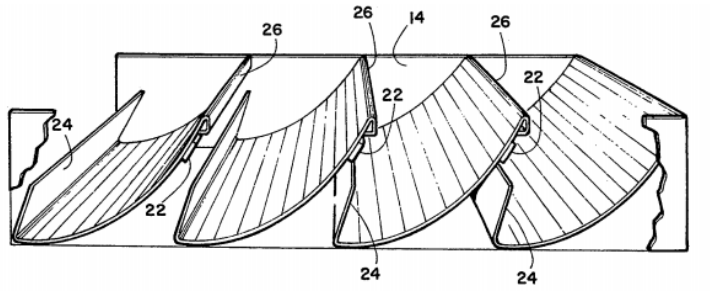

Figure 2.6: A perspective of the solar concentrator cell array from the patent [21].

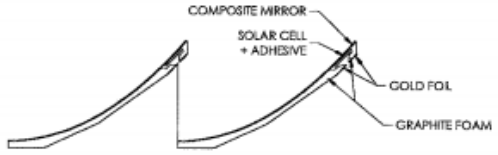

Figure 2.7: Deep Space concentrator element design from the patent [22].

Table 2.2: Comparison of two solar concentrator designs proposed by T. Stern and others [21], [22].

Parameter	**Lightweight solar concentrator cell array**	**A deep-space concentrator for inner and outer solar system missions**
Year	1994	2005
Figure	Fig. 2.6	Fig. 2.7
Mirror material	Highly conductive composite material (for enhancing thermal conductivity). Preferably a suitable advanced organic composite which has the resin and reinforcing carbon element to provide optimum thermal stability. To provide enhanced conductivity (for performance as a radiator fin) the mirror may be doped with high conductivity material (e.g. silver powder).	A composite laminate it used - Graphite Fiber Reinforced Composite (GFRC). It has reduced thermal conductivity at high and low temperatures, which allows thermal switching approach.
Mirror front surface	Coated with highly reflective material (aluminum or silver). Coating should have optimum resistance to UV radiation degradation.	Unknown
Mirror back surface	Thermal emissive coating (for mirror thermal control) to allow the mirror element to act as a **radiator fin** for the string of solar cells. The coating may use white paint with low solar absorption to minimize absorbed thermal load from solar and albedo sources.	Unknown
Panel material	Highly conductive composite material.	Porous graphite material.
Features	The whole structure is made up from one type of material and, therefore, does not pose a problem of differential thermal expansion behavior of different elements.	Uses a modular off-axis reflective concentrator design to achieve thermal control under high flux environments by limiting the total amount of energy to be managed within the thermal mass (also keeping the element small minimizes the conduction path reducing the temperature differences between solar cell and radiator surfaces. An aperture plate in front of the solar cell allows to reject off-axis and de-focused energy providing a means to limit the temperature of the solar concentrator components.

2.2. Theory of Heat Transfer

Heat transfer in general can occur via three different processes: conduction, convection and radiation. In space there is vacuum, so convection is non-existent.

- **Conduction** is heat transfer through a medium via collision of molecules involving a direct contact between the heat source and heated object. It takes place generally in solids. With regard to the *ConCur* concept conduction plays the following role. Having the front side of the substrate panel being constantly oriented in the direction of the Sun, there will be heat transfer by conduction trough the panel's thickness towards the back side of the panel. Similarly, as the cells will be heated up, there will be heat transfer by conduction along the concentrators towards the substrate panel. The reflected light from the concentrator will not all reach the solar cell, but part of it will be concentrated onto the backside of the concentrator, therefore detailed thermal and optical analysis of the concentrator configuration is needed. Since that is the place where the solar cells are connected it should be taken care of that the cell temperature remains below their operational limit, and when too hot the heat must be directed towards the back side of the substrate and dissipated effectively.

- **Radiation** is the main source of heat transfer from the environment to the satellite in space. When considering radiation an important concept to understand is the definition of a black body: black body radiation is an idealized radiation spectrum of a body that is at a uniform temperature. It does not reflect any radiation, but emits at any temperature the maximum possible amount for any wavelength, and absorbs the maximum possible incident radiation. Fig. 2.8 shows the idealized black body spectrum and the radiation spectrum emitted by the Sun. The difference between the two is negligible and thus the Sun is often approximated as a black body.

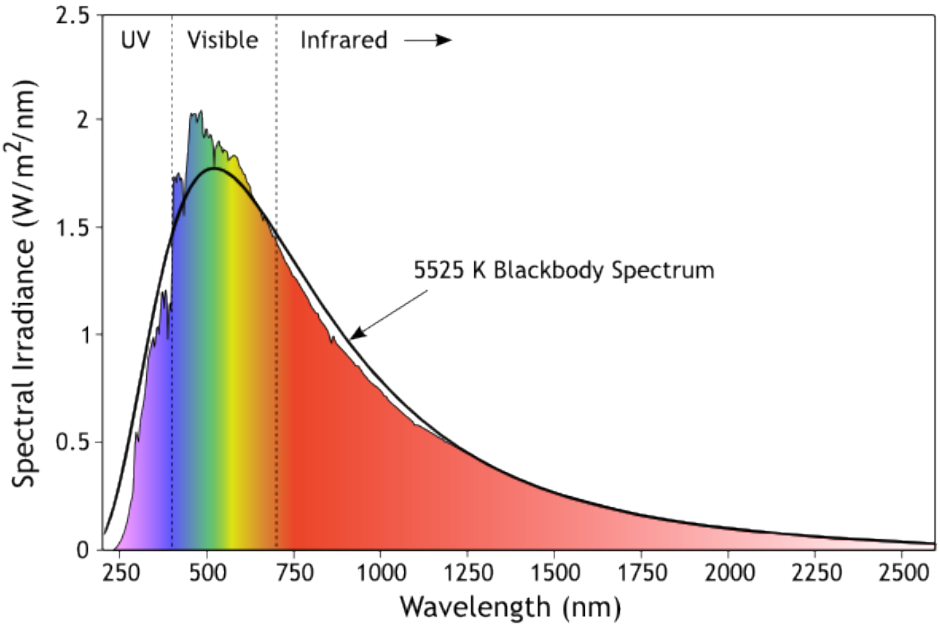

Figure 2.8: Black body radiation spectrum and the spectrum emitted by the Sun [23].

The way heat transfer is incorporated in *ESATAN* software is described further in the report (Chapter 4).

2.3. Environmental Factors

This section briefly summarizes various environmental factors that in space thermal environment will most likely affect performance of the solar array in LEO at an altitude of 1200 km. Table 2.3 lists the most important characteristics of each of the challenges to be taken into account when designing the solar array.

Table 2.3: Summary of environmental factors affecting overall performance of the solar array in orbit.

Env. factor	**Explanation**	**Effect on Solar Array Performance**
Solar UV Radiation	It is made up of particles with wavelength of approximately 10 to 400 nm (high energy, short wavelength).	May significantly affect performance of the solar arrays. With regard to the solar array systems the radiation initiated chemical reaction can cause hardening and weakening of polymers as well as destroy electronics [24]. The positive effect is heating and electrical power generation from solar energy using solar cells.
Electrons and Protons	High energy particles emitted by the Sun.	Degradation of the solar cells occurs as the result of introducing the non-radiative recombination centers that result of displacements of atoms triggered by their collisions with the energetic particles in space. These recombination centers reduce the minority carrier lifetime and, therefore, the amount of charged carriers generated by photon absorption [25]. This is why it is important to account for the cell degradation when estimating the amount of generated power at EOL conditions (using *SPENVIS* software).
Atomix Oxygen	The substance created due to photo-dissociation of molecular oxygen in the upper atmosphere induced by solar radiation of wavelengths $\lambda \leq$243 nm.	It is responsible for metal corrosion in Space. The metal most affected by ATOX is silver resulting in linear degradation. Corrosion by atomic oxygen is considered to be one of the most dangerous hazards to S/C structural elements in orbits with altitudes 200 to 700 km [26].
Thermal Cycling	S/C will experience extreme temp. fluctuations when entering and exiting the eclipse. The combination of extreme temperatures and the sudden change between them pose serious concerns to the ability of the solar array design to sustain the thermal load.	Leads to S/C experiencing very high thermal stresses. The two most common defects induced by thermal cycling are microcracking and delamination.
Contamination	Contamination sources are usually outgassing products of materials exposed to vacuum conditions as well as fragment products from ATOX and/or solar UV radiation interaction with the S/C materials [27].	Solar arrays may be affected by the LEO environment interaction induced contamination. In [27] it is recognized that the power system optical surfaces are being endangered the most, such as the solar cell cover glass and reflective solar concentrators.
Albedo	Solar radiation reflected by the Earth.	The S/C is affected by albedo radiation due to the solar radiation reflected by Earth, reaching maximum values at the poles and minimum for equatorial orbits.
Earth IR Radiation	Earth emits diffuse IR radiation with intensity varying depending on the position in orbit. It can amount to as high as 20% higher orbiting over the desert areas, while being much smaller over the oceans.	Poses a thread to S/C radiators in LEO, because those are emitting the energy at the same wavelength as the Earth IR is hitting them. Thus the Earth radiation can not be reflected away in that case.

2.4. Top 10 Thermal and Electrical Design Requirements

As an essential part of the assignment the literature study lead to deriving top 10 requirements for the *ConCur* wing that need to be satisfied for a successful mission operation.

1. *The separate panel structure parts and the panel as a whole must sustain the **thermal loads** without any significant permanent deformations throughout the lifetime of the satellite of ~ 5 years (including **severe transient temperature variations** throughout each orbit). This also concerns the concentrators as their **focal plane** may change due to unwanted stresses throughout satellite's lifetime. The in orbit cell temperature shall not exceed 150° C in real life, thus should not be higher than +120° C in the simulations taking into account the safety factor (qualification and uncertainty margins, each of 15° C).*

2. *The solar cells must deliver the **required MPP voltage (50 V), MPP current (6 A)** and overall power (~300 W per panel) to the PCU at the specified elevated temperatures (including losses) and EOL conditions (taking into account cell degradation).*

3. *Selected materials must ensure effective heat transport away from the undesired hot spots through conduction and radiation.*

4. *It must be kept in mind that the structures components should have similar **expansion ratios** to avoid differential expansion and contraction due to **extreme temperature gradients** upon entering and exiting the eclipse periods.*

5. *The **adhesive** used for joining the structures must have high thermal conductivity and sufficient glass transition temperature for good heat transport.*

6. *The panel must be **oriented** with respect to the Sun such that the amount of incoming light is enough for solar cells to produce the required voltage and current in illuminated state, taking into account that the solar array will be able to rotate only around single axis (one DOF) and that the offset angle for the SADM is 0.1°. The power output **sensitivity to the misalignment around both axis** shall be investigated.*

7. *The **thermal radiative challenges** posed by the environmental aspects (albedo, planetary radiation etc.) must be taken into account when estimating the radiation-caused damage to the solar panel.*

8. *The cabling material and the **wiring** of cells must be selected/done in such a way to ensure required thermal protection and at the same time minimize losses. Also, the positioning of the wiring harness shall be safe in stowed configuration. In addition the design should account for redundancy.*

9. *The solar panel must be able to sustain thermal loads in the **stowed configuration** during the launch.*

10. *The overall design of an array should result in a minimum of **30-40% lower cost per watt** than the planar solar array, and the **mass** of one completely equipped panel **shall not exceed 6** kg.*

2.5. Material Selection

The choice of materials for the different structural parts are briefly described in this section. Some materials have been already pre-selected by the other graduates/intern students at *Airbus* based on the structural analysis behavior of the panel and other areas.

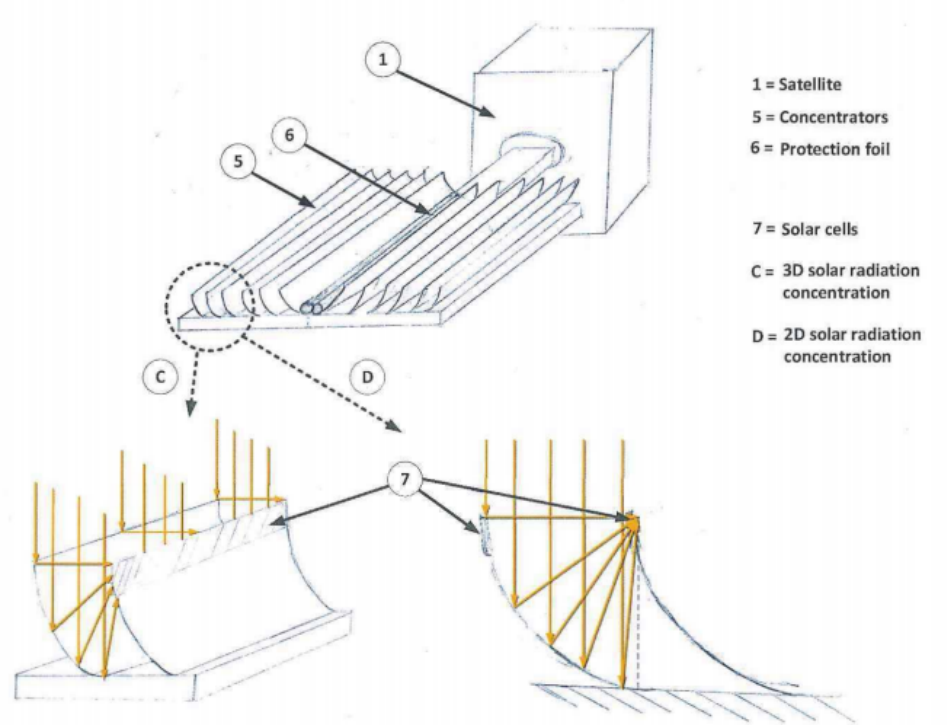

Figure 2.9: Concentrator solar cell concept of the Concur solar array [13].

- Supporting panel

  The supporting panel (also called substrate panel) of the solar array can be seen in Fig. 2.9. It accommodates the mirror concentrators and thermally plays a role in collecting heat from the concentrators and dissipating it towards deep space. The panel itself will be made of CFRP and the surface of its back side will be roughened for achieving higher emissivity value. The type of CFRP is **carbon fiber M55J** carefully chosen by E. van den Abeele in his feasibility study [13].

- Concentrator

  In the feasibility study made by E. van den Abeele [13] several trade-offs and finite element (FEM) analyses have been performed to determine the optimum concentrator material and thickness in order to sustain the pre-determined structural load cases. For that matter the optimum material with various advantages, such as being lightweight and having good thermal conductivity, was concluded to be the **carbon fiber M55J**, same as the supporting panel material. A considerable advantage of choosing the concentrators and the panel being made of the same material is to prevent differential expansion. Such material choice also agrees with Ted Stern's judgment in his patents on the same type of solar concentrator arrays. He specifies that the parabolic concentrators should be preferably made from uncured advanced organic composite with reinforcing carbon element to provide thermal stability at the anticipated service temperature [21]. As a possibility to enhance the thermal conductivity, high conductivity material particles (e.g. silver) may be doped into the concentrator material [21].

  To be able to focus as much light as possible onto the solar cell, the front part of the concentrators is required to have a very high reflectivity. Therefore, the carbon fiber material will be coated with a layer of high-reflectivity material. Ted Stern in his patent [21] proposed to use aluminum or **silver**. He mentions that apart from being highly reflective the coating also has to have optimum resistance to UV radiation degradation. To get the feeling of how the panel temperature distribution varies for different reflective coatings, multiple options were applied to the model in *ESATAN*. The results are analyzed in Chapter 5.

- Adhesives

The interfaces that require adhesive bonding are (1) the solar cell - concentrator interface, (2) the panel - concentrator interface and (3) the coverglass - cell interface. In the first two cases the adhesive should have **high conductivity** for effectively transferring the thermal load from (1) the solar cell to the concentrator, and from (2) the concentrator to the panel, so that ultimately the heat is rejected to the deep space by the rear side of the panel. Apart from conductivity, what has to be kept in mind is the glass transition temperature of adhesive - that is the temperature above which the polymer transitions from a hard, glassy material to a soft, rubbery form. Based on the discussions with Ir. Remco v. d. Heijden (electrical engineer at *Airbus*) the solar cells will be joined to the concentrator using adhesive *RTV 691* (with layer thickness of $\sim 100\mu$m). Its glass transition temperature is very high (well above 160°C) and thus it is thermally suitable. It is also highly conductive. To connect the concentrators to the substrate panel of the same material, the same adhesive is used. For the third interface the adhesive *DC93-500* is used (with 20μm layer thickness). It can sustain very high temperatures, see more specifications in Table F.1.

3

Electrical Design

The electrical design of the *ConCur* solar array is elaborated in detail in this chapter. First, Section 3.1 describes the materials and sizing of relevant electrical components of the design such as the solar cells, diodes, busbars, interconnects, wires etc. Next, the theoretical effect of concentrating light on the solar cell performance is explained in Section 3.2. The electrical power calculations for two typed of orbits are presented in Section 3.3 including the description of the calculations of the cell efficiency change as a function of temperature, as needed to account for in thermal modelling. Finally, Section 3.4 displays some technical drawings for illustration purposes.

3.1. Sizing of the Electrical Components

When establishing detailed electrical design the sizing, placement and choosing materials becomes very important. In this section these parameters are shortly described.

3.1.1. Solar Cells

The type of the solar cells to be used for the concentrator solar array are high efficiency *Azur Space 3G30C Triple Junction GaAs* cells specifications of which can be found in App. A. This cell consists of three layers each covering a part of spectrum illuminated by the Sun, see Fig. 3.1 and 3.2. These three substrate layers are:

- $GaInP$ (gallium - indium - phosphate) absorbing very high energy photons from 300 nm in UV region up to 600 nm in the visible spectrum (short wavelength particles),
- $GaAs$ (Gallium Arsenide) covering the wavelength range between 600 and 900 nm, and
- Ge (germanium) absorbing low energy particles in IR region above 900 nm till ~1600 nm.

The typical dimensions of such a cell are (approximately) 40 x 80 mm, however as concluded by E. van den Abeele [13] in his Feasibility Study on *ConCur* the optimal size of solar cells (according to the spacing between each two adjacent concentrators being 75 mm, and to maximize the utilization of the reflected light by concentrators) was found to be **15 x 80** mm, rectangular shape. Cell specifications in terms of design, mechanical and electrical data, acceptance values and temperature gradients can be found in App. A. Tab. 3.1 summarizes additional solar cell parameters that are used in electrical and thermal calculations.

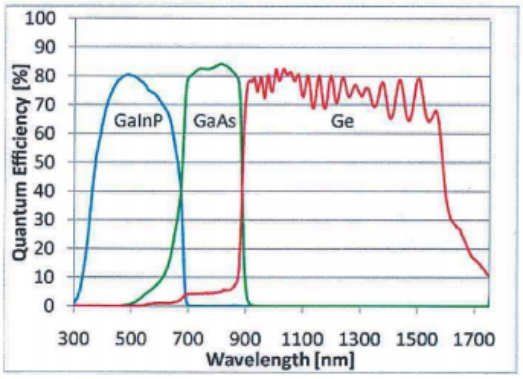

Figure 3.1: Wavelength coverage by a triple junction $InGaP/GaAs/Ge$ solar cell [13].

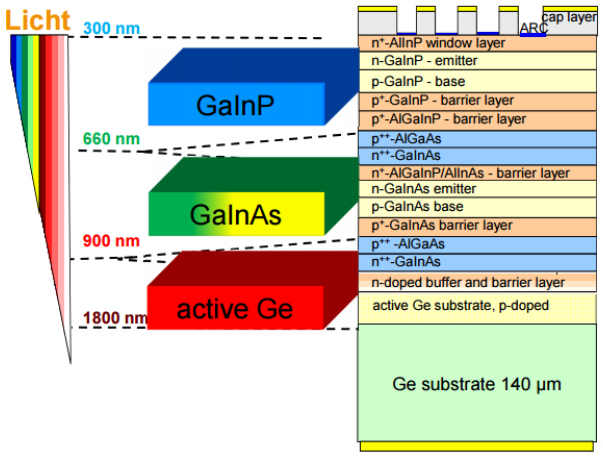

Figure 3.2: Azur Space TJ GaAs solar cell structure [28].

Table 3.1: Solar cell parameters.

Parameter	Value	Unit	Remark
Cell dimensions	15 x 80	mm	
Total cell thickness	311	μm	Excl. coverglass, incl. adhesive and kapton layers
Coverglass thickness	100	μm	
Avg. cell density	2924.38	kg/m^3	Used in thermal design (includes coverglass)
*Avg. out-of-plane conduction	1440	W/m^2K	Cz_{SCA} calculated from the Excel sheet provided by *Airbus*
*Avg. in-plane conduction	0.0085	W/K	Cxy_{SCA} calculated from the Excel sheet provided by *Airbus*

*(starred) Average thermal conductance was calculated as follows (with parameter values listed in Tab. 3.2):

- *Out-of-plane per unit area:*

$$Cz_{SCA}[W/m^2K] = \frac{1}{\sum \frac{t}{k}} = \frac{1}{(\frac{t}{k}_{glass} + \frac{t}{k}_{adh1} + \frac{t}{k}_{germanium} + \frac{t}{k}_{adh2} + \frac{t}{k}_{kapton})} \quad (3.1)$$

- *In-plane between the two nodes:*

$$Cxy_{SCA}[Wm/mK] = \sum k \cdot t = k \cdot t_{glass} + k \cdot t_{adh1} + k \cdot t_{germanium} + k \cdot t_{adh2} + k \cdot t_{kapton} \quad (3.2)$$

Table 3.2: Solar cell assembly specifications.

Parameter	Symbol	Value	Unit	Remark
Conductivity	k_{glass}	2.0	W/mK	Coverglass
	k_{adh1}	0.146	W/mK	DC93-500
	$k_{germanium}$	58.58	W/mK	
	k_{adh2}	0.4	W/mK	RTV 691
	k_{kapton}	0.2	W/mK	
Thickness	t_{glass}	100	μm	Coverglass
	k_{adh1}	20	μm	DC93-500
	$k_{germanium}$	140	μm	
	k_{adh2}	100	μm	RTV 691
	k_{kapton}	51	μm	

3.1.2. Diodes

There are two types of protective diodes used in the electrical design of the solar array:

- **By-pass diodes** are integrated for each separate cell to ensure that in shading/misalignment/failure situation the total current within the string of cells connected in series can by-pass the affected cell. The reason for each cell to have its own by-pass diode as opposed to having a single diode across each string is due to high risk of failure in orbit environment, high cell cost as well as the fact that the chosen cell can only withstand maximum of $4V$ in reverse without failing (compared to $20V$ for silicon solar cells). The by-pass diode is made of the same material as the cell, also with a layer of coverglass (100 μm) on top for protection. It is connected to the cell in parallel, as opposed to the blocking diodes (connected in series). The size of a single by-pass diode is 1 x 7 mm and it is located underneath and between the two adjacent cells, as shown in Fig. 3.3. As will be seen later in this chapter the number of cells per solar panel amounts to 168, hence the number of by-pass diodes is also 168.

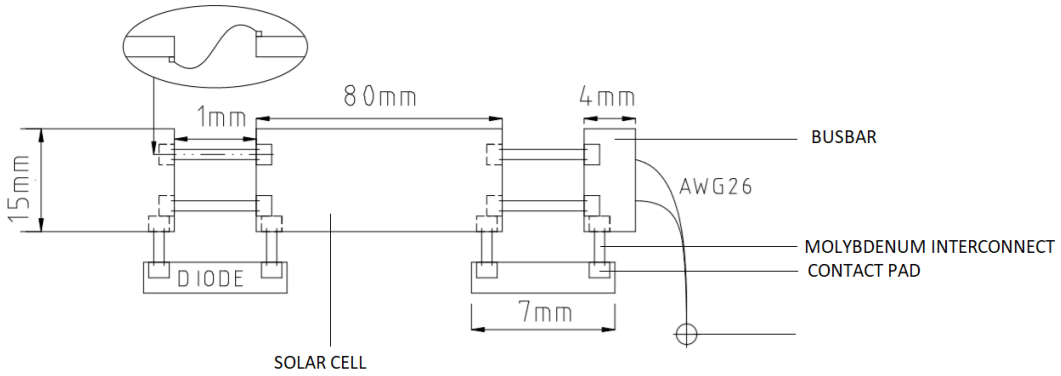

Figure 3.3: Image of the by-pass diode position with respect to the cells and the side view of the cell out-of-plane interconnects.

- **Blocking diodes** are connected to the cells in series at the end of each string to ensure that the current flows in the desired direction. As calculated later in this chapter (preliminary calculations) the required amount of strings per panel is six, therefore, there are six blocking diodes connected in series to the positive side of each string at the rear of the panel, see Fig. 3.11.

3.1.3. Other Components

Interconnects and Contact Pads

The solar cells are interconnected with each other and connected to the by-pass diodes via molybdenum interconnects as shown in Fig. 3.3. They are attached to the metal contact pad that is welded onto the cell. The metal pads are 4 mm^2 each, and there are six pads per cell: 4 for interconnects to the other cells and 2 for connecting to the diodes. This results in a significantly lower cell effective area

which was taken into account when calculating the cell performance parameters (from 1200 mm^2 to 1176 mm^2).

Busbars

Each string of cells in series and each side of the concentrator are bounded at their edges by the busbars, where the electrical charge is concentrated to be further transported to the desired location via two (to account for redundancy) *AWG 20* wires. Busbar is 4 x 15 mm large and is made of Invar (nickel iron alloy), see Fig. 3.3.

Wiring Harness

Electrically conducting wires are used for transporting the electric charges generated by the solar cells to the power conditioning unit inside the satellite. There are two types of wires used: *AWG 20* and *AWG 26*, chosen based on the amount of current they need to carry. *AWG 26* wires will be used to interconnect the cells of two adjacent concentrators into one string. It was calculated that a single string of cells would carry $\sim 1\ A$ current to the rear side of the panel, where the current of all strings would add up (to $\sim 6\ A$) and travel to the PCU through *AWG 20* wire. The relevant properties of both sizes of wires can be found in the following table:

Table 3.3: Electrical wire properties [29].

Property	**AWG 20**	**AWG 26**
Number of cores	1	1
Voltage, maximum rating	600 V_{rms}	600 V_{rms}
Maximum current rating	7.5 A	2.5 A
Operating temp. range	-200°C to +200°C	-200°C to +200°C
Diameter	1.58 mm	1.03 mm
Approximate length	2 m	0.6 m
Resistance	33.31 Ω/km	133.9 Ω/km
Current in the wire	~6 A	~1 A

It should be noted that the above specified maximum current will increase the wire temperature by $\sim$ 50°C in vacuum environment, therefore the wires are chosen such to account that the maximum current rating is at least 20% higher than the maximum current a wire will be carrying. This satisfies the de-rating safety requirement.

3.2. Effect of Concentration on the Solar Cell Performance

Concentrating the light onto the solar cell has various effects on its performance. Under higher illumination the cell produces a higher current, the process of which is discussed shortly in Sec. 3.2.1, but it also introduces additional recombination centres which contributes to worsening of the cell performance, which are discussed in Sec. 3.2.2.

3.2.1. Photocurrent and Fill Factor

The current produced by the solar cell scales linearly with the amount of sunlight received by the cell, hence concentrating the light *n* times will result in *n* times the amount of current of a single sun, as in:

$$J_{SC,n} = n \cdot J_{SC} \tag{3.3}$$

More light concentration and hence higher current directly increase the power output. However, it also contributes to the power loss due to series resistance according to:

$$P_{LOSS} = I^2 \cdot R_{series} \tag{3.4}$$

The increase in solar cell performance (as characerized by the fill factor) as a function of concentration ratio can be seen in Fig. 3.4 [30]. As can be seen, the fill factor generally increases with growing

concentration ratio. The tendency according to which the FF here increases (as a function of CR) is used to estimate its increase in the situation that is investigated in this thesis. The FF versus CR curve from the graph was reconstructed in *MS Excel* and by means of formatting a logarithmic trend-line with displayed equation (see Eq.3.20) of the curvature (with CR as a variable and FF as an output), the fill factor for the desired CR was obtained. The following equation will be used further in electrical power calculations.

$$FF_{Xsuns} = FF_{1sun} + 0.3485 \cdot lnCR \tag{3.5}$$

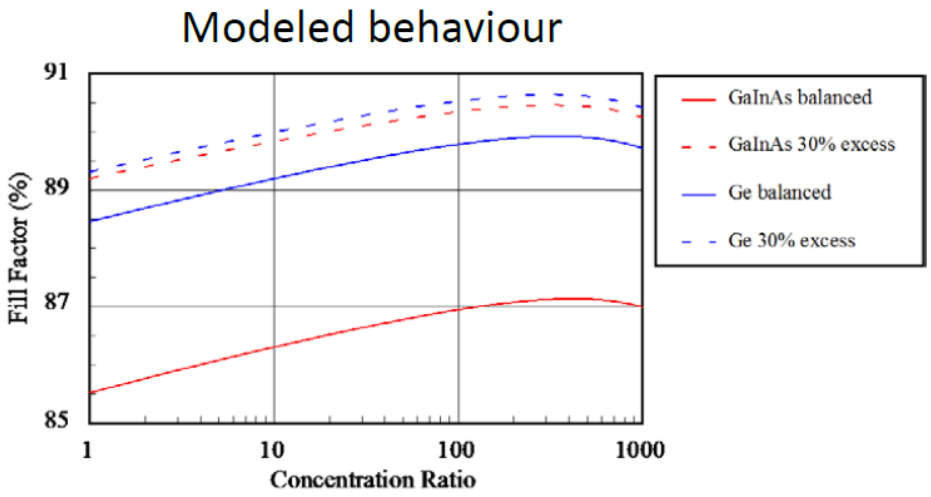

Figure 3.4: Fill factor versus concentration ratio for TJ GaAs solar cells (cell performance behavior tested for various spectral mismatch scenarios [30].

3.2.2. Recombination Mechanisms

Recombination is a process opposite of generation of charge carriers; it is a process where carriers are destroyed [5]. In particular recombination in the bulk is of three types:

Radiative Recombination

Radiative recombination predominantly occurs in **direct bandgap materials** (where an electron can shift from the higher energy state (conduction band) to a lower energy state (valence band) without a change in momentum). It is also referred to as band-to-band recombination. An electron recombines with the hole in the valence band and releases a photon. Gallium Arsenide is a direct bandgap semiconductor, as can be seen in Fig. 3.5.

Auger Recombination

Auger recombination also involves the electron recombination with the hole, but instead of releasing a photon the energy is taken up by the **third carrier** (an electron in the conduction band). This is an important recombination mechanism in indirect and doped semiconductors, or at high carrier concentrations under concentrated sunlight.

Shockley-Read-Hall Recombination

Recombination occurring due to the **defects in the lattice** of the material is called Shockley-Read-Hall recombination. It is a two-step process with (1) an electron (or hole) being trapped in the energy state in the forbidden region introduced through (intentional or unintentional) defects in the crystal lattice, and (2) a hole (or electron) moving up to the same energy level before the electron is thermally re-emitted into the conduction band, then it recombines [31].

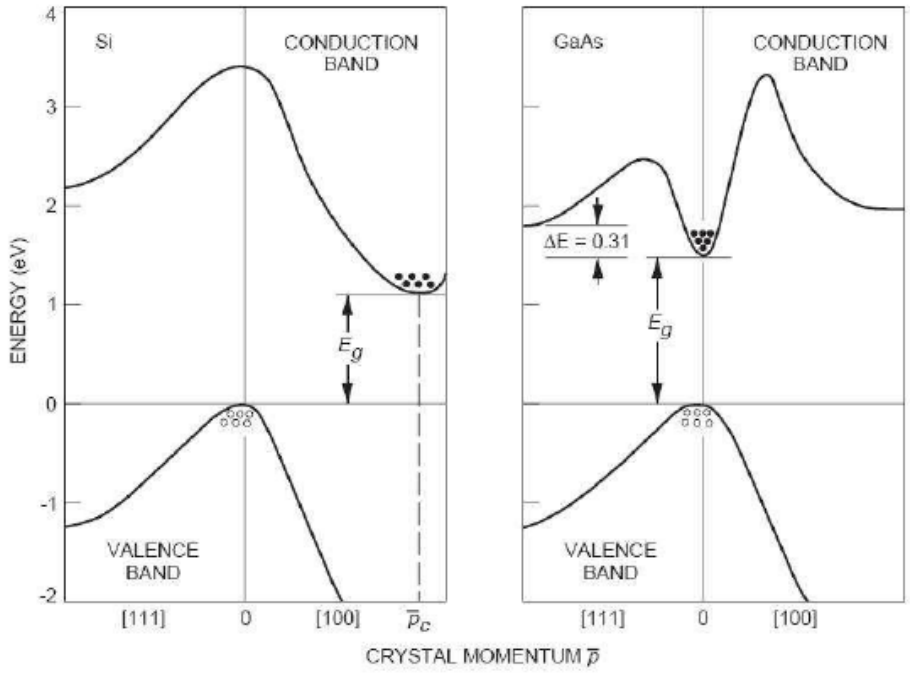

Figure 3.5: Energy band structure of Si and GaAs [32].

Remarks

Out of the three above mentioned recombination mechanisms, the radiative recombination dominates in the GaAs solar cells. Due to light concentration Auger recombination might affect cell performance significantly, too.

3.3. Electrical Power Calculations

This section elaborates upon the electrical power calculations which are done taking into account the panel thermal performance results (see Chap. 5), such as in-orbit temperatures. All constant parameters (inputs and requirements) are listed in Table 3.4.

Electrical power calculations are done for two types of orbit:

- The eclipse-free orbit (90° right ascension) is analyzed, taking into account the temperature values obtained from the radiative *Case 3D OPR*: operational case with cells ON and under EOL conditions (see Chapter 5). The panel temperature in this case is more or less constant throughout the orbit (max. 67° and min. 62°C).

- The second orbit for electrical power calculations is 0° right ascension polar orbit (as in radiative *Case 3C OPR*). The panel temperature in this case varies significantly and its variation will be assessed for electrical power calculations.

3.3.1. Orbit Without Eclipse

Constant Parameters

Electrical power calculations for the solar panel are done based on the set of constant parameters listed in the Tab. 3.4, where *(starred) values were chosen according to the specified amount of radiation in space (see App.B and C), and ** (double starred) values were taken from the thermal *Case 3D OPR* (see Chap. 5).

Table 3.4: Input parameters/constants for panel electrical power calculations.

Parameter/constant	**Symbol**	**Value**	**Unit**
Cell width	w_{cell}	15	mm
Cell length	l_{cell}	80	mm
Cell Area	A_{cell}	1200	mm^2
Metallization area	A_{met}	4	mm^2
Number of met./cell	n_{met}	4	$-$
Total met. area /cell	$A_{met,total}$	16	mm^2
Effective cell area	$A_{cell,eff}$	1176	mm^2
Panel width (initial)	w_{panel}	1300	mm
Panel length (initial)	l_{panel}	1110	mm
Edge busbar width		4	mm
Number of busbars/conc.		2	$-$
Gap between the cells		1	mm
Cells/conc. (initial)	$n_{cells/conc}$	15	$-$
Conc/panel		14	$-$
Cells/panel (initial)		180	$-$
Packing density	PD	0.987	$-$
Required total voltage	V_{panel}	50	V
Required total current	I_{panel}	6	A
Required total power	P_{panel}	300	W
Highest operational cell temp.** (90° asc.)	T_{max}	67	°C
Lowest operational cell temp.** (90° asc.)	T_{min}	62	°C
Open circuit voltage at STC*	$V_{OC,STC}$	2.616	V
Short circuit current at STC*	$I_{SC,STC}$	0.5185	A
Max power point voltage at STC*	$V_{MPP,STC}$	2.345	V
Max power point current at STC*	$I_{MPP,STC}$	0.197	A
Geometric Concentration Ratio	X	5.0	$-$

Equations

The solar cell performance degrades when exposed to high levels of radiation is Space, and also changes depending on the cell temperature. Based on the orbit altitude (1200 km), orbit inclination (88°) and amount of years in orbit (5 years) it was possible to estimate the amount of radiation at end-of-life conditions using *SPENVIS* software. The amount of trapped electrons and protons depending on the cell coverglass thickness can be found in Appendix B. The minimum coverglass thickness that is usually manufactured is 100 μm, hence this is the thickness chosen. Calculations show that at 100 μm the amount of total trapped electrons and protons does not exceed 2.7E+14 cm^{-1} (highest for the voltage). The results indicate the amount of radiation that the cell would receive if it was placed horizontally onto the solar panel, having a view factor equal to half-sphere. The case of attaching cells to the rear side of concentrator reduces the cell view factor by at least a half, since it is protected by the concentrator. Hence, the amount of trapped particles in the cell decreases greatly. It is assumed to not reach more than 2.5E14 cm^{-2} at EOL (which is still a very safe estimation), therefore, the cell temperature gradients were chosen accordingly, see Appendix B.

The power produced by the array strongly depends on the cell temperature and illumination intensity. Therefore, the equations to account for these two variables are listed below. In order to ensure that the amount of power is not underestimated, the maximum and minimum temp. values are used when calculating voltage and current, respectively, according to their lowest values in orbit. In addition, the calculations are performed at EOL conditions (taking into account cell degradation values at the end of a 5-year operational period) with EOL reflectivity value of the concentrator coating (0.85 $[-]$).

- ***Temperature Influence***
  The open circuit voltage of the cell changes with temperature according to the following equation:

$$V_{OC} = V_{OC,STC} + \frac{dV_{OC}}{dT} \cdot (T - 28) \tag{3.6}$$

Using max. temp. (of 67°C) because then the voltage will be the lowest:

$$V_{OC,1sun} = 2.616 - 0.0065 \cdot (67 - 28) = 2.3625V \tag{3.7}$$

Similarly, for V_{MPP}:

$$V_{MPP} = V_{MPP,STC} + \frac{dV_{MPP}}{dT} \cdot (T - 28) \tag{3.8}$$

$$V_{MPP,1sun} = 2.345 - 0.0068 \cdot (67 - 28) = 2.08V \tag{3.9}$$

Similarly for the current: using min. temp. (of 62°C) because then the current will be the lowest:

$$I_{MPP} = I_{MPP,STC} + \frac{dI_{MPP}}{dT} \cdot (T - 28) \tag{3.10}$$

$$I_{MPP,1sun} = 0.196 + 0.0002 \cdot (62 - 28) = 0.2029A \tag{3.11}$$

- ***Concentration / Light Intensity Influence***
  As discussed in Section 3.2 concentrating the light influences the voltage and the current. The current J_{SC} increases linearly with concentration, whereas the change in voltage was estimated based on the fill factor change with concentration (by extrapolating the Fig. 3.4 given for *3J GaAs* cells under concentration).
  - For the change in current:

    $$I_{SC,Xsuns} = I_{SC,1sun} \cdot X \cdot \rho \tag{3.12}$$

    Similarly:

    $$I_{MPP,Xsuns} = I_{MPP,1sun} \cdot X \cdot \rho \tag{3.13}$$

    The lowest short circuit and MPP current of experiencing 5 suns per cell (at 62°C):

    $$I_{SC,5suns,EOL} = 0.213 \cdot 5 \cdot 0.85 = 0.906A \tag{3.14}$$

    $$I_{MPP,5suns,EOL} = 0.2029 \cdot 5 \cdot 0.85 = \mathbf{0.8623\ A} \tag{3.15}$$

  - For the change in voltage:

    $$V_{MPP,5suns,EOL} = \frac{FF_{5suns} \cdot V_{OC,5suns,EOL} \cdot I_{SC,5suns,EOL}}{I_{MPP,5suns,EOL}} \tag{3.16}$$

    Where (ρ - concentrator coating reflectively, n - ideality factor, k - Boltzmann's constant, q - electron charge and T - temperature in Kelvins):

    $$V_{OC,5suns,EOL} = V_{OC,1sun,EOL} + \frac{nkT}{q} \cdot lnX \cdot \rho = 2.4V \tag{3.17}$$

$$FF_{5suns} = FF_{1sun} + 0.3485 \cdot lnX \tag{3.18}$$

The fill factor at 1 sun illumination was obtained using the constants from the solar cell data sheet:

$$FF_{1sun} = \frac{V_{MPP} \cdot I_{MPP}}{V_{OC} \cdot I_{SC}} = \frac{2.08 \cdot 0.2029}{2.3625 \cdot 0.2133} = 83.7\% \tag{3.19}$$

Hence:

$$FF_{5suns} = 84.3\% \tag{3.20}$$

Finally:

$$V_{MPP} = \frac{0.843 \cdot 2.4 \cdot 0.906}{0.862} = \mathbf{2.13\ V} \tag{3.21}$$

As could have been predicted from Fig. 3.4, at the CR of 5.0 the fill factor does not change much, but the change it still taken into account to prevent oversizing the solar panel by underestimating the cell performance.

Amount of Cells

Having calculated the lowest voltage and current produced by the cells when the solar panel is in 1200 km orbit with 90° right ascension (always in the sunlight, no eclipse period), the number of cells that need to be connected in series and parallel can be calculated as follows. In case of changing power requirements to a different voltage/current value, Fig. 3.6 and 3.7 depict the change in required number of cells in series/parallel for slight changes in required voltage/current values.

$$50V/V_{MPP,5suns,EOL} = CellsInSeries \tag{3.22}$$

$$50V/2.13V = \mathbf{24\ Cells\ in\ Series} \tag{3.23}$$

$$6A/I_{MPP,5suns,EOL} = StringsInParallel \tag{3.24}$$

$$6A/0.8623A = \mathbf{7\ Strings\ in\ Parallel} \tag{3.25}$$

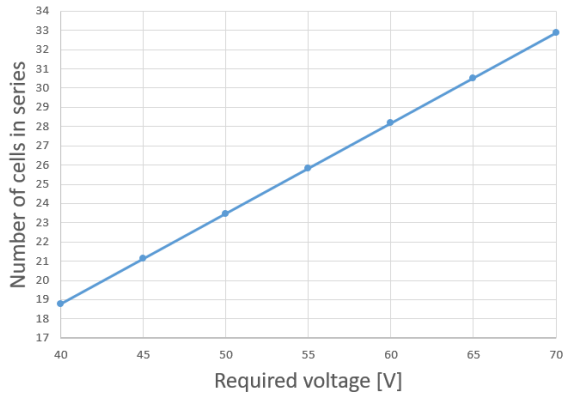

Figure 3.6: Required number of cells in series as a function of voltage.

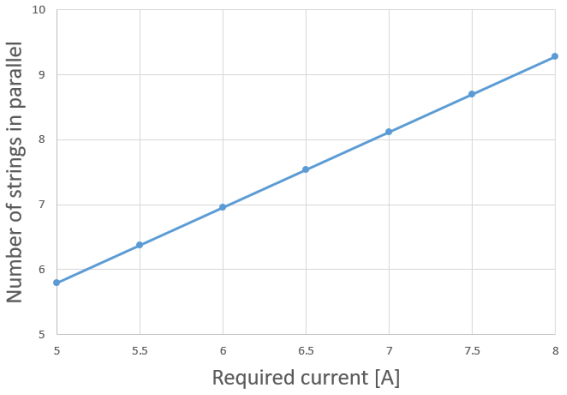

Figure 3.7: Required number of cells in parallel as a function of current.

3.3.2. Orbit With Eclipse

Temperature Variation

Panel temperature distribution for 0° right ascension orbit looks like in Fig. 3.8: with 1/3rd of orbit in eclipse (not producing power), then with the strongly climbing temperature upon exiting the eclipse, reaching the steady-state ($\Delta T \leq 10$°C) for ~1650 seconds (1/4th of the orbit) and again entering eclipse. Upon exiting the eclipse the panel begins to produce power while it's temperature is increasing from roughly -60°C to 80-90°C in 2250 seconds (1/3rd of the orbit). Temperature varying for a considerable amount of time affects the amount of power produced.

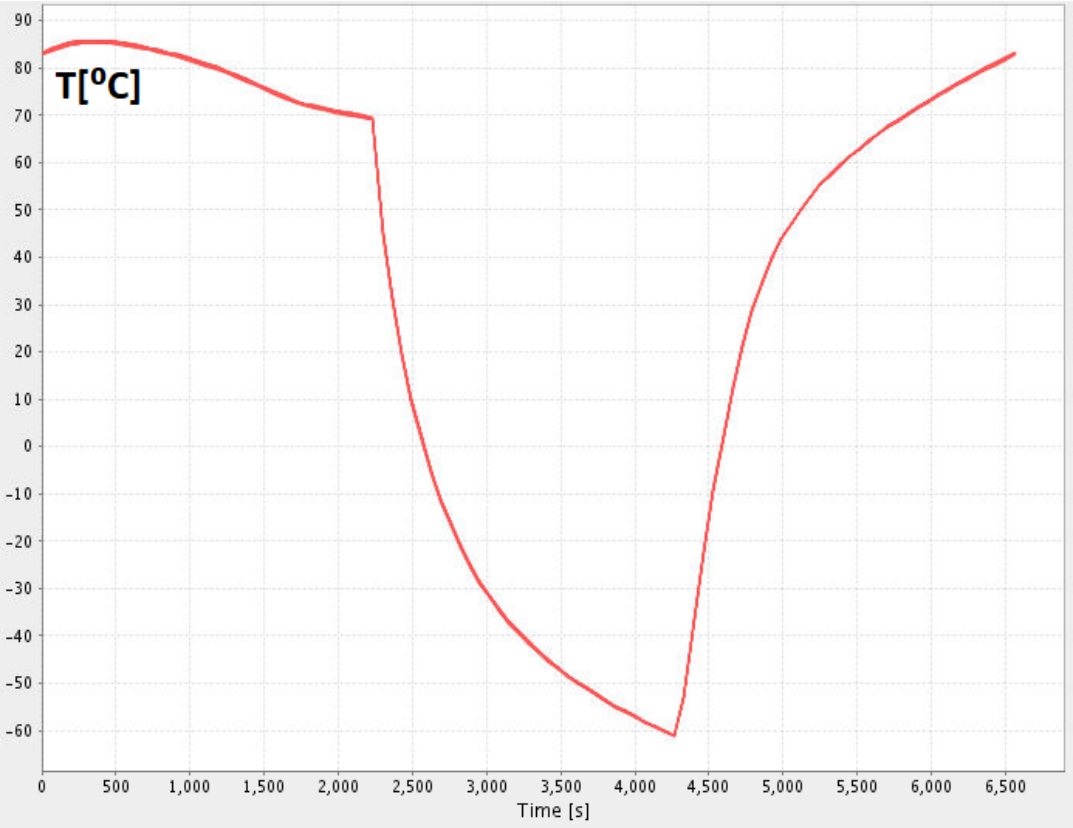

Figure 3.8: Temp. distribution for orbits with eclipse period (*Case 3C OPR*).

Cell Efficiency Change with Temperature

The solar cell efficiency change with temperature was an essential input to thermal modelling to get accurate temperature results. Moreover, these results allow analysis of the amount of power produced during the period of climbing temperature.

It can be seen from the Tab. 3.5 that high temperatures cause the cell voltage to drop, while at the same time slightly enhancing the current. The overall effect of high temperatures, however, is negative, since the cell efficiency decreases with increasing the temperature.

Table 3.5: Fixed solar cell parameters from data sheets and *SPENVIS* calculations.

Parameter	**Symbol**	**Value**	**Unit**
Coverglass thickness	t	100	μm
Total trapped particles	$-$	2.5E+15	cm^{-2}
Temp. gradients:			
Open circuit voltage	V_{OC}	-6.5	$mV/°C$
Short circuit current	I_{SC}	0.33	$mA/°C$
Voltage at max power	V_{MPP}	-6.8	$mV/°C$
Current at max power	I_{MPP}	0.20	$mA/°C$

Based on the parameters in Tab. 3.5 and App. A the efficiency change with temperature can be calculated as follows:

$$\eta = \frac{P_{MAX}}{P_{IN}} = \frac{V_{MPP} \cdot J_{MPP}}{1367W/m^2} \tag{3.26}$$

$$(\frac{d\eta}{dT})_{EOL} = \frac{V_{MPP,EOL} \cdot \frac{dJ_{MPP,EOL}}{dT}}{1367} + \frac{J_{MPP,EOL} \cdot \frac{dV_{MPP,EOL}}{dT}}{1367} = -0.0717[\%/dT] \tag{3.27}$$

$$(\frac{d\eta}{dT})_{BOL} = \frac{V_{MPP,BOL} \cdot \frac{dJ_{MPP,BOL}}{dT}}{1367} + \frac{J_{MPP,BOL} \cdot \frac{dV_{MPP,BOL}}{dT}}{1367} = -0.0679[\%/dT] \tag{3.28}$$

These values are further implemented in *ESATAN* code to approximately calculate the amount of energy that is converted to electricity (at any instant during the orbit), and hence decreases the cell temperature. For thermal analysis the amount of energy converted to electricity is QR (rest heat source), equivalent to the amount of heat that is being dissipated. Fig. 3.9 depicts the QR distribution in watts of the operational radiative *Case 3C OPR*. The values are negative to indicate the heat dissipation for thermal analysis. It can be seen that the amount of power produced by the nodes of the cell is maximum just upon exiting the eclipse (0.2 - 0.275 W per node), because then the panel temperature is coolest and the cells are functioning more efficiently. Within 1000 seconds, however, the amount of generated power reaches steady-state (0.15 - 0.2 W per node).

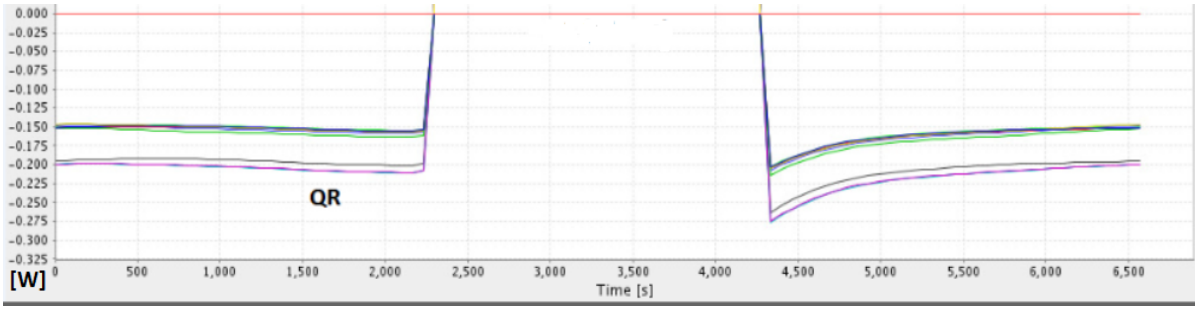

Figure 3.9: Dissipated rest heat (generated electrical power) by the cell nodes (9 lines) throughout the orbit (0° right ascension angle); *Case 3C OPR*.

Equations

At each location in orbit ($\eta = f(T)$):

$$P_{QR} = \eta \cdot I_{absorbed} \tag{3.29}$$

For the first 1/3rd of the orbit (from 0 till 2200 seconds)

$$P_{node,avg} = 0.175W \tag{3.30}$$

Hence:

$$P_{cell,avg} = 0.175 \cdot 9 = 1.575W \tag{3.31}$$
$$P_{panel,avg} = 1.575 \cdot 168 = \mathbf{264.6\ W} \tag{3.32}$$

While in eclipse the panel cools down to very low temperatures (−60°C). Since the solar cells operate more efficiently at low temperatures, electrical power generation peaks upon exiting the eclipse while the panel is at its coolest. At that point (4300 seconds in orbit in Fig. 3.9) the solar panel generates:

$$P_{cell,max} = 0.235 \cdot 9 = 2.115W \tag{3.33}$$
$$P_{panel,max} = 2.115 \cdot 168 = \mathbf{355.3\ W} \tag{3.34}$$

Throughout one orbit (taking into account the average values) the panel will produce the following amount of energy:

$$E = P_{panel_{avg}} \cdot (4400/3600) = \mathbf{323.4\ Wh} \tag{3.35}$$

3.3.3. Conclusions

– *Orbit w/o eclipse*:
The electrical calculation results indicate that it is necessary to have **7 strings** in parallel to satisfy the current requirement, and to satisfy the voltage requirement a minimum of **24 cells** in series are required. Hence in total 168 cells are required (which is less than estimated previously:180). This amounts to 14 cells per concentrator, which amounts to having a panel area of 1.11 x 1.224 m^2. These and other panel parameters are summarized in Tab. 3.6.

The cell layout can be seen in Fig. 3.10. The arrows point in the charge direction within each string. The same color cells are connected in series and form strings which are connected in parallel.

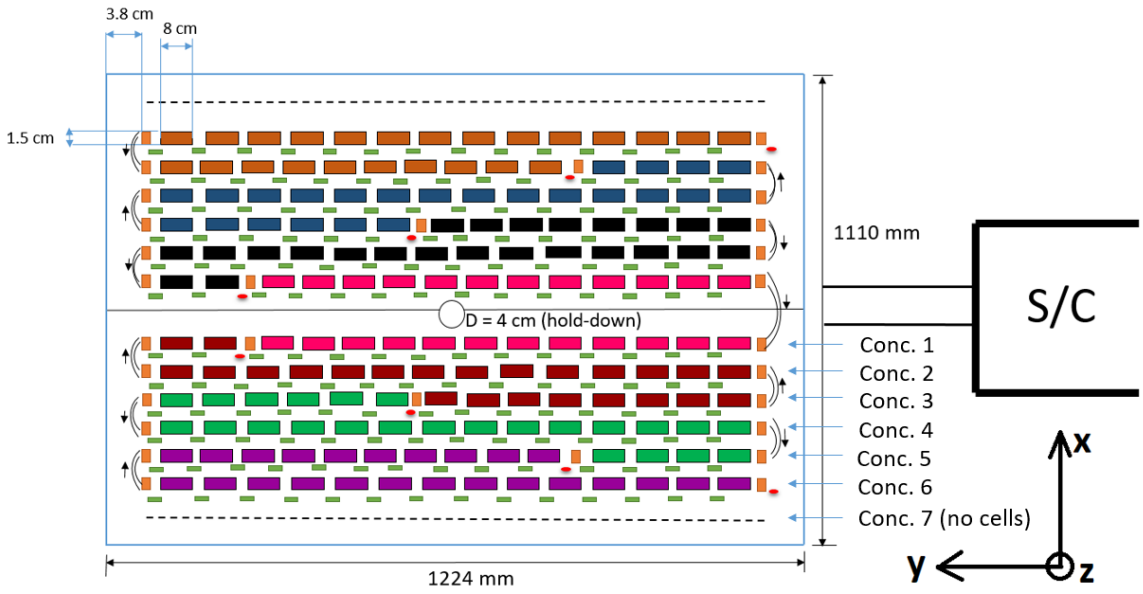

Figure 3.10: Panel cell layout and dimensions with 14 cells per concentrator.

Table 3.6: Parameters of the solar panel.

Summarized parameter/constant	Symbol	Value	Unit
Panel width	w_{panel}	1224	mm
Panel length	l_{panel}	1110	mm
Edge busbar width		4	mm
Number of busbars/conc.		3	–
Cells/conc.	$n_{cells/conc}$	14	–
Conc/panel		14	–
Cells/panel		168	–
Obtained total voltage, EOL	$V_{panel,EOL}$	51.2	V
Obtained total current, EOL	$I_{panel,EOL}$	6	A
Obtained total power, EOL	$P_{panel,EOL}$	$\pm$310	W
Obtained total voltage, BOL	$V_{panel,BOL}$	53	V
Obtained total current, BOL	$I_{panel,BOL}$	6.8	A
Obtained total power, BOL	$P_{panel,BOL}$	$\pm$360	W

– *Orbit w/ eclipse*:
Based on the power calculations made by estimating the efficiency change with temperature, the single solar cell on average will produce 1.575 W of power. However, in case of the orbit without eclipse each solar cell produces 1.84 W. The difference in numbers can be attributed to different assumptions used in both calculation methods. This method of approximating efficiency change with temperature does not take into account the increase in voltage and current due to illumination, but solely focuses on the efficiency behavior with temperature. Hence, the outcome of this method is not as reliable as the separate current and voltage calculations done for the orbital case without eclipse.

The amount of energy that the panel is able to generate throughout one orbit equals **323.4** Wh per panel. To compare, to the amount of energy generated in the eclipse-free orbit:

$$E_{eclipse-free} = 300 \cdot (6500/3600) = \textbf{541.7 Wh} \tag{3.36}$$

– *Losses*:
Some portion of generated power is lost due to wiring. Here it will be briefly estimated how much of the portion is lost given the wire specifications in Table 3.3. The power loss due to electrical resistance is calculated using the following equation:

$$P_{LOSS} = I^2 \cdot R \tag{3.37}$$

$$P_{LOSS,AWG20} = 6^2 \cdot 33.31 \cdot 0.002 = 2.4W \tag{3.38}$$

$$P_{LOSS,AWG26} = 1^2 \cdot 133.9 \cdot 0.0006 = 0.08W \tag{3.39}$$

The solar panel is required to deliver 300 W. Compared to this amount, the percentage of power that is lost in wiring amounts to 0.83%. Since this is a very small portion, the power loss in wiring is neglected in the electrical calculations.

3.3.4. Discussion

Fig. 3.10 depicts how it is possible to put 168 solar cells onto 1.11 x 1.224 m panel while connecting them in the most optimum way to ensure the necessary power production. However, from the electrical point of view this cell layout has certain drawbacks that need to be discussed further:

1. As will be seen later in the thermal results, the temperature of the cells remains more or less constant from cell to cell. Moreover the temperature variation between the concentrators 1 to 5 is insignificant, too. Hence, connecting the cells of different concentrators into one string would not be a problem electrically. However it was found that the temperature of the cells on concentrator 6 gets ~10°C lower which means that connecting the cells of concentrator 5 to cells of concentrator 6 would cause performance mismatch. Hence, ideally it would be optimum to have strings of cells separate on each concentrator for optimal electrical power generation.

2. Since the solar cells are not glued to the panel substrate but are positioned 10 cm above the wiring through which the current flows towards the S/C, there could be some magnetic moments generated if not counteracted by the directions of the current. This has to be taken into account more closely when wiring the panel.

3.4. Schematic Drawings

The panel electrical design can be seen in the following figures. The physical positioning of wiring harness on the rear side of the panel can be seen in Fig. 3.11 and 3.12. Figures in this section are screen-shots of the 3D panel model kindly made by Ir. Peter Datema at *Airbus*.

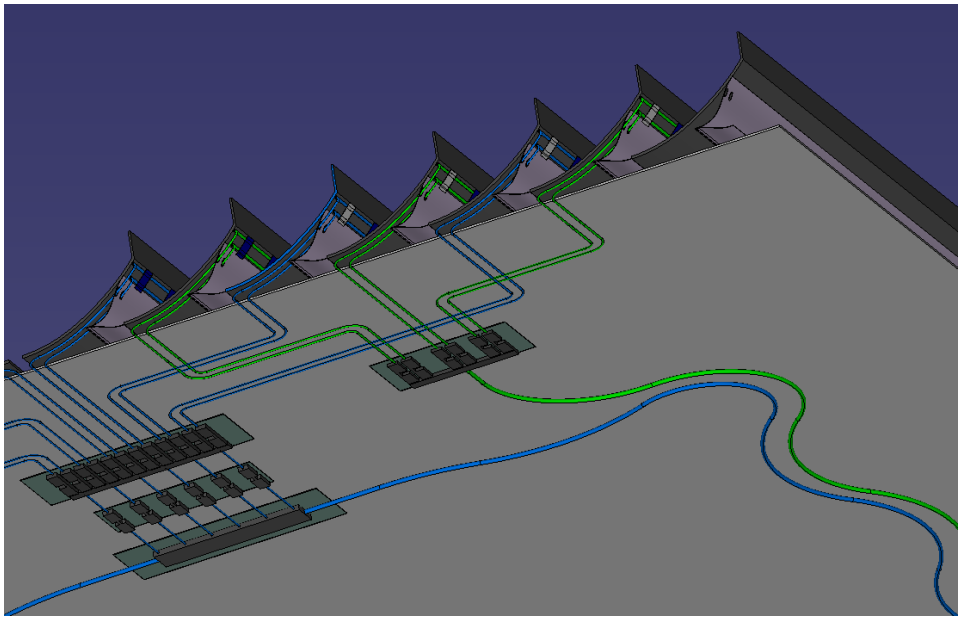

Figure 3.11: Side and rear view of the panel wiring.

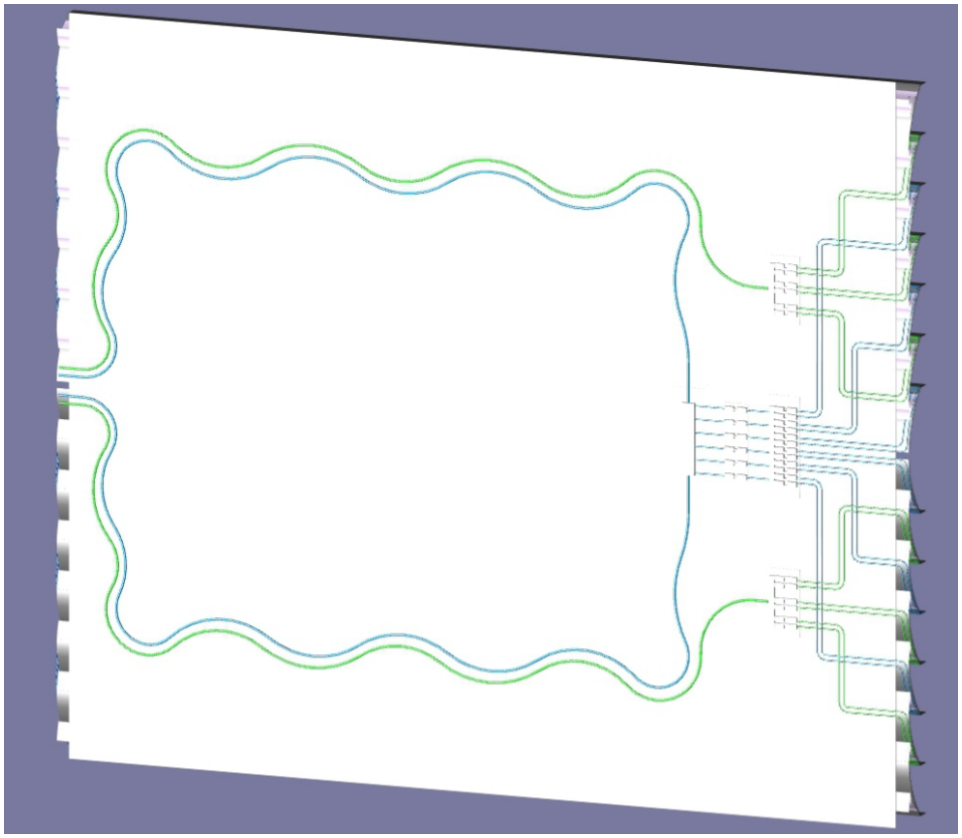

Figure 3.12: Rear view of the panel wiring.

4

ESATAN-TMS Modelling Principles

4.1. Heat Transfer in Space

Heat transfer in general occurs via three different processes, which are **conduction**, **convection** and **radiation** with only two these occurring in space. Conduction, being a process of heat transfer through direct contact, is responsible for cooling the solar panel by means of using high conductivity materials to transfer the heat to the rear of the panel, from where it is radiated into outer space by the process of radiation. These two heat transfer processes are taken into account by *ESATAN* software when calculating the occurring temperatures.

The build-up of the solar array thermal model is elaborated upon in Section 4.2. Once the geometry has been assigned a certain number of nodes, when executing the thermal analysis case *ESATAN* calculates the linear conductance (GL in $[W/K]$) between each two nodes that are connected (automatically or user defined) based on the material properties and the geometry using the following equation (k - material conductivity in $[W/mK]$, A - area of the interface between nodes, L - distance between the two nodes) [33], see Eq. 4.1:

$$GL = \frac{kA}{L} \tag{4.1}$$

In general the radiative heat exchange between the two surfaces can be calculated as follows (see Fig. 4.1 [34]) using the Stefan-Boltzmann's law (F_{12} is the view factor, see Eq. 4.3). The radiative conductance between any two nodes is calculated based on the geometric and radiative characteristics (such as IR emissivity and radiating surface area) taking into account the **view factors**.

$$q_{net} = A_1 F_{12} \sigma ({T_1}^4 - {T_2}^4) \tag{4.2}$$

$$F_{12} = \frac{Energy - from - A_1 - intercepted - by - A_2}{Total - energy - emitted - by - A_1} \tag{4.3}$$

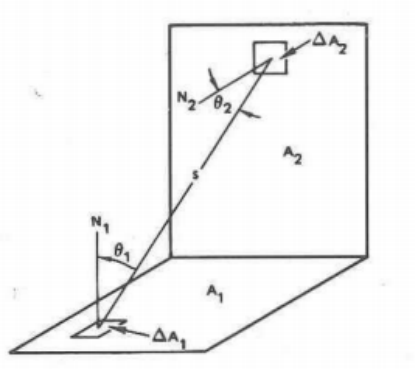

Figure 4.1: Heat exchange by radiation between two small black surface elements [34].

The heat balance equation [35] used to calculate the temperature change in time of an **isothermal** node in *ESATAN* is as follows [33]:

$$(mc_p)_i \frac{dT_i}{dt} = Q_i + (\alpha A^s q^s + \alpha A^a q^a + \epsilon A^e q^e)_i - \sum_j R_{ij}\sigma(T_i^4 - T_j^4) - \sum_j C_{ij}(T_i - T_j) \quad (4.4)$$

Where the represented parameters are:

- $(mc_p)_i$ is thermal mass (mass times the heat capacity)
- A_i is the area of the radiating surface
- T_i is the temperature of the radiating area
- Q_i is the internally dissipated heat
- $\alpha A^s q^s$ is the Sun radiation (absorptance times area times heat)
- $\alpha A^a q^a$ is Albedo radiation (solar radiation reflected by the Earth towards the spacecraft)
- $\epsilon A^e q^e$ is the Earth radiation
- $\sum_j R_{ij}\sigma(T_i^4 - T_j^4)$ are the radiation couplings
- $\sum_j C_{ij}(T_i - T_j)$ are the conductive couplings

View factor (F_{12} in the previous equations) is the proportion of the radiation that leaves one surface which strikes another surface. In case of the conventional planar solar array in space, for instance, the view factor of space radiation towards the solar cells is much higher than the view factor with which the radiation in space sees the cells when in *ConCur* concept, since a lot of radiation is blocked by the concentrator. For a little more detailed explanation of the heat transfer processes and equations, see the Literature Study Report [2].

4.2. Modelling Principles

ESATAN-TMS is an integrated thermal modelling environment that supports complete thermal analysis process from geometry creation, radiative and thermal analysis to the post-processing of results. The entire process includes the following steps:

1. Modelling of the geometry and setting material properties: creation of *GMM* (geometric mathematical model) and materials library,
2. Execution of the radiative analysis case: calculates view factors, radiative exchange factors, heat fluxes and directed UV emission (albedo and solar flux values are set in the radiative case definition),
3. Definition of boundary conditions (if any),
4. Generation of *TMM* (thermal mathematical model) by choosing the previously defined radiative analysis case and (if necessary) specifying the environment temperature. Including generation of linear conduction pathways between the nodes (GLs),

5. Application of different solution control mechanisms to execute the thermal analysis case (steady-state or transient analysis),
6. Post-processing of the results using *ThermNV* software and *Notepad++* coding environment.

After executing the thermal analysis cases there are several output files, some of which include useful information on the procedure and steps *ESATAN* uses, and others including the results.

4.2.1. Benchmarks

To get acquainted with *ESATAN* software and get familiar with the heat transfer in space more closely, several different geometries/structures were modelled and thermally tested. The detailed analysis of these benchmark models was drawn in the Midterm Report [15], hence here the concepts are only briefly shown, and lessons learned in modelling and thermal analysis can be found in App. E. The following models have been built:

1. Geometry with a surface as a UV source, see Fig. 4.2 and 4.3,
2. Geometry with a Heat Load and BCs, see Fig. 4.4 and 4.5,
3. Flat mirror concentrators in orbit environment, see Fig. 4.6 and 4.7,
4. Honeycomb solar panel, see Fig. 4.8 and 4.9.

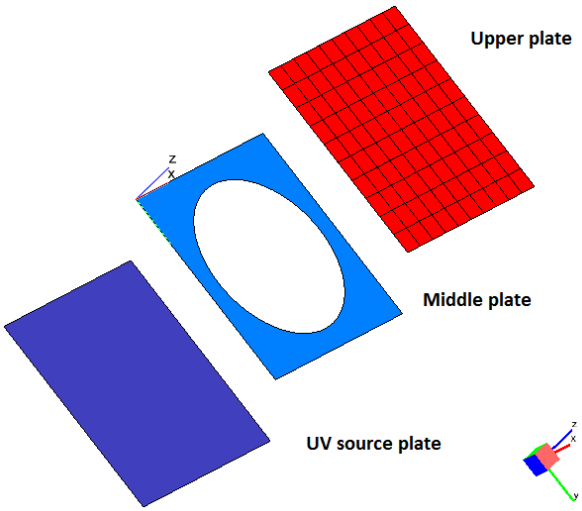

Figure 4.2: Model of three plates.

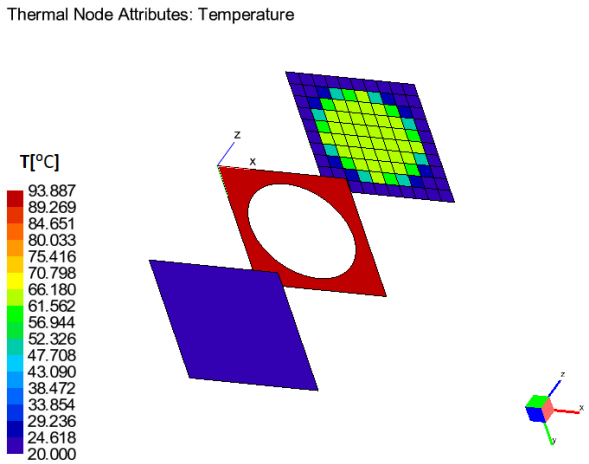

Figure 4.3: Temperature distribution due to active UV source.

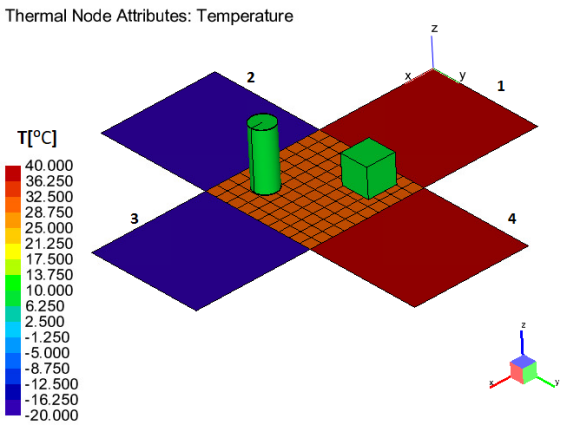

Figure 4.4: Model with a heat load and pre-defined BCs.

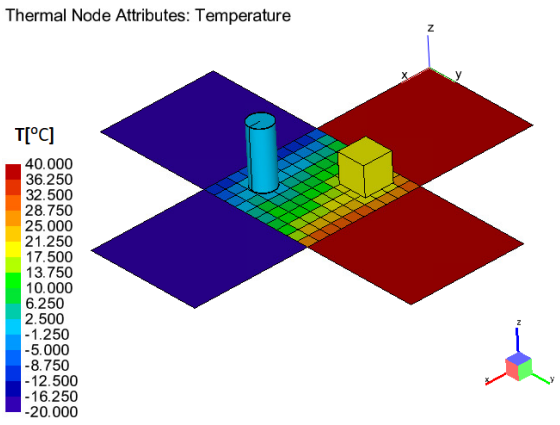

Figure 4.5: Steady state solution of the model.

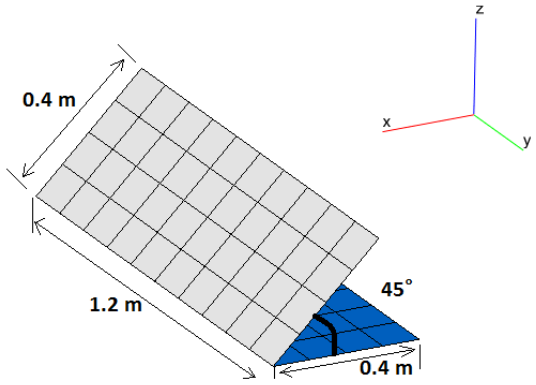

Figure 4.6: Flat mirror concentrator model.

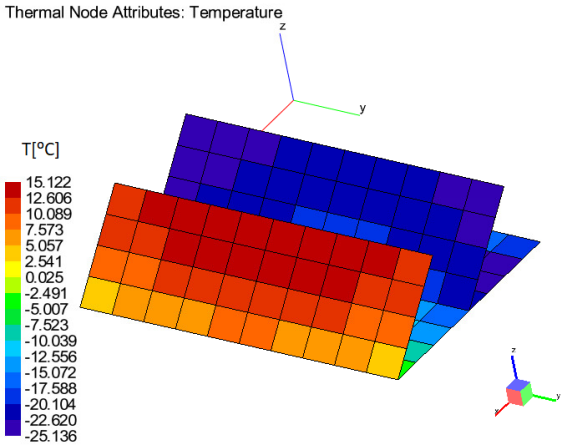

Figure 4.7: Temperature distribution of the model in orbit (transient analysis).

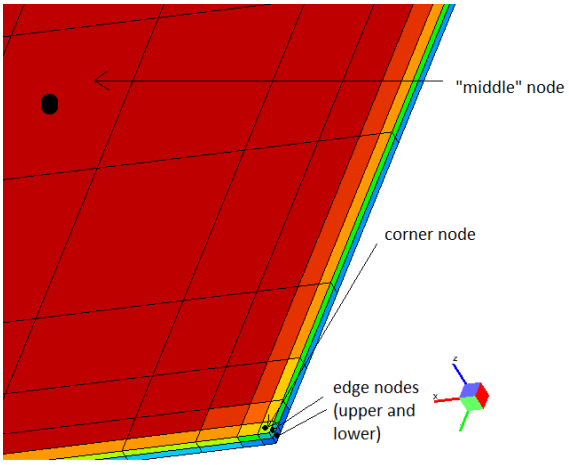

Figure 4.8: Honeycomb solar panel model.

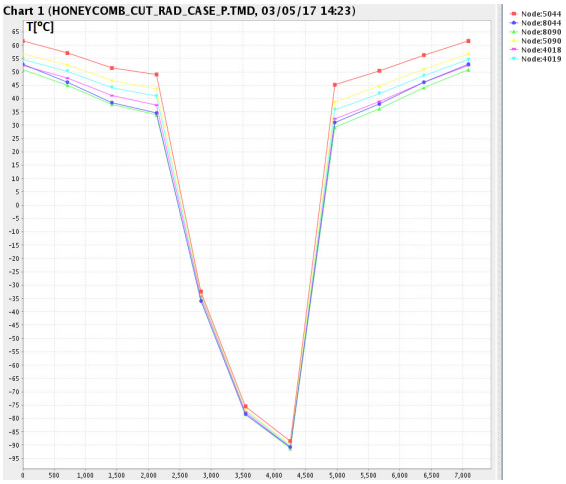

Figure 4.9: Temperature variation of the panel throughout the orbital position.

4.2.2. Step by Step Guide followed for *ConCur* Detailed Thermal Model

1. Set bulk and optical material properties. Create a library file to ease changing concentrator optical coatings later on during sensitivity analysis.
2. Create the desired geometry and assign its materials, nodal mesh, node numbers, dimensions and color.
3. If the model consists of more than one shell select the option *"Autogenerate conductive interfaces"* between the shells.
4. Assemble the solar panel by combining the separately made submodels.
5. Create the contact zones between the different submodels.
6. Create and execute the "Test" radiative case and run "Test" thermal model analysis specifying to use automatically generated conductive links (GLs).
7. Divide one complete conductance file for the entire assembly model into separate conductance files for each submodel.
8. Check manually the separate conductance files and change if necessary, and add conductive links if any are missing. Special attention should be given to the conductance calculations through the contact zones.

9. The contact zones created in the submodels are not automatically added to the main assembly (e.g. contact zones between the cell and concentrator in the concentrator submodel are not present in the panel assembly), so it is necessary to add those manually to the template file.
10. Create a constants file for each conductance file with according material conductivity values.
11. Add checked/corrected conductance files, the constants files and solar cell heat dissipation files to the main model **template file** using command **INCLUDE**.
12. Run thermal analysis with the new template and conduction files to check whether *ESATAN* reads it correctly.
13. Export each submodel as a geometry file (this way in case of any geometric changes to the submodels it is possible to just update its geometry file and reload the main assembly file in *ESATAN*, as opposed to having to assemble the main file again from scratch, because by changing submodels the main assembly model does not change).
14. Execute the necessary radiative case.
15. Run thermal analysis (steady state or transient) of that case.
16. Post process the results in *ThermNV* software.

4.3. Model Verification Check

After the model is built it is important to verify whether it indeed works as it is supposed to. The model is checked by means of analyzing the results in *ThermNV* software where the following can be visually displayed:

- Conductive links between the nodes and the models,
- Value of linear conductance between any two nodes that are thermally connected,
- Radiative links between the nodes and the models,
- Value of radiative links between the two nodes.

The calculations were also verified by manually calculating the conductive links between the models for some nodes.

5

Thermal Design

This chapter elaborates upon optimizing and analyzing the detailed solar panel thermal design. In Section 5.1 it is explained how the model was built up in *ESATAN*, including the used materials. Next, Section 5.2 presents some design iterations resulting in choosing the optimal solution. Section 5.3 described the radiative cases that are used for testing the model in orbit. Hence, the results are discussed in Section 5.4, followed by some additional remarks and assumptions in Section 5.5.

5.1. Model Assembly - Baseline Model

The concentrator solar array was modelled in *ESATAN* by modelling the cells (with by-pass diodes), parabolically-shaped concentrators, the substrate panel and the support mechanisms (U-beam and two side beams) separately at first and integrating them all together in one assembly.

5.1.1. Solar Cell

The solar cell assembly includes the cell, coverglass and the bypass diode. The cell is modelled as a **rectangular shell** with length and width dimensions of 80 x 15 mm, as these have been previously found to be the optimal cell dimensions. The dimensions of the by-pass diodes are 7 x 1 mm, as discussed with Remco v.d. Heijden at *Airbus* (electrical engineer). For the purpose of being able to see the temperature and illumination (solar flux) gradients within each cell, it was chosen to split each cell into 18 nodes (9 on each side/surface), see Fig. 5.1.

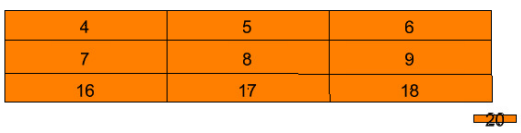

Figure 5.1: Model of a solar cell and diode, with node numbers.

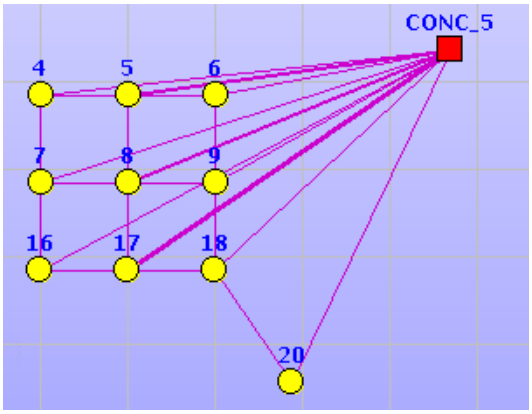

Figure 5.2: Conduction pathways generated between the nodes within the cell and between the cell and diode. It can be seen that the cell nodes are conductively connected to the concentrator.

The cell material properties that were used can be found in Table F.1. The cell in-plane and through (out-of-plane) conductions were calculated using an *MS Excel* file by *Airbus* and the equations used can be found in Appendix C. The conduction pathways within the solar cell assembly can be seen in Fig. 5.2.

The cell was thermally coupled to the concentrator by creating a *contact zone* between the concentrator back surface and cell back surface. The contact conductance was initially set at 1600 W/m^2K which amounts to the adhesive (RTV 691) conductivity divided by adhesive layer (250 μm).

Implementing solar cells in thermal analysis

Several radiative cases involve having the solar panel being in operational mode, meaning that the cells will be turned on and will be converting a significant amount of incoming solar flux into electrical energy. For thermal analysis in *ESATAN* the solar cells are approximated as being the rest heat source to account for the drop in temperature due to energy conversion. Turning ON the cells thermally is made equivalent to having a negative *Rest Heat Source QR* at each cell node, and the value for that (in watts) is calculated as in the following equation:

$$QR(node) = -1.0 \cdot PD \cdot \frac{QS(node) + QA(node)}{\alpha_{SOLAR}} \cdot (\eta + \frac{d\eta}{dT} \cdot (T(node) - 28.0)) \tag{5.1}$$

Where PD is cell packing density (assumed to be 1.0), QS and QA are the solar and albedo heat sources (in watts), respectively. α_{SOLAR} is the cell solar absorptivity (equals 0.91), η is cell efficiency at STC (28°C, AM0 and 1367 W/m^2) and $\frac{d\eta}{dT}$ is the change in cell efficiency with temperature (calculated to be -0.0717%/$^\circ C$), see Section 3.3.

5.1.2. Concentrator

The concentrators are parabolically shaped to reflect all incoming light onto a common focal point. However, modelling such as geometry is difficult in *ESATAN*, therefore, the concentrator geometry was modelled using multiple shells, each approx. 0.5 cm wide and 1.3 m long, each being fused to the other. The model appears to approximate the curvature in enough detail to concentrate the reflected light onto a solar cell, see Fig. 5.3 and 5.4.

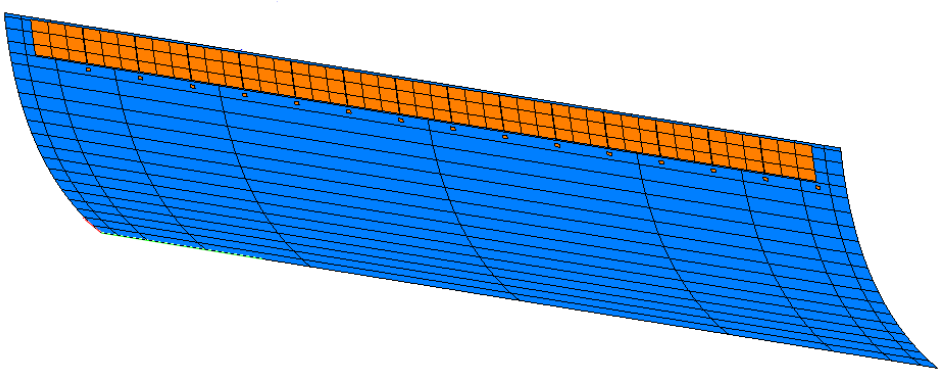

Figure 5.3: Model of a concentrator and solar cell assembly.

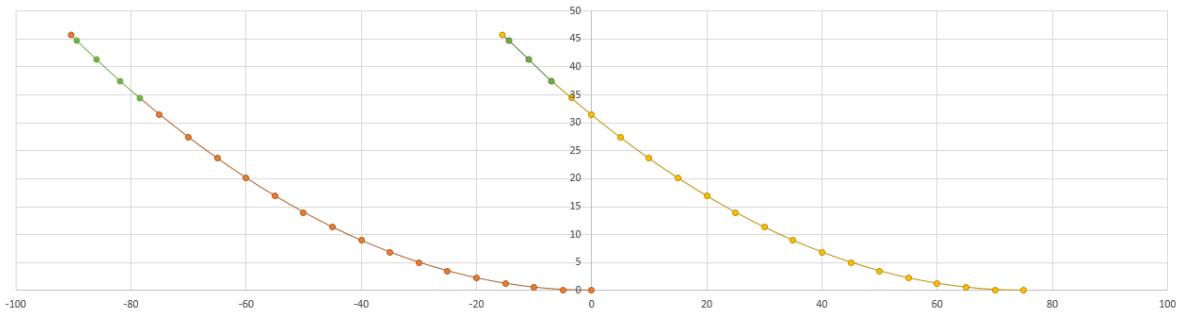

Figure 5.4: Concentator curvature.

To conductively connect the concentrator to the substrate panel, the contact zones are created the same way as they are created between the cell and concentrator. Any other model parameters including material properties can be found in Appendix C.

5.1.3. Substrate

The panel substrate was modelled as a single CFRP shell of dimensions 1.3 x 1.11 m with 1.5 mm thickness. Originally the panel length and width dimensions were set at 1.2 and 1.0 m, however after performing some iterations the panel was increased to accommodate more concentrators for enhanced electrical performance of the array. In Fig. 5.5 also the chosen nodal mesh can be seen. This type of mesh was chosen to be able to spot the edge effects better (same mesh was used for the honeycomb panel benchmark in the Midterm report, see App. D).

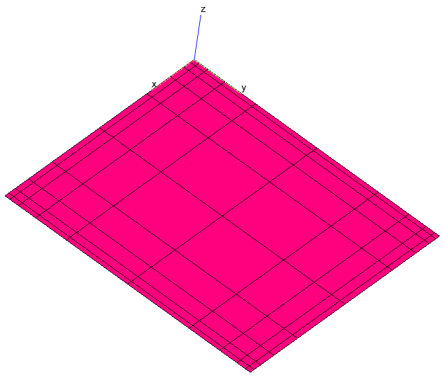

Figure 5.5: Model of the substrate panel - top view.

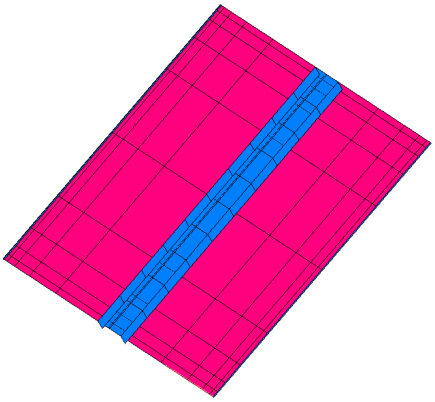

Figure 5.6: Model of the substrate panel - rear view.

CFRP Beams

To ensure structural stability of the panel and also being an important part of the array deployment mechanism, a CFRP **U-beam** is attached to the rear side of the panel. Similarly, two **side beams** are attached to the rear side for panel protection during stowage, and adding more stiffness to it to cope with the vibrational loads during launch. The models of beams can be seen in Fig. 5.6. The geometrical features of the panel are listed in the following table.

Table 5.1: Dimensions of the CFRP beams.

Geometry	Length (y-dir.)	Width (x-dir.)	Thickness	Material
U-beam	1.3 m	0.12 m	0.5 mm	CFRP
Side beams	1.3 m	5 mm	2 mm	CFRP

The final model has to satisfy the temperature constraints of separate assembly components as listed in the Tab. F.1.

5.2. Thermal Concept Analysis - Design Iterations

The solar array assembly as described in Section 5.1 (baseline model) has been tested by putting it in LEO at 1200 km altitude and setting the conditions equivalent to the most extreme hot case (*Case 1A Hot*). As a result due to the concentration of the light onto the solar cells, the highest temperature is found there reaching 243°C (see Fig. 5.7). The big difference between the concentrator temperatures at the cell location (rear side) and at the top side means that the out-of-plane heat conduction through the concentrator is not enough to transport enough heat from the cells to the back of the panel. The main two reasons for such elevated cell temperatures are (1) sunlight concentration and (2) significant lack of heat transport by radiation. Based on the operational temperature limit of the panel materials (see Tab. F.1 in App. F), at this temperature the panel will not be able to operate, therefore the sensitivity analysis is needed to optimize the model. The highest acceptable temperature that the model would be able to sustain in orbit is approx. 150°C (maximum cell operating temp. and maximum temp. that epoxy resin can sustain). However, to keep some margin, it is desirable to not exceed **120°C in the hottest possible case**. To lower the temperature of the cells of the baseline model certain design modifications have to be made. Hence, the solutions that are investigated are:

- 5.2.1. Changing concentrator in-plane conductance
- 5.2.2. Changing optical reflective coatings
- 5.2.3. Adding a PG thermal doubler
- 5.2.4. Changing contact conductance in *ESATAN*
- 5.2.5. Combined effects
- 5.2.6. Adding vertical radiator
- 5.2.7. Using aluminum concentrators and substrate panel instead of CFRP.

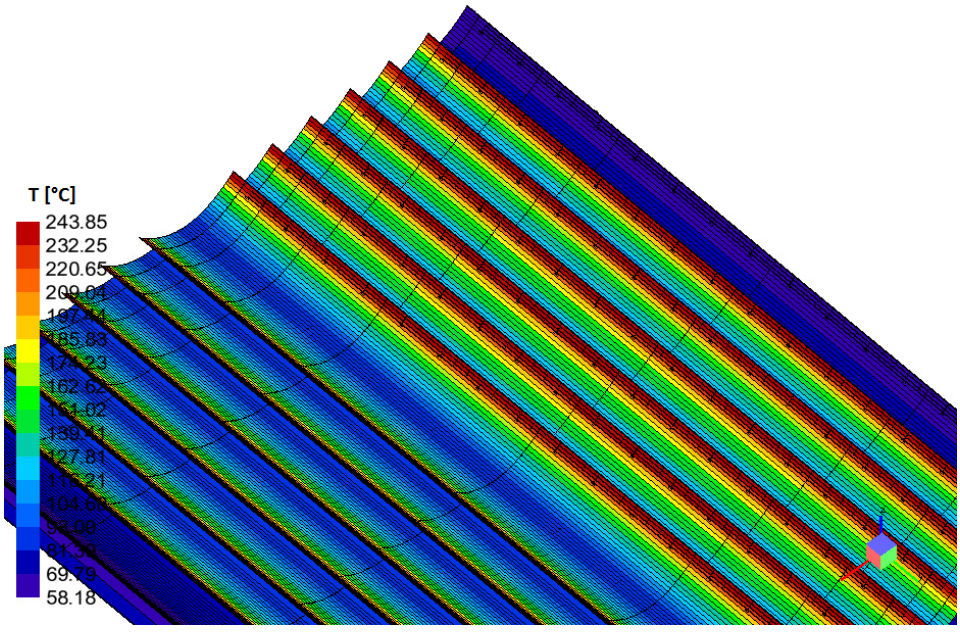

Figure 5.7: Temperature distribution over the solar panel at the hottest location in orbit - **BASELINE MODEL**.

5.2.1. Changing concentrator in-plane conductance

The cell temperature can be decreased by enhancing the heat transport in the concentrator structure. This can be done by increasing its thickness, hence the concentrator conduction is changed by varying the thickness in this case. The thickness variation can be found in Table 5.2. Increasing the concentrator thickness twice thermally equals to doubling the in-plane conduction. It should be noted that the out-of-plane conduction will also change when changing the concentrator thickness, but the change is expected to be insignificant due to relatively low concentrator thickness.

Fig. 5.8 shows the change in cell temperature with respect to the the change in concentrator conductivity. It can be concluded that an increase in thickness/conductivity of the concentrator results in better heat transport and, hence, lower cell temperature values. The effect seems to be leveling out at around 140°C, meaning that a huge increase in conductivity at that point will not contribute to a substantial temperature drop.

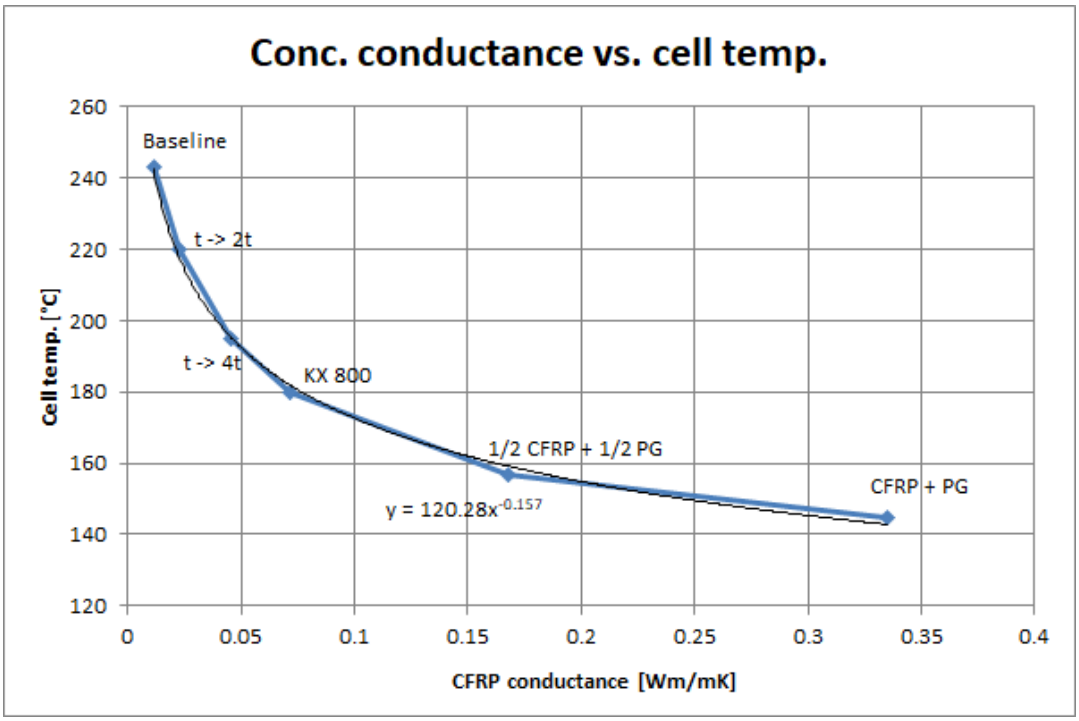

Figure 5.8: Solar cell temperature as a function of conductance.

Table 5.2: Parameters used for sensitivity analysis: varying concentrator conductivity/thickness.

Case	**Conc. t [mm]**	**In-plane conduction [Wm/mK]**	**Remark**	**Max cell temp. [°C]**
Baseline	0.24	0.0114	CFRP M55J	243
t -> 2t	0.48	0.0228	CFRP M55J	220
t -> 4t	0.96	0.0456	CFRP M55J	195
KX 800	0.24	0.0720	Using KX 800 material (higher cond. CFRP) with baseline thickness	180
1/2 CFRP + 1/2 PG	0.24	0.1677	0.12 mm of CFRP M55J and 0.12 mm of PG material (3 layers)	157
CFRP + PG	0.48	0.3354	0.24 mm of CFRP M55J and 0.24 mm of PG material (6 layers)	145

5.2.2. Changing optical reflective coatings

Another way to cool the cell could be by changing the concentrator reflective coating material. The coatings with higher emissivity values theoretically would have a beneficial effect on lowering cell temperature. Table 5.3 lists four different coating materials that are all highly reflective, and all have different α/ϵ values.

Table 5.3: Parameters used for sensitivity analysis: varying reflective coatings [36].

Case	**Coating**	α	ϵ	α/ϵ	**Cell temp. [°C]**
Baseline	Al	0.15 (EOL)	0.05	3.0 (EOL)	243
	FEP	0.09	0.4	0.225	211
	OSR	0.084	0.665	0.126	191
	Gold	0.19	0.025	7.6	237

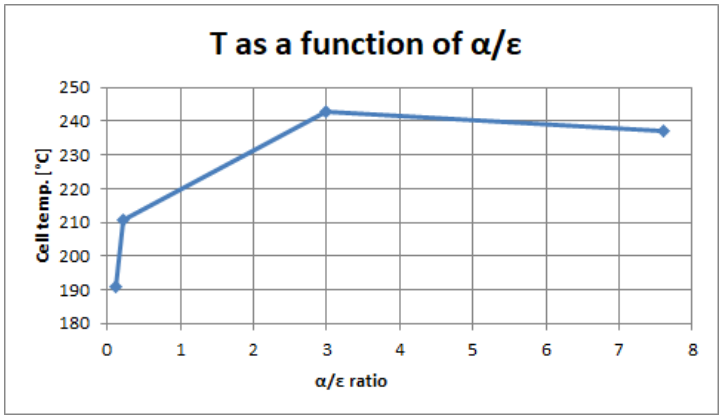

Figure 5.9: Solar cell temperature as a function of α/ϵ of the coating material.

Fig. 5.9 shows that lower α/ϵ values result in lowest cell temperatures. It was expected since higher emissivity means the heat is expelled more effectively to the environment. However, gold having the highest ratio still seems to cause slightly lower cell temperatures than aluminum coating. This indicates that the values of α/ϵ ratio alone can not accurately be related to the change in temperature. Coating reflectivity has high importance in this solar array model, hence it could be that there is no simple relationship between the cell temperature and α/ϵ ratio in this

case due to other optical properties, such as reflectivity. Also, only changing the concentrator reflective material does not seem to solve the problem of having too high temperature, hence further iterations at this point are required.

5.2.3. Adding a PG thermal doubler

Another solution to lower the temperature locally at the cell location is by using a thermal doubler that is made of a highly conductive PG material (pyrolytic graphite) and encapsulated by kapton from both sides for protection. A single layer of PG can be seen in Fig. 5.10, and it's conductivity as a function of temperature can be found in Fig. 5.14. There are two ways that were investigated in implementing such a doubler, see Fig. 5.12 and 5.13. In Fig. 5.12 it is physically attached to the concentrator right underneath the cell, and on the other end attached to the panel. For this configuration cases A to D (see Tab. 5.4) are executed to see whether the temperature of the cells would decrease. The second configuration (Fig. 5.13) is to attach the doubler between the concentrator and the solar cell, instead of underneath it (cases E to G). For both configurations the amount of PG layers is varied. For both cases the width and length of the thermal doubler were assumed to be 7 cm and 1.3 m. Figure 5.11 depicts the heat pathways by conduction and radiation. It can be seen that radiation is limited due to small view factor towards space (the cell is facing a concentrator), hence the high conductivity PG thermal doubler would significantly enhance the cooling of the cell.

Figure 5.10: Single layer of pyrolytic graphite.

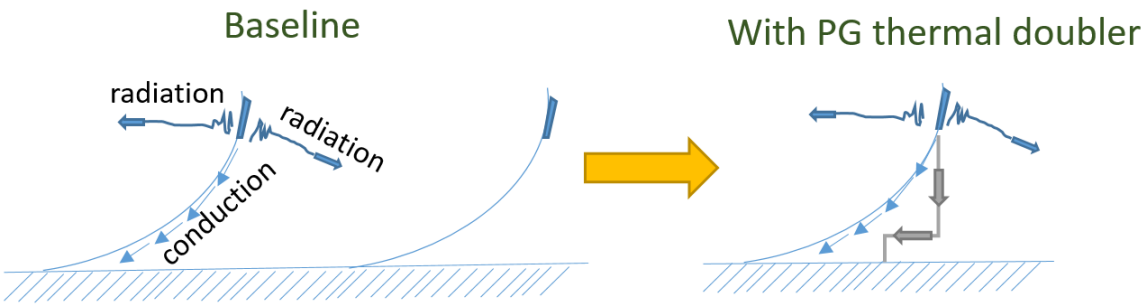

Figure 5.11: Thermal pathways through which the heat of the solar cell can dissipate (conduction and radiation); enhanced heat transport by extra conduction using a PG thermal doubler (right image).

The thermal doubler conductance was implemented in the *ESATAN* model using the following equation (with w_{PG} being the width of the concentrator node, PG conductivity k_{PG}, layer thickness t_{PG} and length of the thermal doubler l_{PG}).

$$GL(panel, concentrator) = \frac{w_{PG} \cdot k_{PG} \cdot t_{PG}}{l_{PG}} \tag{5.2}$$

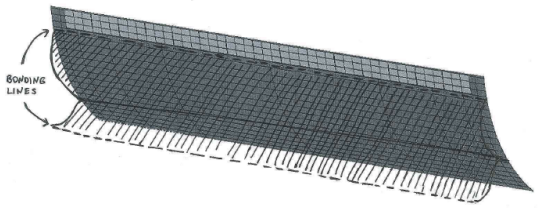

Figure 5.12: Case 1: Thermal doubler addition to the concentrator (bonded underneath the cell).

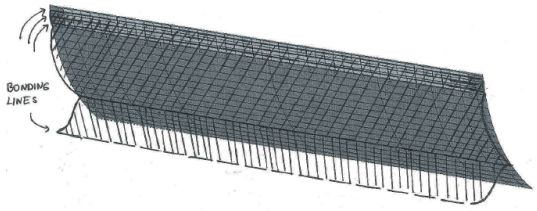

Figure 5.13: Case 2: Thermal doubler addition to the concentrator (bonded between the cell and concentrator).

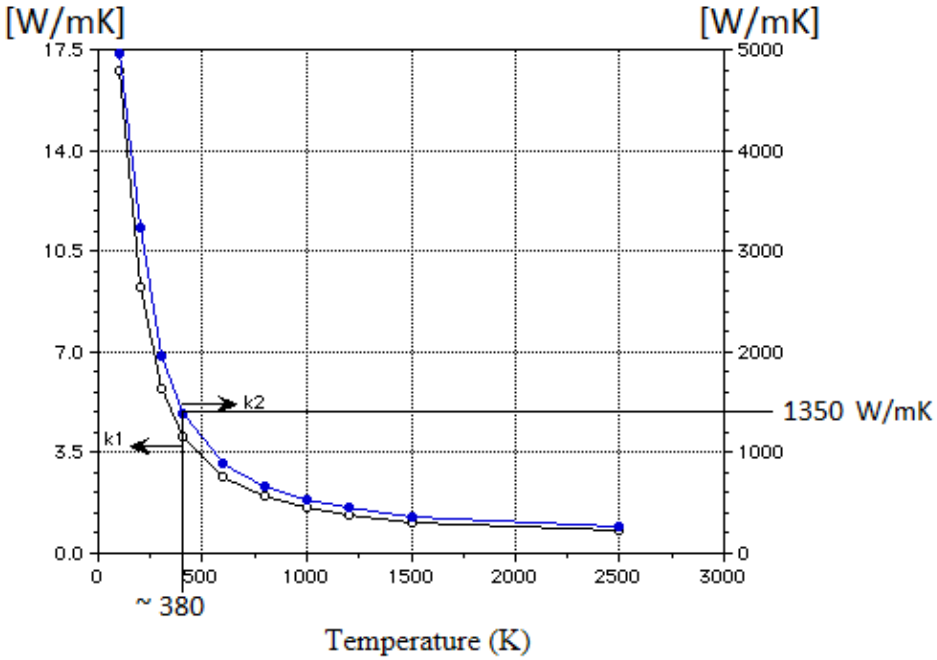

Figure 5.14: PG conductivity as a function of temperature (left scale for trough conductance, and right scale for in-plane conductivity) [37].

Table 5.4: Parameters used for design iterations: varying number of PG layers in the thermal doubler.

Case	**Number of PG layers**	**Thickness** $[mm]$	**In-plane conductance** $[Wm/mK]$	**Cell temp.** $[^{\circ}C]$
Baseline	0	–	0.0114	244
Case 1: A	1	0.04	0.054	200
Case 1: B	3	0.12	0.162	187
Case 1: C	10	0.40	0.54	180
Case 1: D	30	1.20	1.62	177
Case 2: E	1	$0.24_{CFRP} + 0.04_{PG}$	0.0654	174
Case 2: F	3	$0.24_{CFRP} + 0.12_{PG}$	0.1734	149
Case 2: G	10	$0.24_{CFRP} + 0.40_{PG}$	0.5514	135

As can be seen from Fig. 5.15 the addition of a conductive flexlink decreases the cell temperature significantly. Adding more than one layer of PG continues to enhance cooling of the cell, although the temperature does not change by much as the layers are being kept added after having 10 layers. It can be seen that in case 2 when the flexlink is attached to the cell directly, the cell temperature decreases more than in case 1. This makes sense since the flexlink is directly bonded to the back side of the cell, and is able to get rid of the heat more efficiently. The case 2 with 30 layers was left out, since the temperature curve is expected to have the same behavior as in case 1.

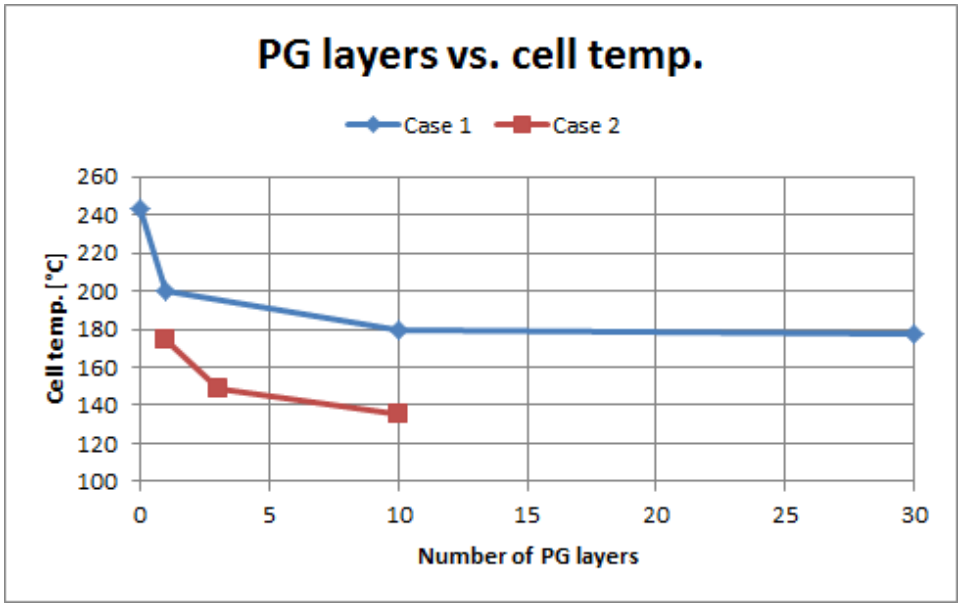

Figure 5.15: Solar cell temperature versus number of PG layers.

5.2.4. Changing contact conductance

In the model geometry certain adhesive thickness had to be assumed to calculate the contact conductance between the panel and concentrator, and between the concentrator and the cell. It was initially assumed to be 250 μm thick, which resulted in 1600 W/m^2K contact conductance (*RTV 691* adhesive). Later on it was found out that this layer can be much thinner, hence the hottest radiative case was run with 100 μm adhesive (4000 W/m^2K). Despite the contact conductance increasing more than twice due to this change, the cell temperature only decreased by 1-2 degrees. This can be explained by the fact that contact conductance is very high in general when compared to other conduction terms (such as through conduction in in-plane concentrator conduction). Hence, relative to the other conductive terms around the contact nodes, the contact conductance has little effect on the temperature.

5.2.5. Combined effects

Having seen an improvement in heat transport at the cell separately due to the flexlink (attached at the cell) and changing the CFRP material from *M55J* to *KX 800*, now some changes are combined and the resulting cell temperatures are listed in Tab. 5.5.

Table 5.5: Combinations of changes implemented.

Case	**Coating**	**Temp. [°C]**
PG doubler (case 2) + KX 800	Al	130
PG doubler (case 2) + KX 800	OSR	104.5

5.2.6. Adding vertical radiator

Another option that is investigated is adding a vertical radiator (made of PG material) above the concentrator in combination with having the PG thermal doubler (case 2), as shown in Fig. 5.16.

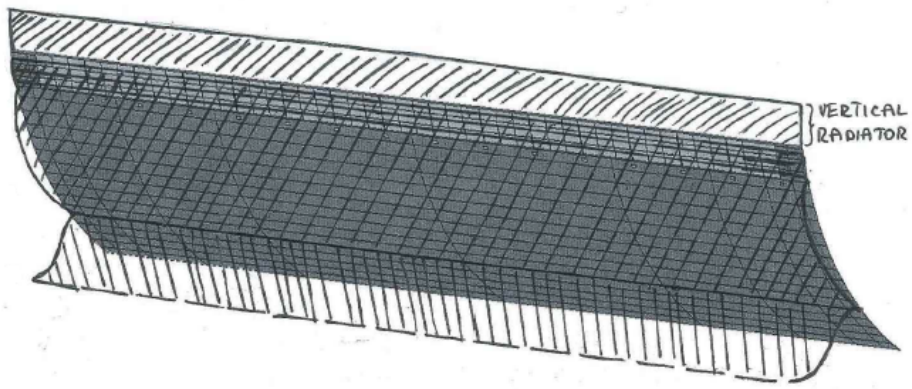

Figure 5.16: Sketch of the vertical radiator attached to the concentrator.

The width, height and thickness of the vertical radiator are 1.3 m (concentrator length), 2 cm and 0.4 mm (10 layers of PG), respectively. In fact, the configuration shown in Fig. 5.16 could use a single long thermal doubler.

The resulting highest cell temperature for the hottest case scenario for this configuration is 122°C, which is considered to be a safe zone for the optimized solution. Note that the concentrator material remains CFRP *M55J*. In case the CFRP with higher conductivity values is used (*KX800*) the cell temperature drops to 115°C. Despite it being lower with the latter CFRP material, it is decided to stick with the *M55J* due to it's advantage of having much better flexibility than *KX800*, which is important since the structure will be bent parabolically.

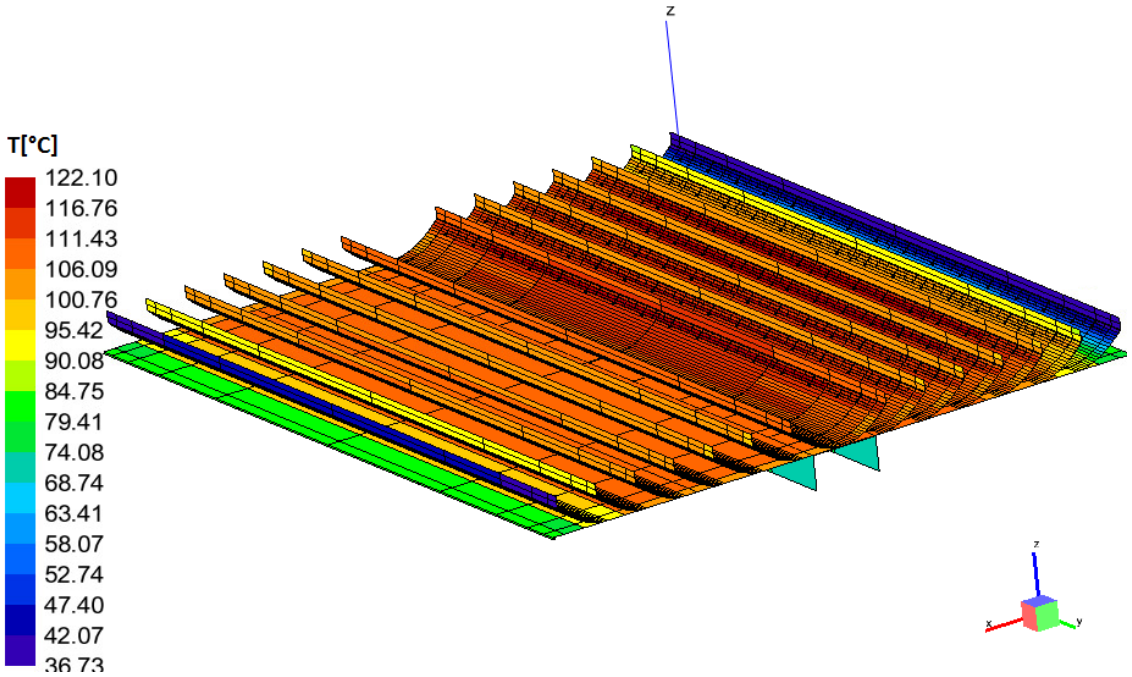

Figure 5.17: Temp. distribution (hottest location in orbit) over the panel with vertical radiator made from PG material - **OPTIMIZED SOLUTION**.

5.2.7. Using Aluminum instead of CFRP

CFRP was chosen as the main panel substrate, concentrator and support beams material due being a strong, flexible and very lightweight material. However due to its low conductivity thermal requirements are not met without the help of additional high-conductive materials (PG) which introduces complexity to the design. To keep it simpler in this case CFRP panel and concentrators are substituted by aluminum material keeping the thickness and geometry the same. Fig. 5.18 depicts the temperature distribution for this case, and it can be seen that the maximum cell temperature reaches 135°C, which is a very good improvement as compared to the baseline case. One of the drawbacks is increased weight, however it has been calculated to still weigh less than 6 kg [14]. Some other things to consider would be its elasticity (as the panel needs to be able to bend in stowed configuration).

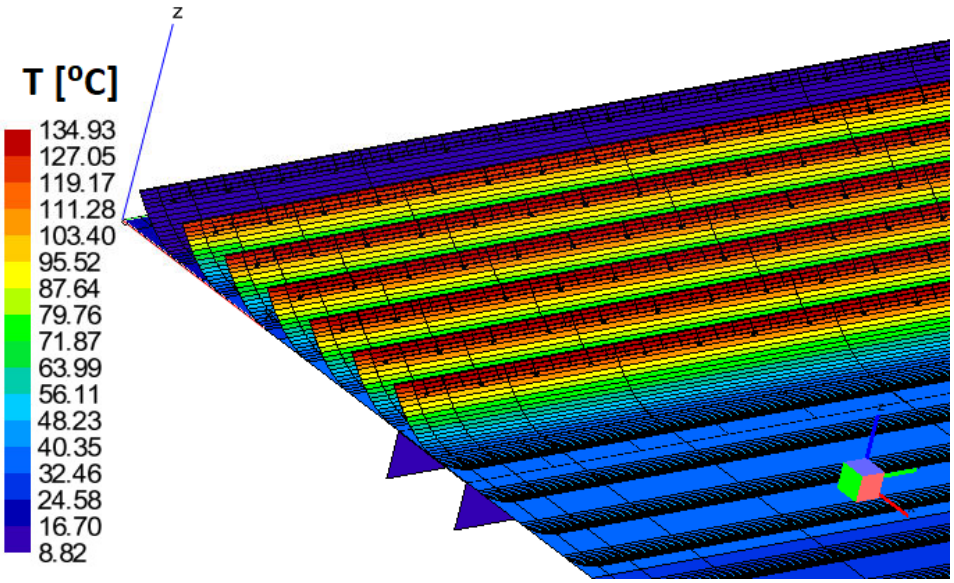

Figure 5.18: Temperature distribution at the hottest location in orbit (Radiative *Case 1A HOT*).

Table 5.6: Comparison of aluminum versus CFRP material characteristics.

Parameter	**AL 2024 T6**	**CFRP M55J**
Density $[kg/m^3]$	2700	1630
Max. operating temp. [°C]	400	150
Conductivity $[W/mK]$	121	55 and 1.3
Max temperature [°C]	135	244

5.2.8. Optimized baseline design

Having varied many different parameters the baseline design can be optimized by applying multiple changes at the same time. The summary of the changes made to the design are listed in the Tab. 5.7, and the optimized design temperature distribution for the hottest case scenario (Case *1A HOT*) can be seen in Fig. 5.17.

Table 5.7: Changes made to the baseline model.

Case	**Vertical radiator**	**Thermal doubler**	**Max cell temp. [$^{\circ}C$]**	**Remarks**
Baseline	No	No	244	–
Optimized solution	Yes	10 layers of PG bonded between the cell and concentrator.	122	PG flexibility decreases exponentially with an increase in the amount of layers, so it might be problematic to shape it into the desired geometry.

5.3. Description of Radiative Cases

As mentioned earlier, the main research objective of this thesis is to determine the thermal behavior of the solar panel in orbit. Throughout satellite's lifetime the solar panel will experience a variety of different configurations, depending on the time of the year, satellite's position, orbit definition etc. In total 16 different radiative cases were analyzed, divided into 4 main categories - hot, cold, operational and misalignment cases. This section aims at describing the purpose and specifications of each case separately at first, and summarizing them all in Tab. 5.26.

Various parameters change for each radiative case, however the orbit altitude and inclination are held fixed for all radiative analysis cases, see Tab. 5.8. Among the varied parameters are:

- Concentrator surface coating reflectivity, see Tab. 5.9,
- Distance between the satellite and the Sun in terms of extremes (WS and SS, see Tab.5.9; 152 and 177 million km are the Sun-Earth distances),
- Albedo values,
- Amount of Earth IR radiation,
- Orbit right ascension angle (0° or 90°). Note that both types of orbits are assumed to be *sun-synchronous*, which means that the movement of the satellite always looks the same when viewed from the Sun (synchronized with respect to the Sun).

Table 5.8: Fixed orbit parameters.

Parameter	**Value**	**Unit**
Orbit altitude	1200	km
Orbit inclination	88	°

Table 5.9: Varied parameters.

Property	**BOL**	**EOL**	**WS (152 million km)**	**SS (177 million km)**
Coating reflectivity	0.95	0.85	–	–
Solar flux	–	–	1461.62	1270.38

Fig. 5.19 depicts a 2D drawing of the orbit trajectories for 0° and 90° right ascension angles. In both cases it takes the S/C ~6500 seconds to orbit the Earth once. At 0° right ascension angle the S/C orbits the Earth as shown in the figure by the dotted circle (in the clockwise direction). The software *ESATAN* sets the starting point (0 or 6500 seconds) when the S/C is positioned slightly above the 300 seconds mark. at 300 seconds it reaches a location where it is positioned exactly between the Earth and the Sun, as shown. The orbit for 90° right ascension angle is shown as a dotted vertical line, and in Fig. 5.19 comes out of the picture, such that throughout the orbit the satellite is in the sunlight.

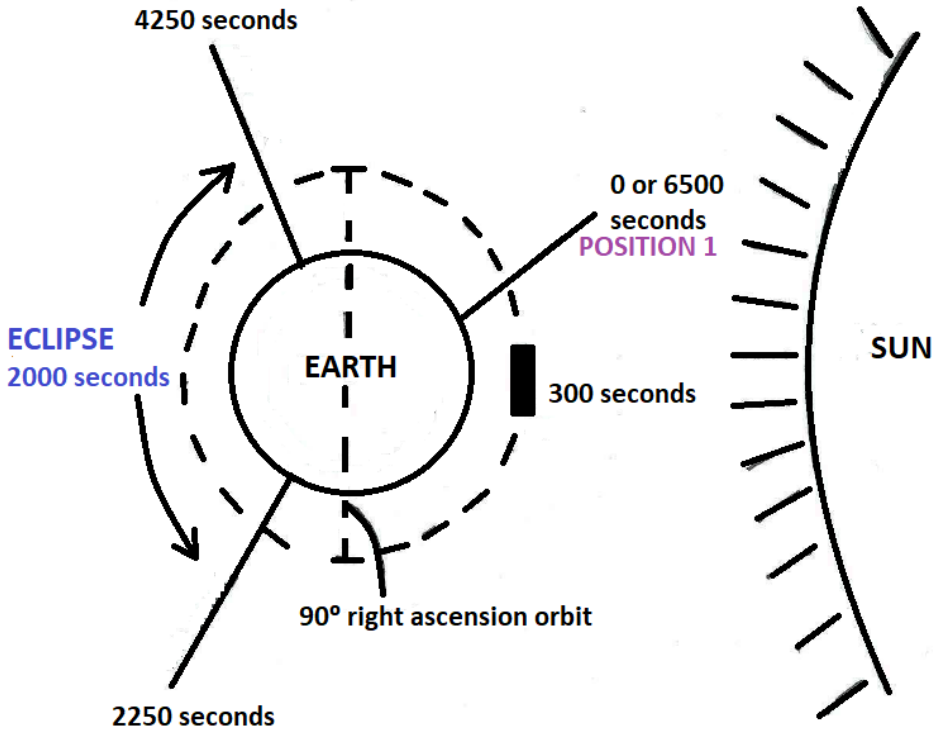

Figure 5.19: Orbit trajectories for 0 and 90° right ascention angles and relevant positions around the orbit.

5.3.1. Hot Cases

To ensure that the solar panel does not fail in orbit due to extremely high temperatures, the following four radiative cases were executed to predict the panel temperature distribution in the worst (hottest) conditions in orbit. It is especially crucial for the concentrator solar array, since light concentration introduces hot spots.

A set of the following parameters is assumed constant for all the hottest cases in orbit:

1. As can be seen from Tab. 5.9 the end-of-life coating refectivity is assumed to drop considerably, which will result in higher absorptivity leading to increased temperature. Therefore, EOL conditions are assumed for all hottest cases.
2. During the Winter Solstice the Earth is at its closest to the Sun and, hence, receives the highest amount of radiation, see Tab. 5.9. Higher incoming solar flux implies higher temperature, therefore, WS conditions are assumed for all hottest cases.
3. Depending on the inclination of the orbit, albedo (solar reflection) values vary from 0.2 to 0.4 $[-]$, reaching maximum near the poles (for polar orbits). Higher albedo means more incoming light which results in higher temperature. Therefore, the maximum albedo values are assumed for all hottest cases.
4. Another important environmental aspect kept constant for the hot cases is the Earth IR radiation. The average amount of radiation emitted by the Earth is equivalent to the amount emitted by the black body of 251 K. Throughout the year the amount of radiation generally varies to correspond to that of a black body of $\sim$ 244 K to 264 K. For the hot radiative cases the higher limit is considered.

1A HOT

This case is the extreme hot case. Apart from the above-mentioned parameters, the three additional characteristics for this particular case are as follows:

- Right ascension angle of the orbit is 0°, which means that (in the low Earth orbit of 1200 km altitude) it will spend 1/3rd of its lifetime in eclipse not being able to produce electric power.

- Cell operation is OFF when analyzing this hottest case. Then thermally there is no heat dissipation by converting the incoming light into electricity which means that all absorbed flux is converted into heat, therefore, simulates the hottest case. During normal operations some sections of the solar panel will be turned off in order to limit the power generation. When the batteries are charged and the S/C uses little power, then generation of extra power may cause issues in the S/C electrical systems, hence the solar cells in some parts of the solar panel are shunted. Since it is impossible to predict which sections will be shunted, this case allows to analyze the effect of a shunted section anywhere on the solar panel.

- In this case (as in the ideal case in orbit) the solar panel is oriented in such a way that the cells receive maximum illumination, hence the substrate of the panel is facing the Sun and oriented perpendicularly to the incoming sun rays. This direction is noted as TRUE SUN direction.

Table 5.10: Case 1A HOT.

Case	**Mat. prop.**	**Right asc. [°]**	**Solar flux**	**Albedo**	T_{EARTH} **[K]**	**Cells**	**Panel orient.**
1A Hot	EOL	0	WS	0.4	264	OFF	TRUE SUN

1A HOT ZERO ALBEDO

This case is a variation of the *Case 1A HOT* with zero albedo. It is executed to see if/by how much the temperature is influenced by albedo.

Table 5.11: Case 1A HOT ZERO ALBEDO.

Case	**Mat. prop.**	**Right asc. [°]**	**Solar flux**	**Albedo**	T_{EARTH} **[K]**	**Cells**	**Panel orient.**
1A Hot ZERO ALBEDO	EOL	0	WS	0.0	264	OFF	TRUE SUN

1B HOT

This case also represents the extreme hot case with only one parameter difference as compared to the previous case:

- Right ascension angle of the orbit is 90° meaning that the S/C orbital plane is shifted in such a way that it never enters eclipse but instead is always receiving solar illumination. This way there is only minimum energy storage required on board of the S/C (for emergency cases) as the cells are able to produce power constantly.

Table 5.12: Case 1B HOT.

Case	**Mat. prop.**	**Right asc. [°]**	**Solar flux**	**Albedo**	T_{EARTH} **[K]**	**Cells**	**Panel orient.**
1B Hot	EOL	90	WS	0.4	264	OFF	TRUE SUN

1C HOT

In this case the solar panel being under the same thermal conditions as in *Case 1A HOT* now is turned by 180° with respect to the Sun, pointing it's rear side towards the incoming sunrays.

Depending on the satellite's pointing requirements it might happen that the satellite at times will have to change its pointing direction and the panel might end up in the configuration of rearside facing the Sun. This might happen on purpose to shield the cells from excess sunlight in case they overheat.

Table 5.13: Case 1C HOT.

Case	Mat. prop.	Right asc. [°]	Solar flux	Albedo	T_{EARTH} [K]	Cells	Panel orient.
1C Hot	EOL	0	WS	0.4	264	OFF	BACK SIDE

1D HOT

This case is equivalent to *Case 1A HOT* but with the panel in operational conditions. It is executed to see the thermal effect of drawing power versus short-circuited case.

Table 5.14: Case 1D HOT.

Case	Mat. prop.	Right asc. [°]	Solar flux	Albedo	T_{EARTH} [K]	Cells	Panel orient.
1D Hot	EOL	0	WS	0.4	264	ON	TRUE SUN

5.3.2. Cold Cases

Just as the solar panel is expected to reach extremely high temperatures when illuminated by the Sun, when in eclipse it is expected to experience very low temperatures. The following three radiative cases were executed to predict the panel temperature distribution in the worst (coldest) conditions in orbit.

A set of the following parameters is assumed constant for all the coldest cases in orbit:

1. BOL values are assumed for the concentrator coating reflectivity,
2. Lowest incoming solar flux implies lower temperatures, therefore, SS conditions are assumed for all coldest cases,
3. Minimum albedo values are considered in all cold cases (equivalent to 0.2 [$-$]),
4. The lower limit of the Earth IR radiation is assumed (equivalent to 244 K).

2A COLD

In this cold case apart from the above-mentioned parameters, the three additional characteristics for this particular case are as follows:

- Right ascension angle of the orbit is 0°, which means that the S/C experiences regular eclipse periods where the structure will reach lowest temperatures,

- Cell operation is ON when analyzing this coldest case because substantial part of the incoming radiation will, therefore, get converted into electric power which will cool the panel,

- The solar panel is oriented in the TRUE SUN direction allowing the cells to receive solar illumination and produce electric power.

Table 5.15: Case 2A COLD.

Case	Mat. prop.	Right asc. [°]	Solar flux	Albedo	T_{EARTH} [K]	Cells	Panel orient.
2A Cold	BOL	0	SS	0.2	244	ON	TRUE SUN

2B COLD

This case is almost entirely equivalent to the previous cold case with only one parameter difference:

- Right ascension angle of the orbit is 90° meaning there is no eclipse, hence lowest temperatures here are expected to be much higher than of the previous case.

Table 5.16: Case 2B COLD.

Case	Mat. prop.	Right asc. [°]	Solar flux	Albedo	T_{EARTH} [K]	Cells	Panel orient.
2B Cold	BOL	90	SS	0.2	244	ON	TRUE SUN

2C COLD

In this case the solar panel under the same thermal conditions as in *Case 2A COLD* with two differences:

- The panel is turned by 180° with respect to the Sun (safe mode), pointing it's rear side towards the incoming sun rays,
- The solar cells are turned OFF meaning that the panel is in a non-operational mode.

Table 5.17: Case 2C COLD.

Case	Mat. prop.	Right asc. [°]	Solar flux	Albedo	T_{EARTH} [K]	Cells	Panel orient.
2C Cold	BOL	0	SS	0.2	244	OFF	BACK SIDE

5.3.3. Operational Cases

First two sets of thermal cases are executed to determine the highest and lowest temperature extremes that the panel can reach in orbit. This set of four cases aims at determining panel temperatures in operational mode with:

1. Lowest incoming solar flux (SS conditions),
2. Cells ON,
3. Average albedo values (equivalent to 0.33 [$-$]),
4. The Earth IR radiation is assumed to be equivalent to that of a black body of 254 K (average),
5. Panel orientation in the direction of TRUE SUN for all cases.

3A OPR

The additional two properties for this case are:

- BOL panel characteristics,
- 0° right ascension angle.

Table 5.18: Case 3A OPR.

Case	Mat. prop.	Right asc. [°]	Solar flux	Albedo	T_{EARTH} [K]	Cells	Panel orient.
3A OPR	BOL	0	SS	0.33	254	ON	TRUE SUN

3B OPR

This case is the same as the previous case (*Case 3A OPR*) with one parameter difference:

– Right ascension angle of the orbit is 90° meaning the absence of eclipse periods.

Table 5.19: Case 3B OPR.

Case	Mat. prop.	Right asc. [°]	Solar flux	Albedo	T_{EARTH} [K]	Cells	Panel orient.
3B OPR	BOL	90	SS	0.33	254	ON	TRUE SUN

3C OPR

This case is also the same as *Case 3A OPR* with the difference of having:

– EOL panel characteristics. Hence the differences between the two cases in thermal performance can be attributed due to the change in concentrator reflectivity.

Table 5.20: Case 3C OPR.

Case	Mat. prop.	Right asc. [°]	Solar flux	Albedo	T_{EARTH} [K]	Cells	Panel orient.
3C OPR	EOL	0	SS	0.33	254	ON	TRUE SUN

3D OPR

This case is the same as *Case 3C OPR* with the difference of having:

– The right ascension angle of the orbit is 90° meaning the absence of eclipse periods.

Table 5.21: Case 3D OPR.

Case	Mat. prop.	Right asc. [°]	Solar flux	Albedo	T_{EARTH} [K]	Cells	Panel orient.
3D OPR	EOL	90	SS	0.33	254	ON	TRUE SUN

5.3.4. Misalignment Cases

The next four cases are executed specifically to determine the sensitivity of the solar flux distribution over the cells for two misalignment angles around two different axis. For all four cases the following parameters are fixed constant:

1. The cells are kept turned ON, meaning that the panel is in operational mode,
2. The right ascension angle of the orbit is kept at 90° meaning that there is constant sunlight and no eclipse,
3. EOL material characteristics are considered.

⇒ 5° Misalignment around y-axis

The next two cases are executed to determine how a small misalignment angle of 5° influences the thermal and electrical performance of the panel. Fig. 5.20 depicts the slight misalignment in the panel orientation around it's y-axis. In real life this may be caused by the imperfections of pointing accuracy of the Solar Array Drive Mechanism (SADM), although it will not reach 5° offset in reality (Δ1° max is predicted). Fig. 5.20 depicts the panel at position 1 in orbit. Note, that the side closer to the Earth at that location is denoted as "R" side.

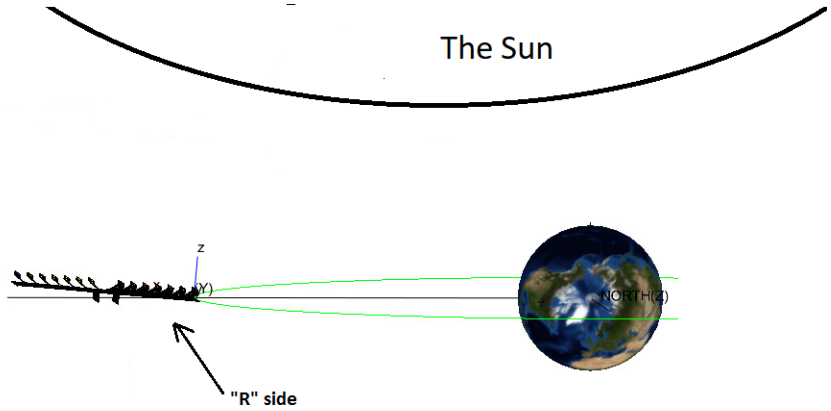

Figure 5.20: CASE 4A MIS-HOT: The panel cross-section with the misalignment of 5° (with the Sun positioned in the positive z-direction). The right side of the panel that is inclined as shown here is denoted as"R" side.

- **4A MIS-HOT**
  Apart from above-mentioned properties the following additional characteristics to simulate hot conditions for this case are:
  - Highest incoming solar flux (WS conditions),
  - Maximum albedo values are considered here (equivalent to 0.4 $[-]$),
  - The upper limit of the Earth IR radiation is assumed (equivalent to 264 K),
  - Panel orientation is TRUE SUN with 5° misalignment as see in Fig. 5.20.

Table 5.22: Case 4A MIS-HOT.

Case	Mat. prop.	Right asc. [°]	Solar flux	Albedo	T_{EARTH} $[K]$	Cells	Panel orient.
4A MIS-HOT	EOL	90	WS	0.4	264	ON	TRUE SUN, 5° misalignment around y axis

- **4B MIS-OPR**
  This case deviates slightly from *Case 4A MIS-OPR* due to changes in the following parameters to simulate operational conditions:
  - Solar flux (SS considered in this case),
  - Abledo (0.33 $[-]$ in this case),
  - The Earth IR radiation (equivalent to 254 K here (average)).

Table 5.23: Case 4B MIS-OPR.

Case	Mat. prop.	Right asc. [°]	Solar flux	Albedo	T_{EARTH} $[K]$	Cells	Panel orient.
4B MIS-OPR	EOL	90	SS	0.33	254	ON	TRUE SUN, 5° misalignment around y axis

⇒ 30° Misalignment around x-axis

Similarly, the next two cases are executed to determine the absorbed solar flux sensitivity for this concentrator solar panel design, for 30° misalignment around a different axis as can be see in Fig. 5.21 and 5.22. In reality such a misalignment can occur due to the changing position of the Sun with respect to Earth, and absence of the mechanism that would correct misalignment error around double axis.

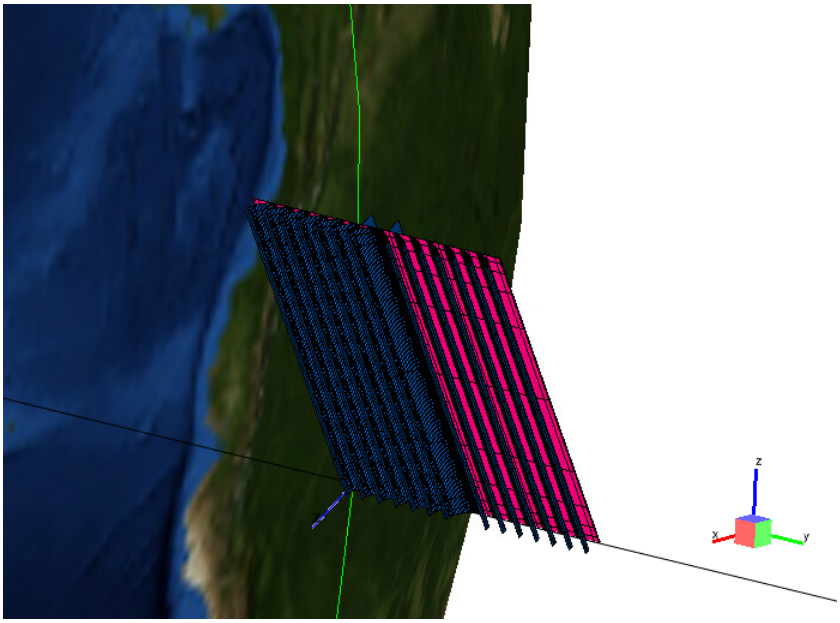

Figure 5.21: CASE 4C MIS-HOT: The representation of the panel misalignment angle of 30° around the y-axis.

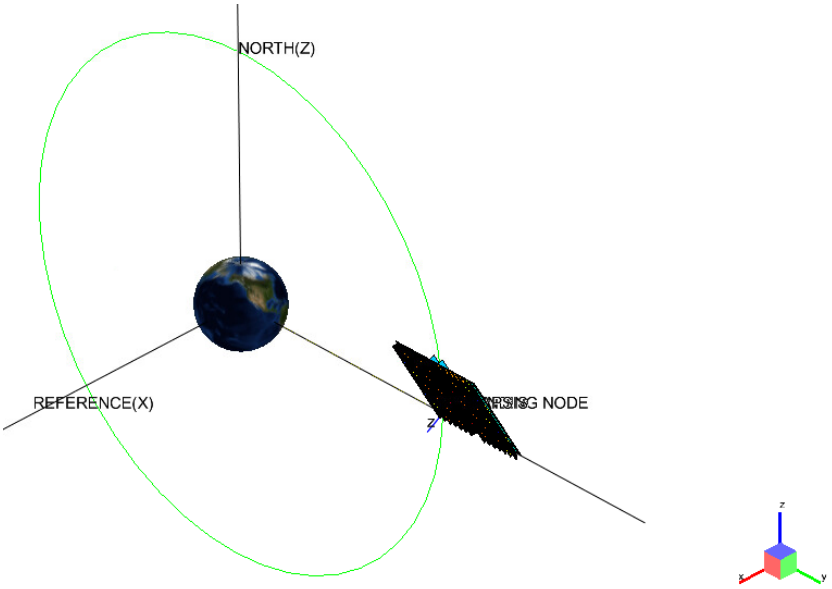

Figure 5.22: CASE 4C MIS-HOT: Panel orientation with a 30° angle of misalignment (green circle - orbit trajectory; x-axis direction of the Sun).

– **4C MIS-HOT**
In this case the exact same thermal characteristics are used as in *Case 4A MIS-HOT* with the only difference in misalignment angle and the axis around which it occurs.

Table 5.24: Case 4C MIS-HOT.

Case	Mat. prop.	Right asc. [°]	Solar flux	Albedo	T_{EARTH} [K]	Cells	Panel orient.
4C MIS-HOT	EOL	90	WS	0.4	264	ON	TRUE SUN, 30° misalignment around x axis

– **4D MIS-OPR**
This case uses the same properties as in *Case 4B MIS-OPR* with the only difference in misalignment angle and the axis around which it occurs.

Table 5.25: Case 4D MIS-OPR.

Case	Mat. prop.	Right asc. [°]	Solar flux	Albedo	T_{EARTH} [K]	Cells	Panel orient.
4D MIS-OPR	EOL	90	SS	0.33	254	ON	TRUE SUN, 30° misalignment around x axis

5.3.5. Overview of All Radiative Cases

An overview of all radiative cases and their orbital, environmental and performance parameters can be found in Table 5.26.

Table 5.26: Summary of Radiative cases.

Case	Mat. prop.	Right asc. [°]	Solar flux	Albedo	T_{EARTH} [K]	Cells	Panel orient.
1A Hot	EOL	0	WS	0.4	264	OFF	TRUE SUN
1A Hot ZERO ALBEDO	EOL	0	WS	0.0	264	OFF	TRUE SUN
1B Hot	EOL	90	WS	0.4	264	OFF	TRUE SUN
1C Hot	EOL	0	WS	0.4	264	OFF	BACK SIDE
1D Hot	EOL	0	WS	0.4	264	ON	TRUE SUN
2A Cold	BOL	0	SS	0.2	244	ON	TRUE SUN
2B Cold	BOL	90	SS	0.2	244	ON	TRUE SUN
2C Cold	BOL	0	SS	0.2	244	OFF	BACK SIDE
3A OPR	BOL	0	SS	0.33	254	ON	TRUE SUN
3B OPR	BOL	90	SS	0.33	254	ON	TRUE SUN
3C OPR	EOL	0	SS	0.33	254	ON	TRUE SUN
3D OPR	EOL	90	SS	0.33	254	ON	TRUE SUN
4A MIS-HOT	EOL	90	WS	0.4	264	ON	TRUE SUN, 5° misalignment around y axis
4B MIS-OPR	EOL	90	SS	0.33	254	ON	TRUE SUN, 5° misalignment around y axis
4C MIS-HOT	EOL	90	WS	0.4	264	ON	TRUE SUN, 30° misalignment around x axis
4D MIS-OPR	EOL	90	SS	0.33	254	ON	TRUE SUN, 30° misalignment around x axis

5.4. Thermal Analysis Results

The optimized baseline panel design is tested in orbit at various radiative conditions. Thermal inspection of the panel is mainly analyzed based on the solar array temperature (Section 5.4.1) at various locations over the panel. In addition to that, several absorbed heat flux figures (solar, albedo, planetary and rest heat) are presented in Section 5.4.2.

5.4.1. Temperature

HOT CASES

- **Case 1A HOT**

  Fig. 5.23 depicts the temperature variation of nodes at the cell, U-beam, panel and edge beam througout the orbit. One full revolution around the Earth at a given altitude takes roughly 6500 seconds. All nodes are (geometrically) middle nodes, where the temperature reaches maximum value for each separate structure. It can be seen that the highest temperatures are reached at the cells (122°C during illuminated phase), which makes sense because it experiences roughly five times the solar flux.

  The highest temperatures are reached at 300 seconds, which is when the panel's position is right between the Sun and the Earth, see Fig. 5.19. At this position the rear side of the panel (which is supposed to radiate heat away to the open space) is exposed to the planet flux the most (largest view factor). At 2250 seconds the panel enters eclipse, and the temperature begins to suddenly drop. The lowest temperature is reached at the edge beams (-67°C) while the cells experience -58°C. At the beginning of eclipse the temperature decreases nearly vertically for the first 500 seconds, and then continues to decrease more slowly, until (at 4250 seconds) it exits eclipse and the temperature begins to rise again. It can be seen that the cell temperature drops by 115°C within 8 minutes, and increases by 130°C within 8 minutes when exiting eclipse. These temperature fluctuations are very high and, therefore, it is important to mention that the differential thermal expansion should be taken into account. In this case the panel substrate, concentrators and beams are all made of the same material (CFRP *M55J*). Also it is important to take into account the thermal expansion coefficients of different materials to predict whether the structure will be able to sustain the thermal loads mechanically.

  The difference between cell temperatures along the panel can be seen in Fig. 5.24, where it is compared for two locations on the panel. Each cell contains 9 nodes and their temperatures are combined in Fig. 5.24 for two cells. The difference in temperatures between the two sets of nodes reaches 15°C during the sunlit period. This is due to the edge effects, and as will be seen later, the cell temperatures on the 6th concentrator are significantly lower than on the previous five. Note that the temperature variation within each cell (between the cell nodes) increases with concentrators being positioned farther away from the center of the panel, for instance, the cell in the middle of the panel experiences the temperature mismatch of ~1°C, while the cell on the edge and at the back of the panel: up to 4°C difference. This indicates that the edge effects play a more significant role towards the end and corners of the panel.

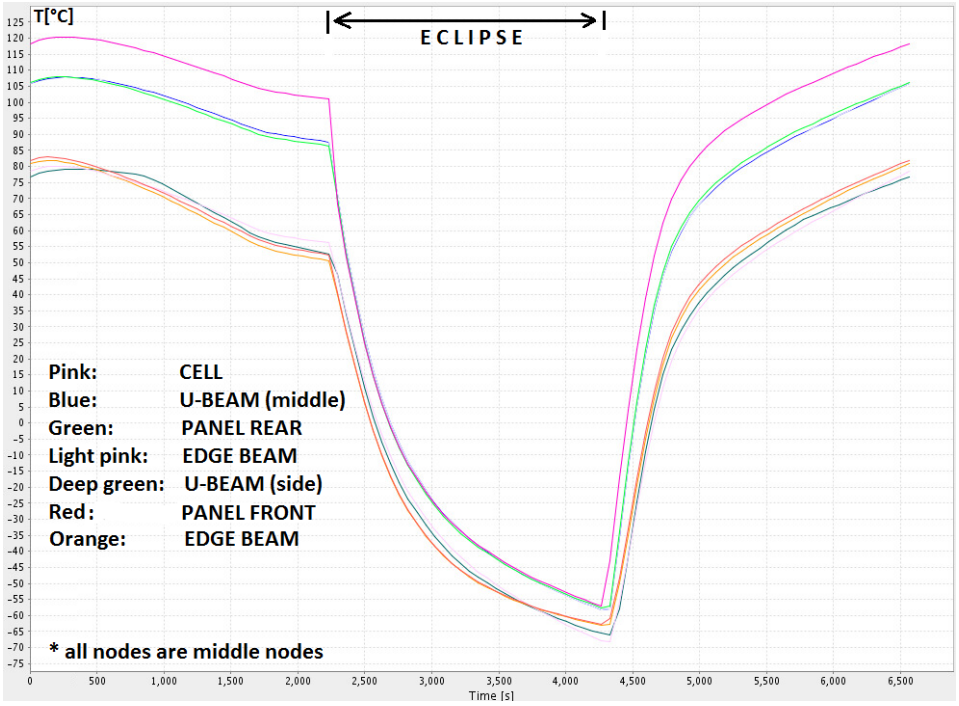

Figure 5.23: CASE 1A HOT: Temperature of several nodes throughout the orbit (middle of the panel). Note that every line represents a single node.

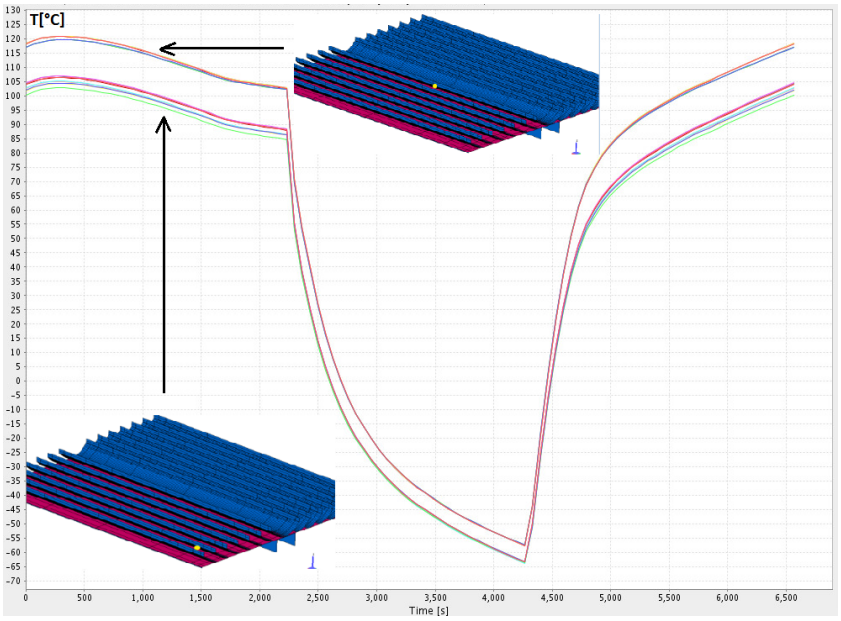

Figure 5.24: CASE 1A HOT: Cell temperature distribution (middle (concentrator 1) vs. edge of the panel (concentrator 6)).

– **Case 1A HOT *ZERO ALBEDO***

To understand the thermal behavior of the solar panel during the sunlit phase as a function of position, the exact same radiative case is analyzed with **zero albedo** to see the influence of the Earth. Fig. 5.25 depicts the temperature distribution of one of the cell nodes (at the middle of the panel). In comparison to Fig. 5.24 the temperature distribution during the sunlit phase appears to be nearly constant. This is an indication that the temperature increase from 104°C to 122°C (for the cell in the middle of the panel) is purely due to the planetary effects.

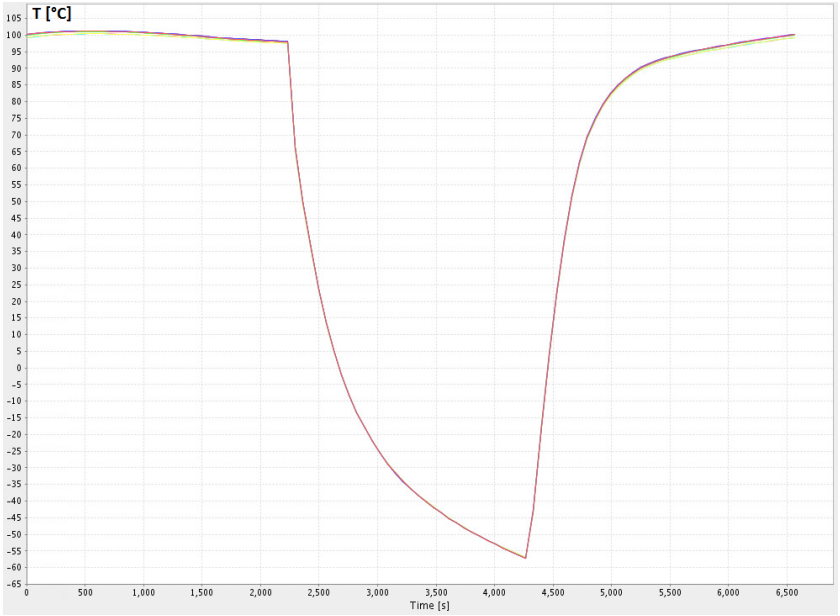

Figure 5.25: CASE 1A HOT: Cell temperature variation throughout the orbit with **zero albedo**, for comparison.

– **Case 1B HOT**

In Fig. 5.26 the upper and middle curves show the cell temperature distribution over one orbit in different positions on the panel. The lower curves represent the temperature change of the vertical radiator at the edge concentrator, as this is where the lowest temperatures occur (side beams on the rear reach minimum 40°C). This is due to the fact that the radiator has a very small view factor with respect to the Sun, the sunlight travels in parallel to the radiator and since its thickness is very small it remains cool. Since the panel does not experience eclipse, the cell temperature never gets lower than 78.5°C (the edge cell at the edge concentrator) and higher than 101.5°C.

The cell temperature fluctuates by $\pm$ 2 degrees throughout the orbit partly due to the way the panel is assumed to be orbiting the Earth (albedo and planetary effect): the panel orientation is fixed with respect to the orbital coordinate frame, hence any node on the panel will experience variable temperature throughout the orbit, because it's position with respect to the planet changes (e.g. different sides of the panel are receiving planet radiation (facing the Earth) at different positions in orbit). Also, the absorbed solar flux varies (insignificantly) throughout the orbit (see next section) which partly also accounts for slight temperature fluctuations for 90° right ascension orbit. Either the solar array has a fixed frame with respect to it's orbit or not is very mission specific and the way solar array is mounted onto the satellite with respect to its communication system and other payload.

The maximum cell temperature in this case is lower than in *Case 1A HOT* because the view factor of the panel with respect to the Earth is very small, so albedo and Earth induced radiation only fall on one side of the panel at a time (the side that faces the Earth).

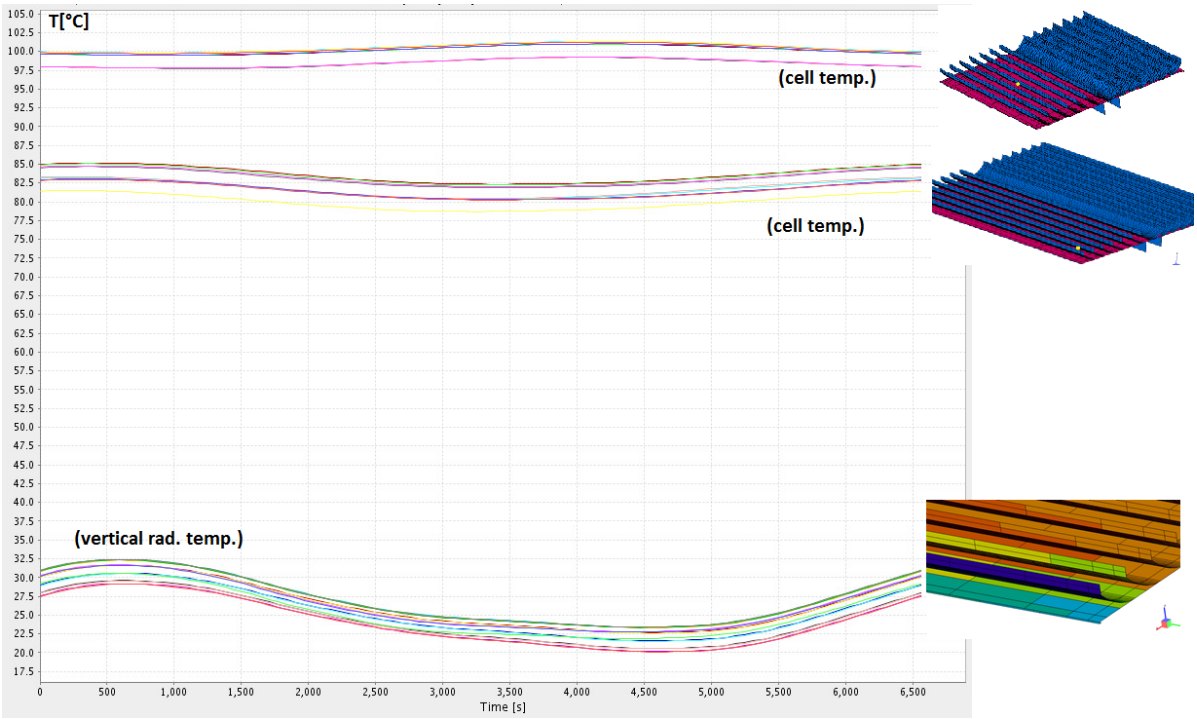

Figure 5.26: CASE 1B HOT: Cell and vertical radiator temperature variation through orbit with 90° right ascension angle.

– **Case 1C HOT**

Depending on the satellite's pointing requirements it might happen that the satellite at times will have to change its pointing direction and the panel might end up in the configuration of rearside facing the Sun, see Fig. 5.27. This might happen on purpose to shield the cells from excess sunlight in case they overheat. To summarize in this case the solar array is

- under the highest possible solar illumination (at winter solstice) of 1461.62 W/m^2,
- under the highest albedo of 0.4 [−],
- experiencing Earth radiation with its emitting temperature of 264 K,
- under end-of-life reflective coating conditions,
- non-operational, with no energy to electricity conversion (short-circuited cells),
- oriented such that the rearside of the panel faces the Sun.

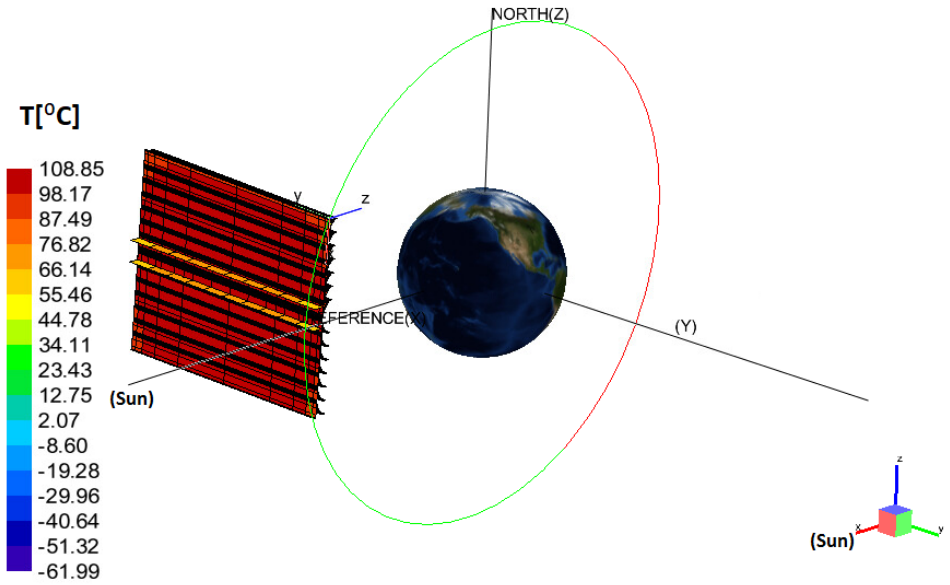

Figure 5.27: CASE 1C HOT: Temperature distribution over the rear side of the panel at the hottest location in orbit (at 300 seconds).

In case something goes wrong with the solar panel, it will be put into a safe configuration to shield the front side from the sunlight. Hence it is important to find out the temperature limits that the rear side of the panel will be exposed to. The highest temperatures the panel experiences when in position as shown in Fig. 5.27, and the rearside substrate reaches 109°C. Fig. 5.28 and 5.29 depict temperature distribution over the front and rear of the panel at the hottest location in orbit. It can be seen that the middle section of the panel is being heated up the most. The edge effects are clearly seen, as the heat disperses more towards the edges of the panel where the structure has a larger view factor to the open space, hence it radiates heat much better than in the middle of the panel.

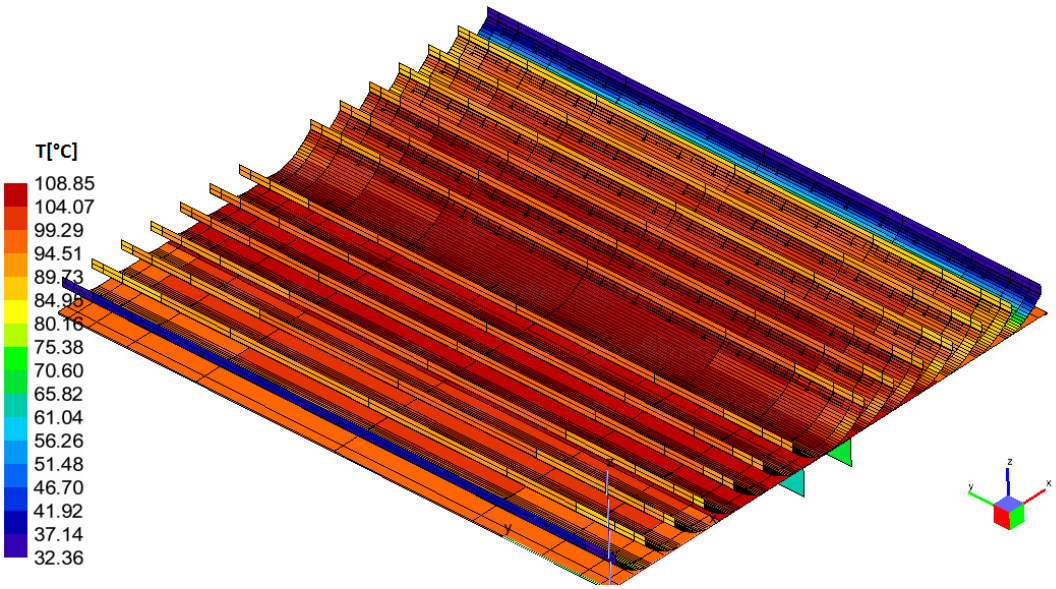

Figure 5.28: CASE 1C HOT: Temp. distribution over the front side of the panel at the hottest location in orbit (at 300 seconds).

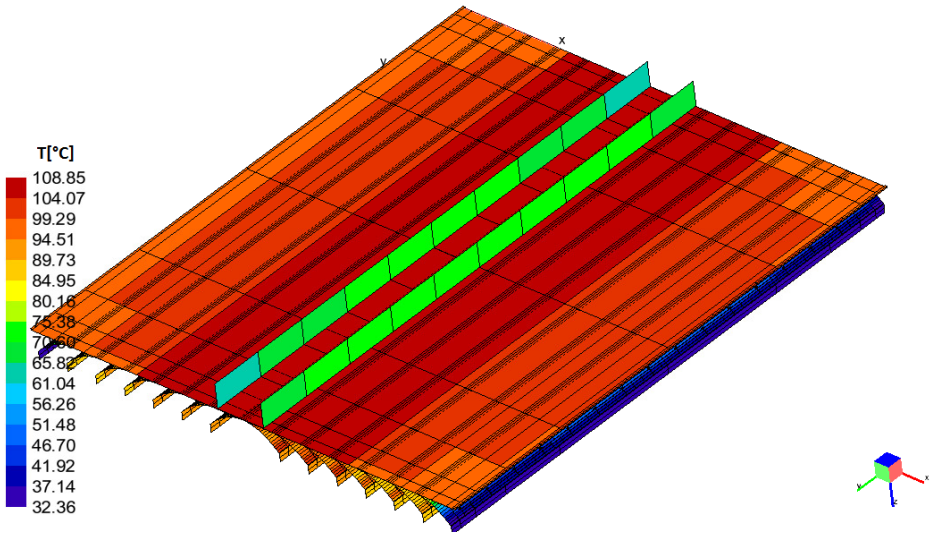

Figure 5.29: CASE 1C HOT: Temp. distribution over the rear sie of the panel at the hottest location in orbit (at 300 seconds).

The lowest temperatures are observed just before exiting eclipse, as expected from having seen the temperature behavior in the previous cases. The minimum panel temperature is roughly -60°C and occurs at the vertical radiators at the edges of the panel. (This again depends on the panel orientation. In case it is oriented as shown in Fig. 5.30, then the edge vertical radiator closer to the Earth will be warmer than that which is further away. In case the panel is turned by 90°C around its z-axis both edge radiators would experience the same temperature, as both would be equally away from the Earth.)

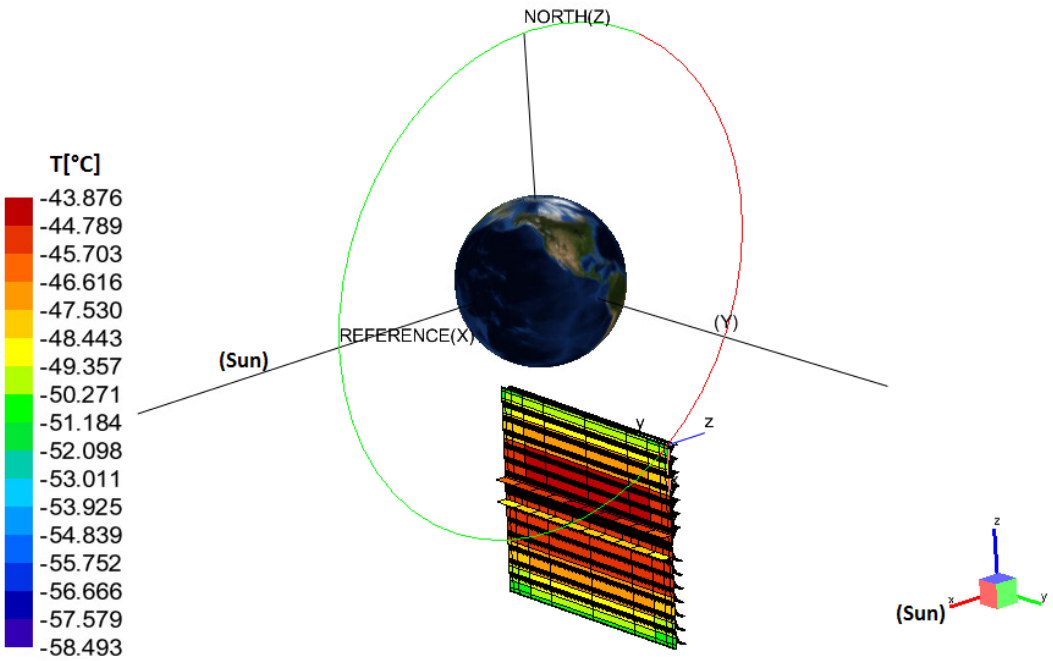

Figure 5.30: CASE 1C HOT: Temp. distribution over the rear side of the panel upon exiting the eclipse (coldest location in orbit).

– **Case 1D HOT**

The cell temperature variation can be seen in Fig. 5.31. As compared to the *Case 1A HOT*, the maximum cell temperature here is 105°C as compared to 122°C. This is due to the cells converting part of the incoming sunlight into electricity (implemented as the **rest heat source QR** in the model). Having solar cells ON only changes panel thermal behavior during the illuminated phase in orbit. Hence, it can be seen that the eclipse cell temperatures are equivalent to those in Fig. 5.23 (with minimum of -58°C).

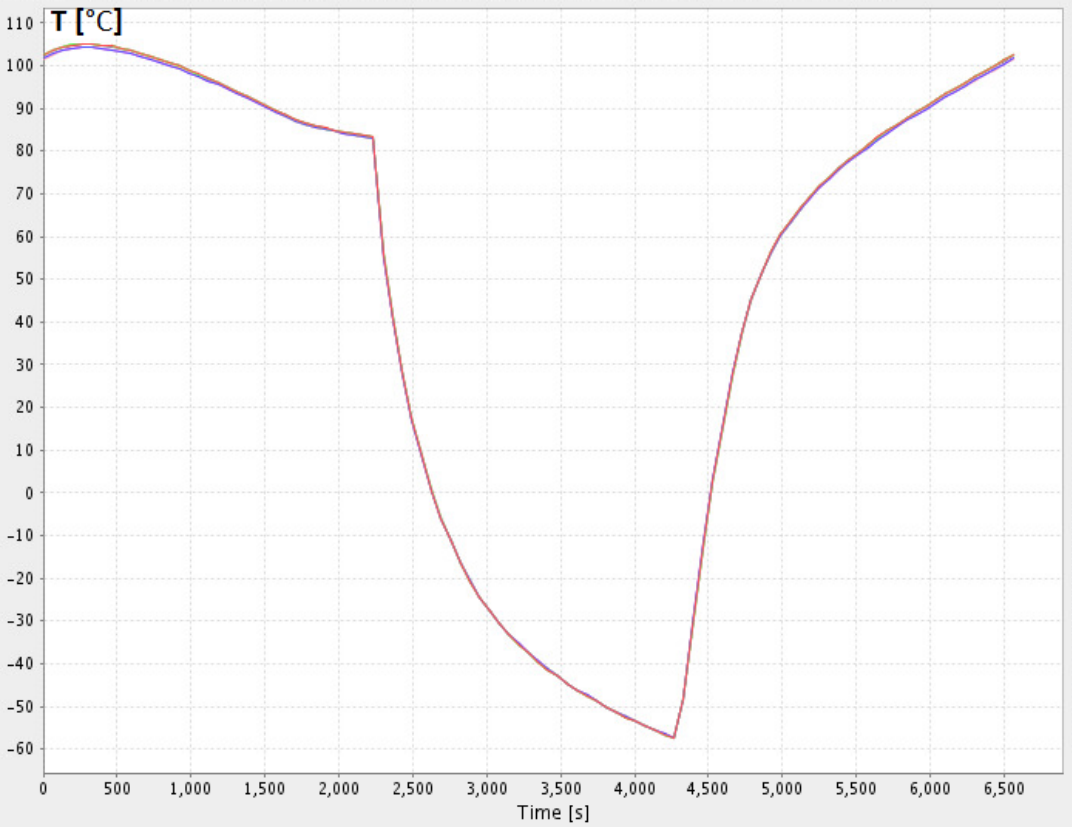

Figure 5.31: CASE 1D HOT: Cell temp. variation throughout the orbit (at the middle of the panel).

COLD CASES

– **Case 2A COLD**

At the coldest location in orbit the temperature distribution can be seen in Fig. 5.32. Fig. 5.33 shows the temperature distribution of the cell (at the edge), edge beams and the U-beam over the entire orbit. It can be seen that the coldest location on the panel is the edge beams and the temperature there during the eclipse reached -75°C. It makes sense since it is expected that the temperatures at the edges get significantly lower than in the middle of the panel because of the edge effects, which can also be seen more clearly in Fig. 5.34.

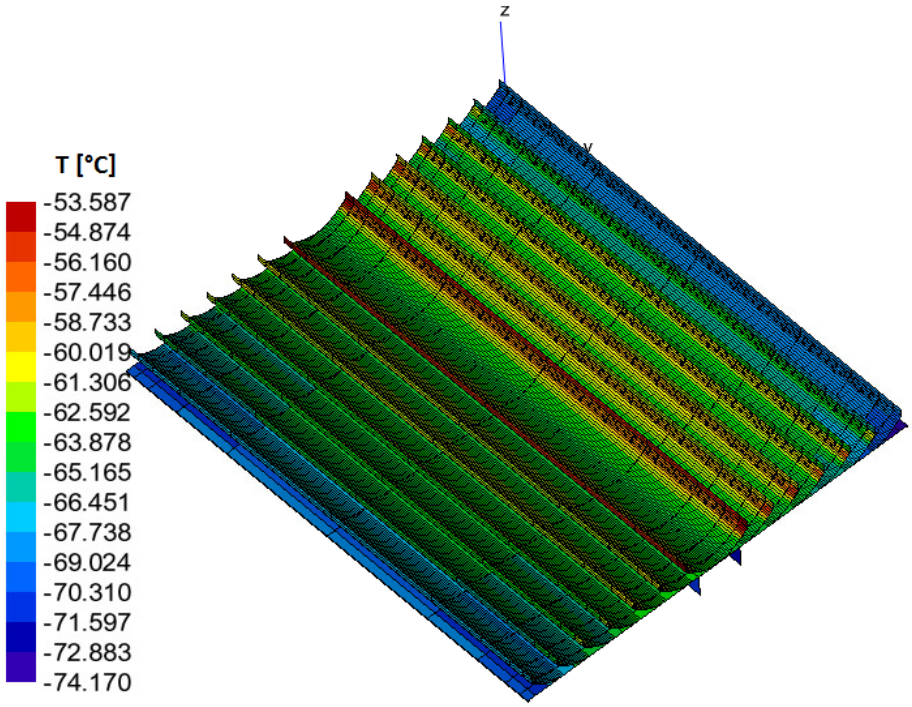

Figure 5.32: CASE 2A COLD: Temperature distribution of the front side of the panel upon exiting the eclipse (coldest location in orbit).

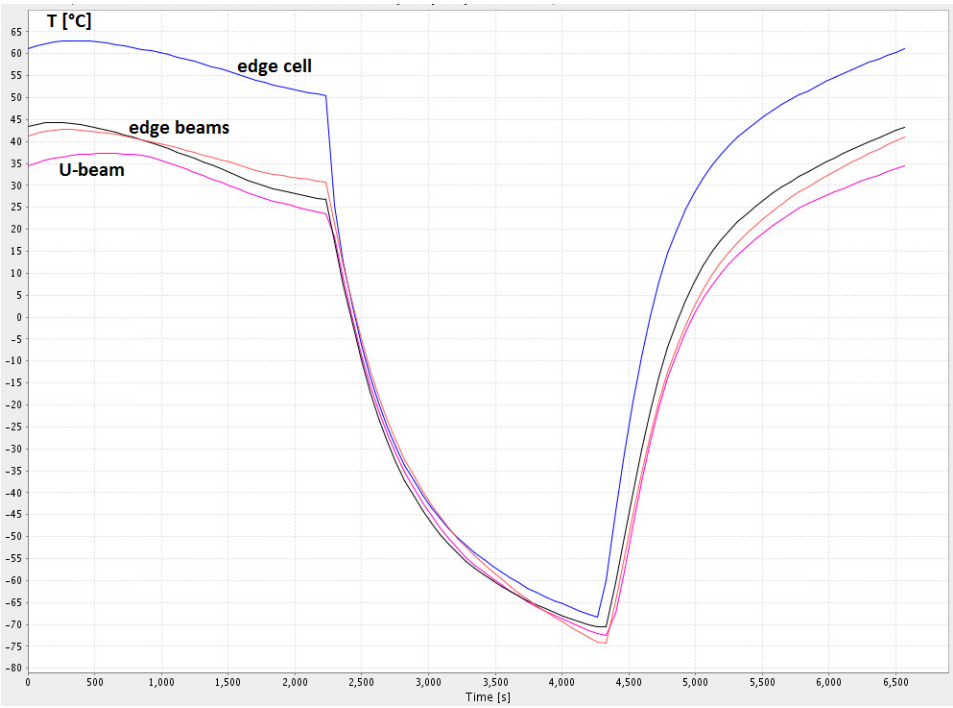

Figure 5.33: CASE 2A COLD: Temperature distribution of the edge cell, edge beams and U-beam.

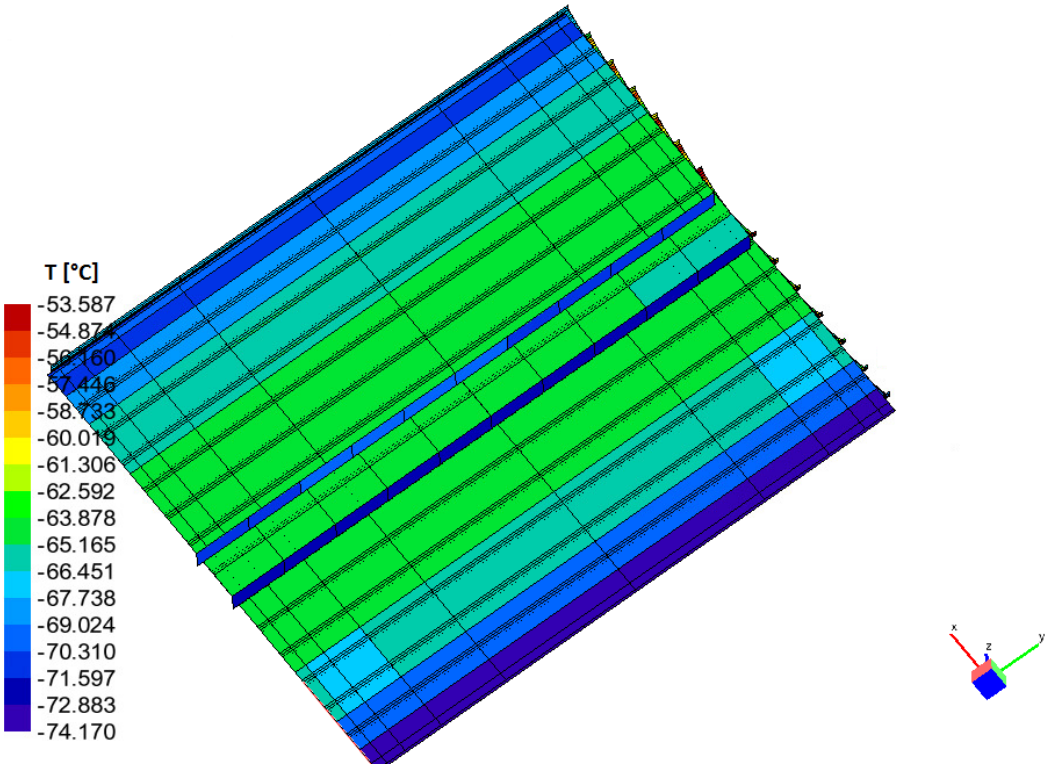

Figure 5.34: CASE 2A COLD: Temperature distribution over the rear side of the panel when in **coldest location** in orbit.

– **Case 2B COLD**

This case is executed to see what are the coldest temperatures reached by the panel. Fig. 5.37 depicts temperature distribution of the edge cell, vertical radiator (at the edge), edge beams at the rear and the U-beam. It can be seen that the U-beam reaches lower temperatures than the edge beams. Temperature fluctuates but ±3 degrees throughout the orbit, and it seems to change its behavior (from decreasing to increasing and the other way around) at around 1500 and 5000 seconds in orbit, as in *Case 1B HOT*. This mild temperature fluctuation can be explained by the absorbed flux figures (see next pages). Figures 5.35 and 5.36 show the panel position at 1500 and 5000 seconds in orbit, respectively.

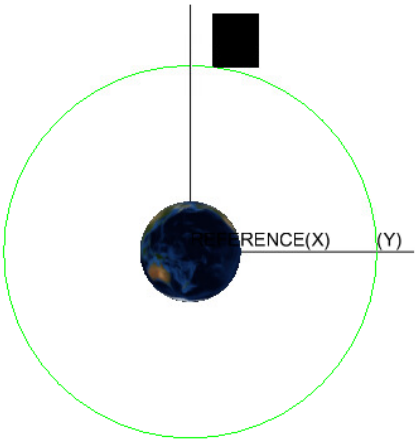

Figure 5.35: CASE 2B COLD: Panel position with respect to the Earth as seen by the Sun at 1500 seconds in orbit, 90° ascension orbit.

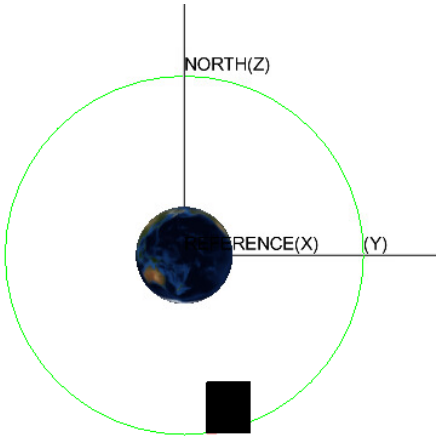

Figure 5.36: CASE 2B COLD: Panel position with respect to the Earth as seen by the Sun at 5000 seconds in orbit, 90° ascension orbit.

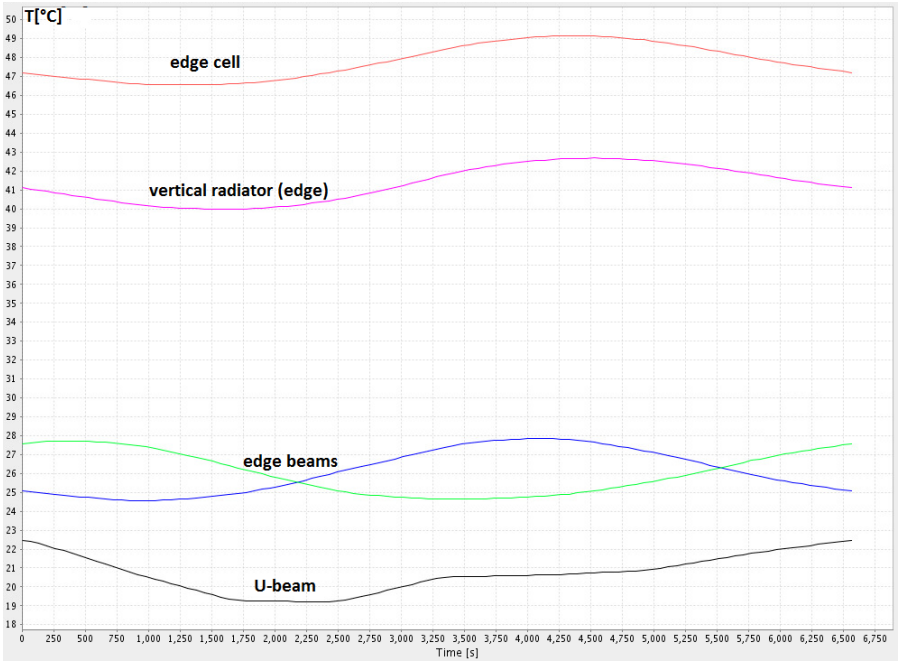

Figure 5.37: CASE 2B COLD: Temperature variation of the edge cell, vertical radiator (at the edge), edge beams and the U-beam.

– **Case 2C COLD**

Figures 5.38 and 5.39 depict the temperature distribution over the rear and front sides of the panel, respectively. As can be seen, the lowest temperatures take place at the edge concentrators, specifically, at their rear side. Slight asymmetry effects take place with 0 to 1 degree difference in temperatures between the right and left half of the panel. This variation is insignificantly small and can be attributed to the difference in view factors towards the Earth (left side in this case closer to the Earth and the right side slightly shaded by the U-beam). It can be seen that the lowest temperatures occur at the edge concentrator (its vertical radiator, specifically): -65°C. This occurs at around 4300 seconds in orbit, hence just before exiting eclipse. It was expected since **the rear of the panel is facing the Sun** in this case, as in the *Case 1C HOT*. The edge effects on the temperature can be seen clearly also in Fig. 5.40.

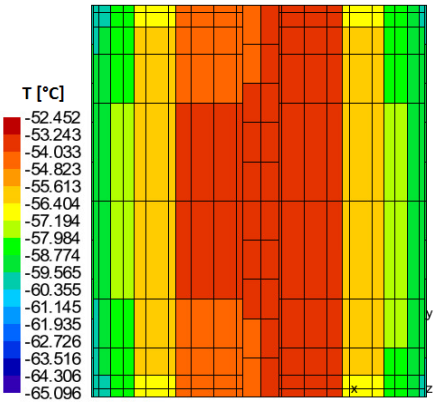

Figure 5.38: CASE 2C COLD: Temp. distribution over the rear side of the panel at the coolest location in orbit (in eclipse).

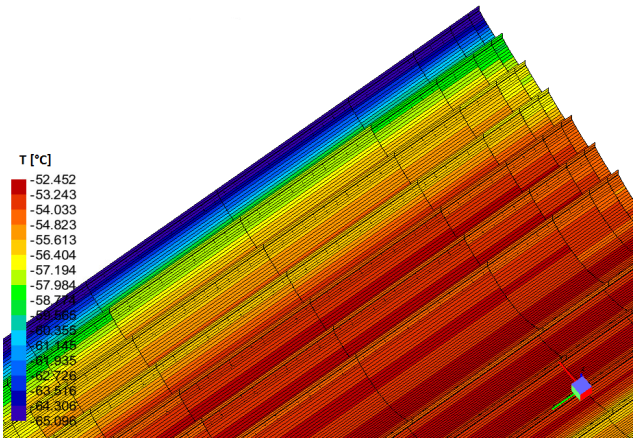

Figure 5.39: CASE 2C COLD: Temp. distribution over the front side of the panel at the coolest location in orbit (in eclipse).

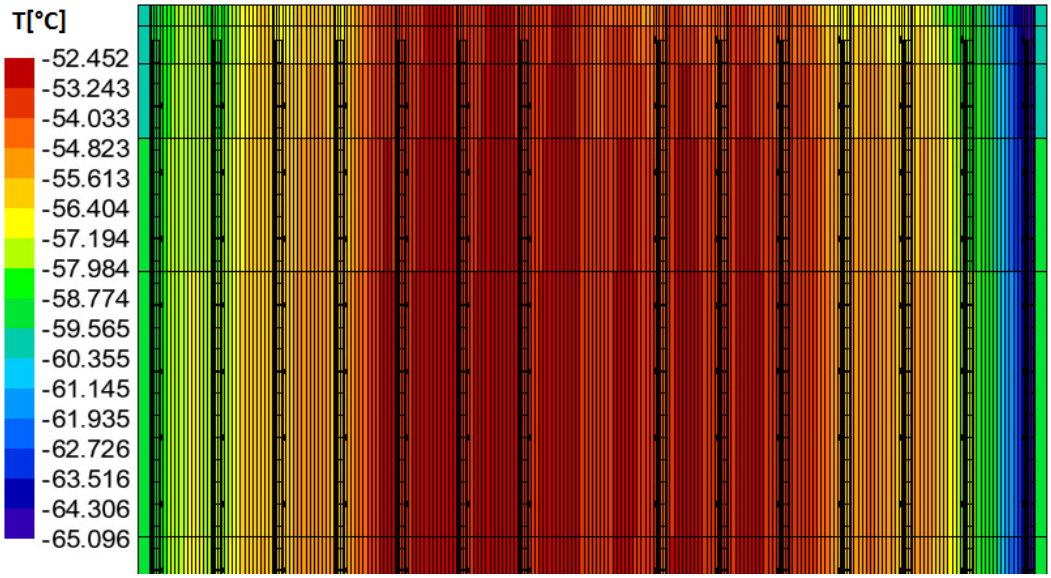

Figure 5.40: CASE 2C COLD: Temp. distribution over the front side of the panel at the coolest location in orbit: see the edge effects.

Fig. 5.41 depicts the temperature variation throughout the orbit of the middle node of all cells along the edge concentrator.

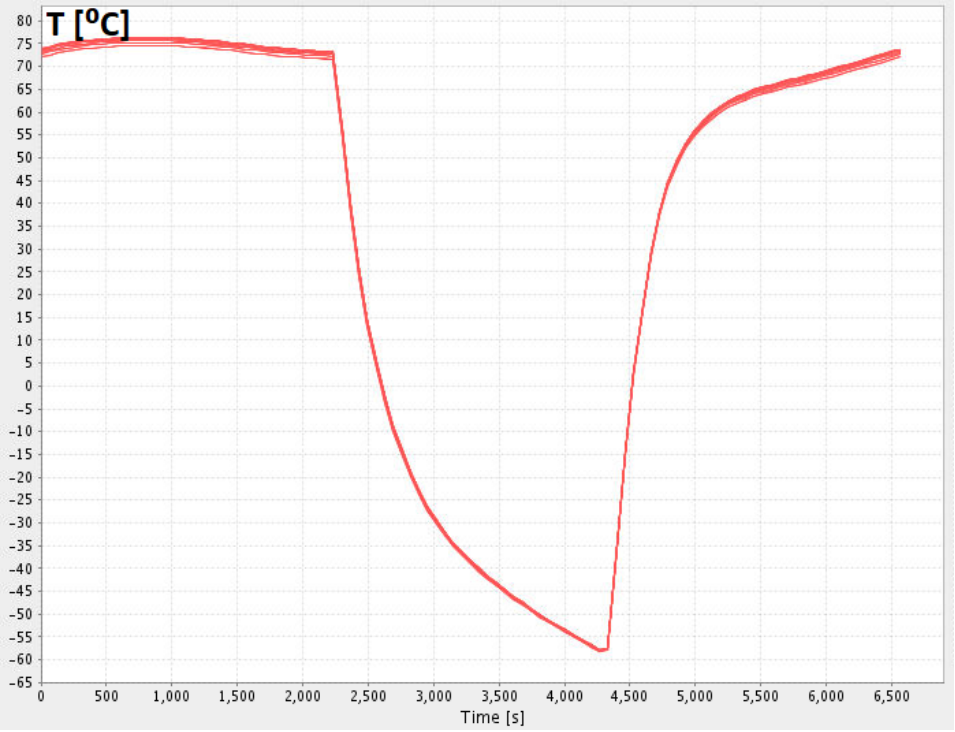

Figure 5.41: CASE 2C COLD: Temperature variation of the middle cell node for all cells on concentrator 6 (edge of the panel).

OPERATIONAL CASES

- **Case 3A OPR**

  The temperature distribution of the panel in the hottest location in orbit on this operational case can be seen in Fig. 5.42. The highest temperature reaches 84°C and is experienced

by the solar cells. Here it can also be seen how the temperature distribution over the first 5 concentrators (counting from the middle of the panel) appears similar to each other, whereas concentrator 6 is much cooler. This solar panel thermal behavior can be explained partly due to edge effects, and also because it is positioned next to a very cool concentrator (last one) which does not contain cells), so it dissipates heat more easily.

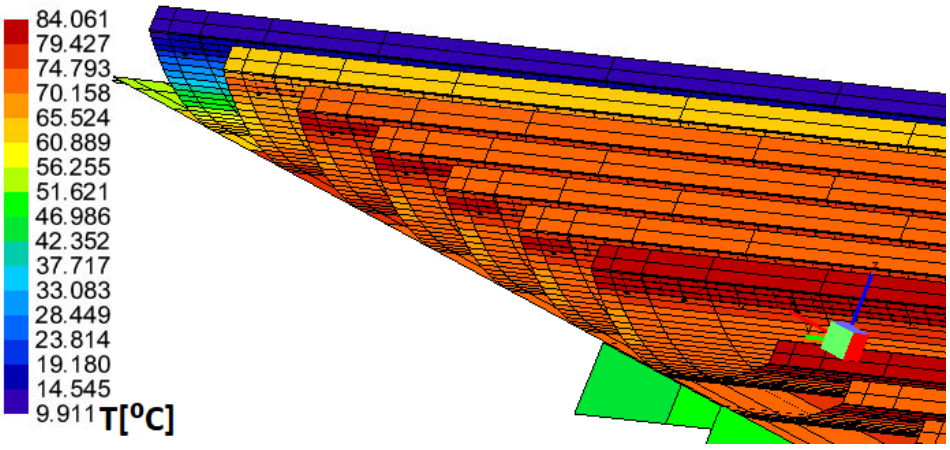

Figure 5.42: CASE 3A OPR: Temperature distribution at the hottest location in orbit (400 seconds).

Fig. 5.43 depicts the temp. variation of the middle nodes of all cells of concentrator 1 (middle of the panel) as a function or orbital position. The temperature for all nodes is the same, hence proving the point that cell temperature does not depend its position within the limits of one concentrator. However, the variation in temperature is observed between the concentrators, see Fig. 5.44: it depicts the temp. variation between the nodes belonging to different concentrators. It can be seen that the cells on the first 5 concentrators experience the same temperatures with ± 2°C difference, while the cells on concentrator 6 are **10°C cooler** than the rest.

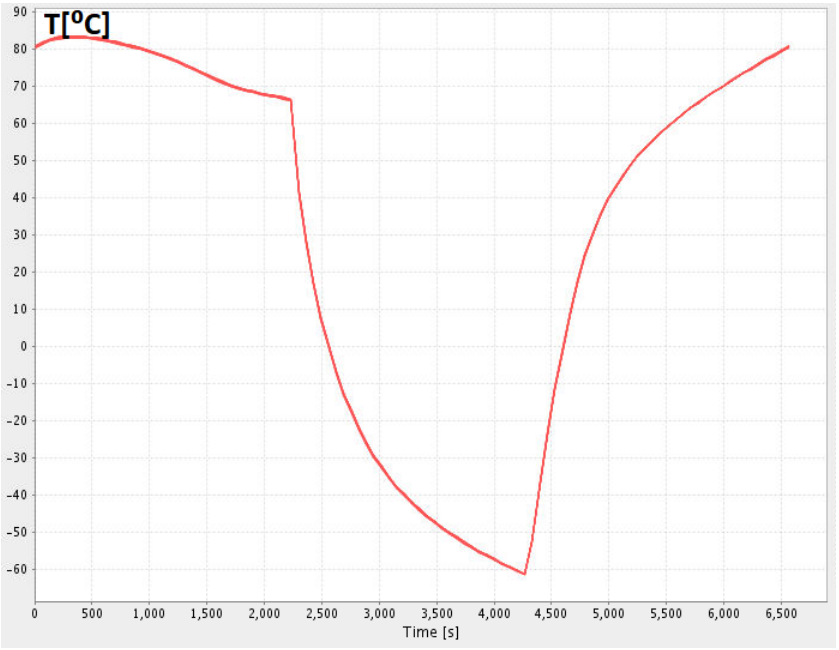

Figure 5.43: CASE 3A OPR: Temperature variation of the middle nodes of all cells of concentrator 1 (middle of the panel).

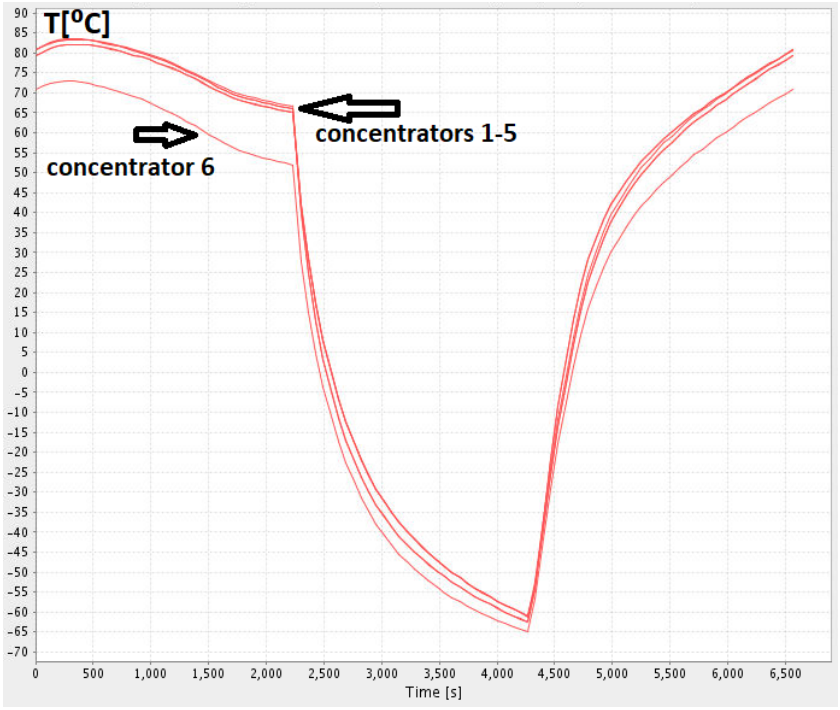

Figure 5.44: CASE 3A OPR: Temperature variation of the middle node of the middle cell for each concentrator (half of the panel, so on 6 concentrators).

– **Case 3B OPR**

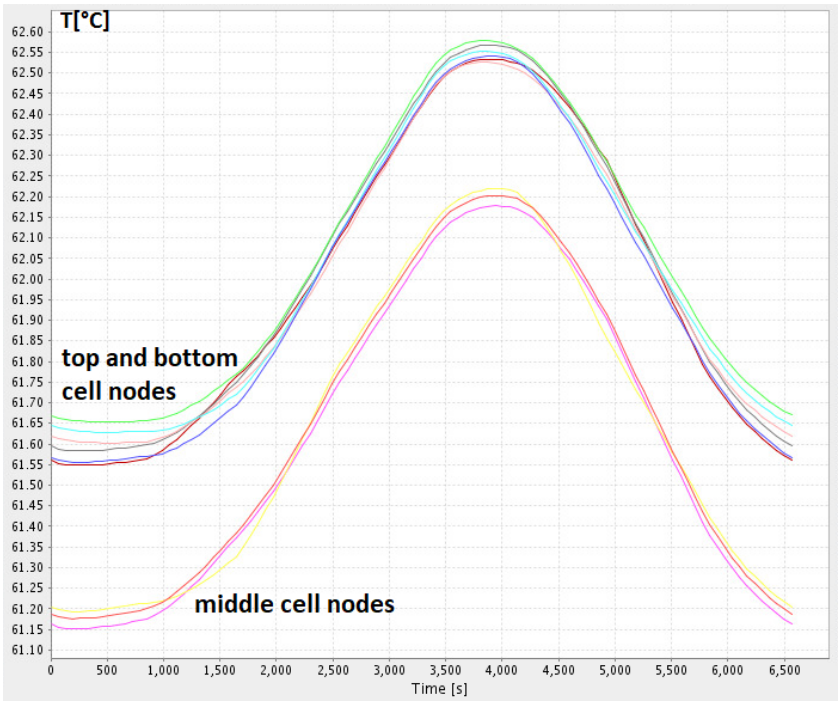

Figure 5.45: CASE 3B OPR: Temp. variation of the **middle cell** nodes of the concentrator number 1 (in the middle of the panel). Note that the temperature change for the nodes does not exceed 1°C.

Fig. 5.45 shows the temperature fluctuation of all the nodes of the middle cell of the concentrator number 1, while Fig. 5.46 depicts additionally the temperature variation of the edge beams and the vertical radiator of the edge concentrator. It can be seen that within

the cell the temperature varies no more than 0.5°C from node to node (note the scale of vertical axis); the middle nodes are found to have slightly less temperature. At around 4000 seconds in orbit the temperature peaks due to the the positioning effects as discussed earlier in *Case 2B COLD*. Fig. 5.46 shows the temperature variation of the edge beams and the vertical radiator (due to the same effects as in *Case 2B COLD*. The coolest temperatures are reached at the vertical radiator (-7.5°C) when it is farthest from the Earth (at around 4500 seconds). In this case the maximum cell temperature is lower than in *Case 3A OPR* due to lower effect of the albedo because of change of orbit.

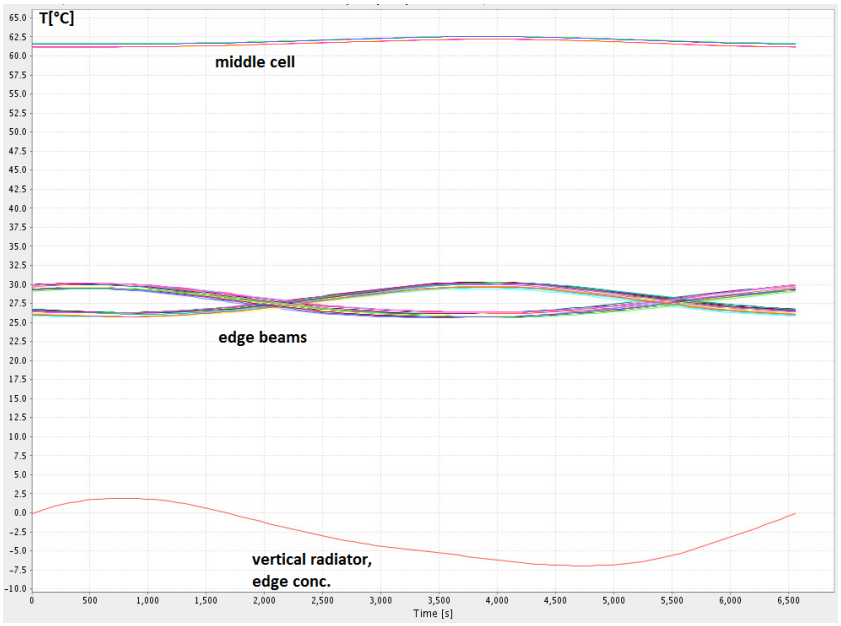

Figure 5.46: CASE 3B OPR: Temp. variation of the middle cell nodes compared to that of edge beams and the edge node of the vertical radiator.

– **Case 3C OPR**

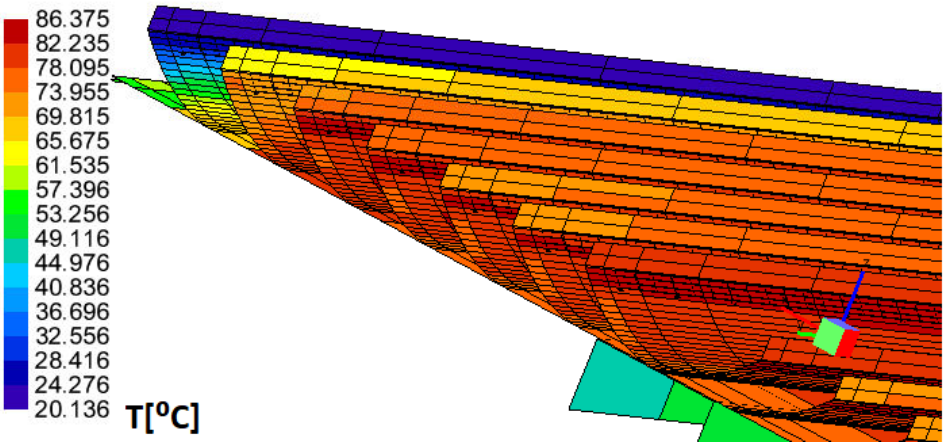

Figure 5.47: CASE 3C OPR: Temperature distribution at the hottest location in orbit (400 seconds).

Similar to Fig. 5.42 temperature distribution for this case is depicted in Fig. 5.47, with similar values also. The difference is in coating reflectivity value being lower in this case (EOL). Hence, the panel temperature increased slightly (by ~2°C) due to increased absorptivity.

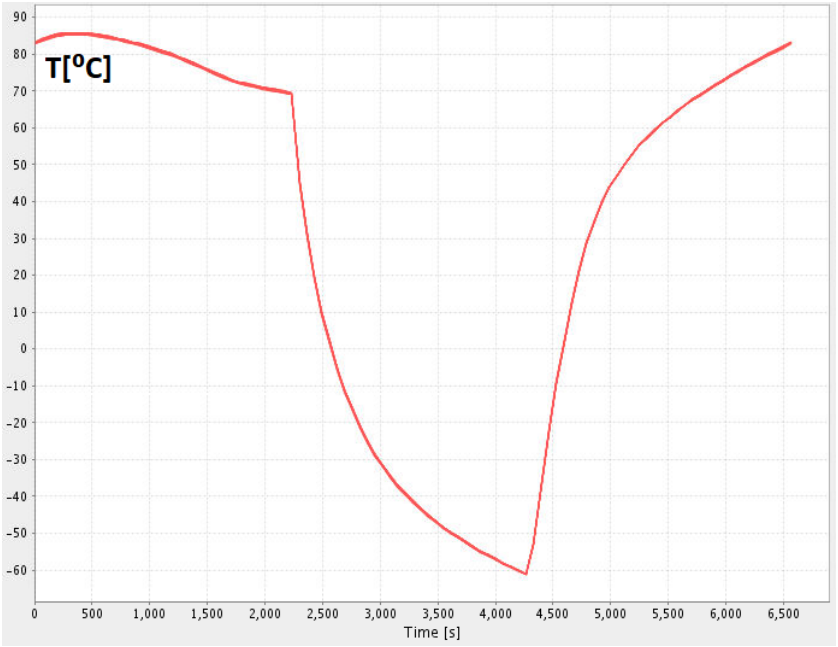

Figure 5.48: CASE 3C OPR: Temperature variation of the middle nodes of all cells of concentrator 1.

– **Case 3D OPR**

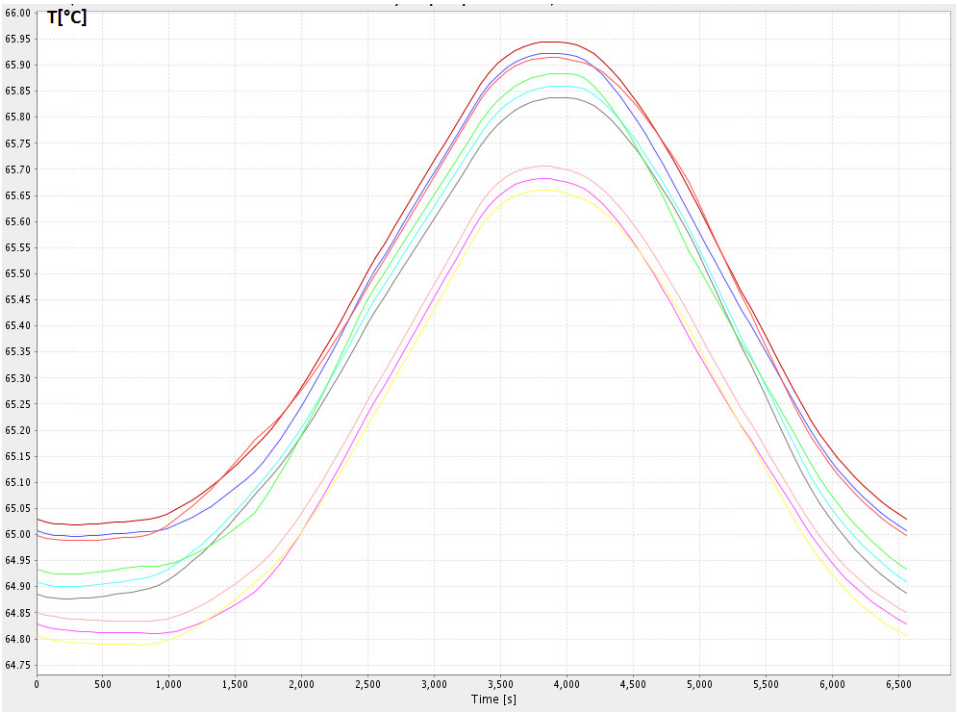

Figure 5.49: CASE 3D OPR: Temperature variation of the nodes of **middle** cell of the concentrator 1. Note that the temperature for all nodes does not vary more than 1°C.

The temperature variation of the nodes of the middle cell of concentrator 1 is shown in Fig. 5.49. Compared to the temperature distribution in *Case 3B OPR* in Fig. 5.45 it can be seen that the temperature increased by ~4°C. The decrease in reflectivity results in increase in absorptivity, hence the concentrator will warm up more from the front side at EOL conditions. Hence, the cell temperature also increases. The difference between the nodal temperature

within the cell in this case is less than 0.5°C (note the scale of the vertical axis), and the increase in temperature around 4000 seconds is less than 1°C increase, hence insignificant.

The temperature variation of the node number 4 of the edge cell of all concentrators can be seen in Fig. 5.50. The curve with the highest temperature belongs to the cell that is located closest to the middle of the panel. The cells further away from the centre experience cooler temperatures due to having a larger view factor and hence being able to radiate the heat more effectively. The two coolest curves represent the temperature variation of the two edge concentrators which do not have cells. The temperature fluctuation around 1500 and 4500 seconds in Fig. 5.50, as previously, can again be attributed to the changing S/C position with respect to the Earth, hence due to the changing Albedo and planetary effect on the edges of the panel. Similarly to Fig. 5.50 the temp. variation of the middle node of the middle cell of all concentrators is shown in Fig. 5.51. Similar thermal behavior is observed. It can be seen that the temperature of middle cells in Fig. 5.51 is slightly higher (by ~0.7°C) than that of the edge cells in Fig. 5.50, which happens due to the edge effects - objects located closer to the edge of the panel have a higher view factor, hence they radiate the heat more effectively, but still insignificant amount in this case.

The temperature variation throughout the orbit of the edge beam, vertical radiator and the middle cell is shown in Fig. 5.52. As compared to the same figure in *Case 3B OPR* the increase in temperature can be observed by 6°C for the middle cell and the edge beams, and 10°C for the vertical radiator. As mentioned before, this increase can be attributed to the increase in absorptivity of the concentrator coating material.

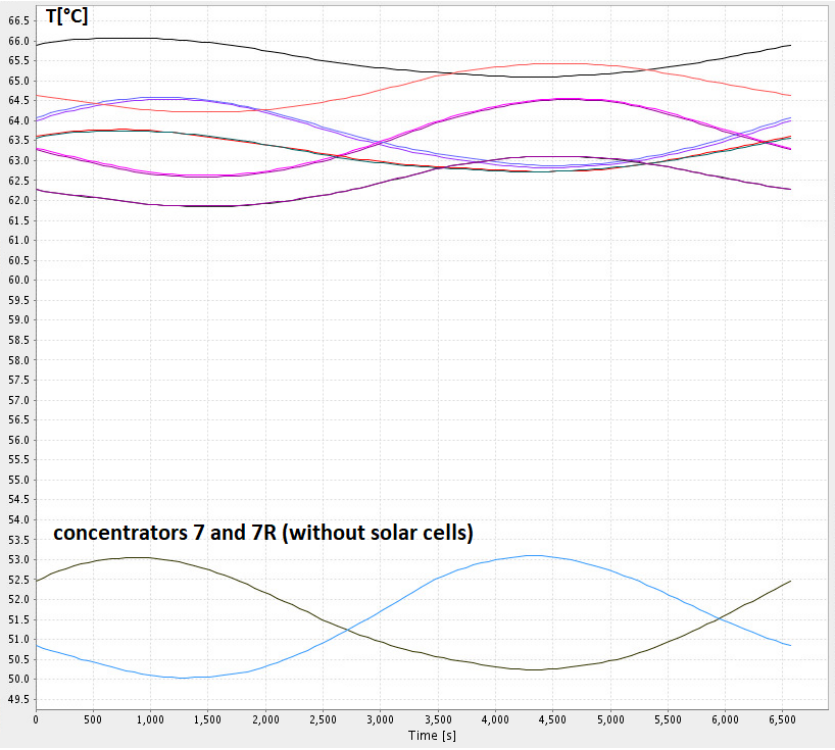

Figure 5.50: CASE 3D OPR: Temperature variation of the node 4 of the **edge** cell of all concentrators (hence, 14 curves) throughout the orbit.

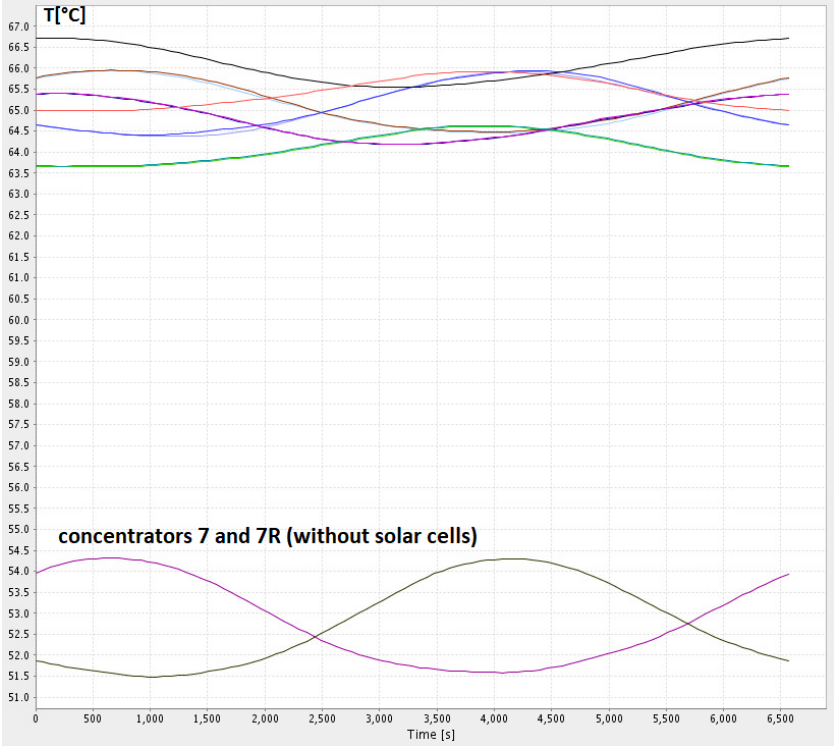

Figure 5.51: CASE 3D OPR: Temperature variation of the node 8 of the **middle** cell of all concentrators (hence, 14 curves) throughout the orbit.

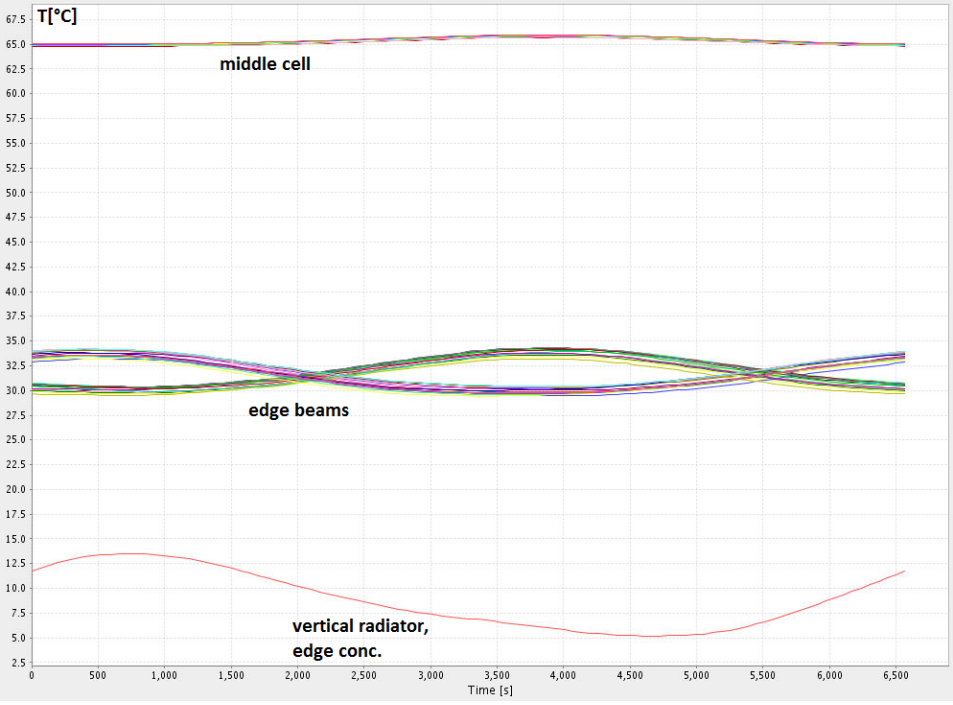

Figure 5.52: CASE 3D OPR: Temperature variation throughout the orbit of edge beam nodes, vertical radiator edge nodes and the middle cell in the middle of the panel, for comparison.

MISALIGNMENT CASES

- **Case 4A MIS-HOT**

Due to the misalignment angle both panel sides experience different illumination, hence the temperature distribution slightly varies from side to side, as can be seen in Fig. 5.53. Note that "R" side in this figure is the left side of the panel. As depicted in Fig. 5.55 on the "R" side of the panel the 5° misalignment causes the reflected sunlight to be concentrated onto the vertical radiator, hence the highest temperatures are observed there and not at the cells. However, as seen in Fig. 5.54 on the other side of the panel the reflected light falls onto the concentrator part below the cell, hence the highest temperatures on that panel side are reached below the cells (partly at the diode). From the figures so far it can be concluded that the misalignment of 5° creates a big difference since much less light is hitting the solar cell, which points out the extreme sensitivity of the design to this much of the pointing offset.

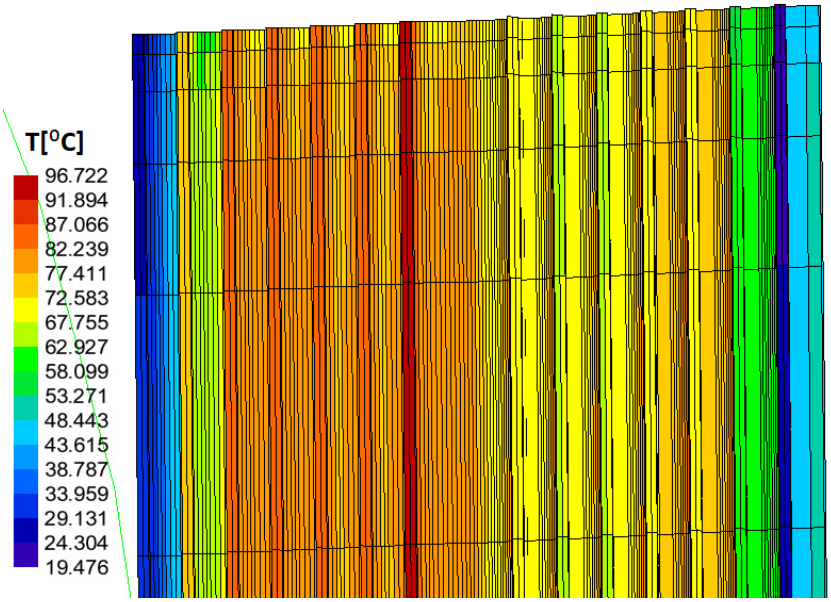

Figure 5.53: CASE 4A MIS-HOT: Temperature distribution over the front side of the panel when in orbit, position 1 (left side being side "R").

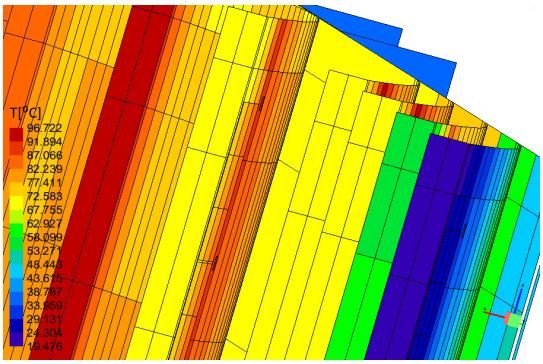

Figure 5.54: CASE 4A MIS-HOT: Temperature distribution over the front side of the panel when in orbit, position 1.

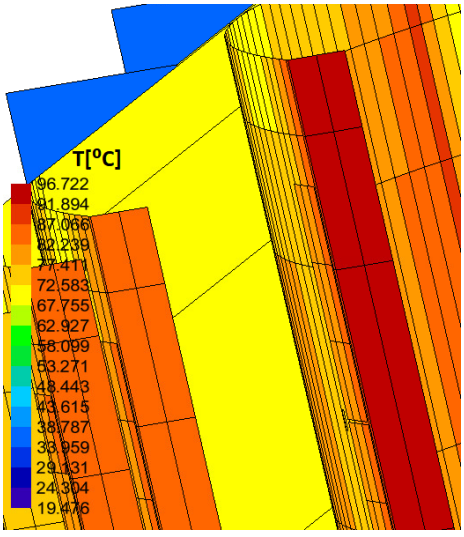

Figure 5.55: CASE 4A MIS-HOT: Temperature distribution over the front side of the panel when in orbit, position 1; panel side "R".

The temperature variation of all nodes of the middle cell is shown in Fig. 5.56, black lines representing its variation of the nodes on ”R” side of the panel, and red lines - of the opposite side. As seen in previous figures, the bottom cell part on the panel side opposite of the ”R” side is exposed to significantly more sunlight than the other parts of that cell or the cells on ”R” side, hence the cell temperature at that location is highest (the upper most curve in red color) reaching 85°C. However, (not shown in the figure) the maximum panel temperature on that side of the panel is experienced by the diodes and not cells, due to misalignment: 97°C. The diodes being small can easily heat up quickly, hence it is important to attach the diode to the PG thermal doubler (as well as the cells) to reduce their temperature. This step was not accounted for in the modelling.

There is slight variation in the temperature throughout the orbit for all nodes (less than 0.5°C, note the vertical axis scale). This can be explained by the fact that throughout the orbit the view factor of each panel side with respect to Earth is changing. Hence, the mild temperature changes (or $\pm 1^{\circ}$) can be attributed to the planetary effects.

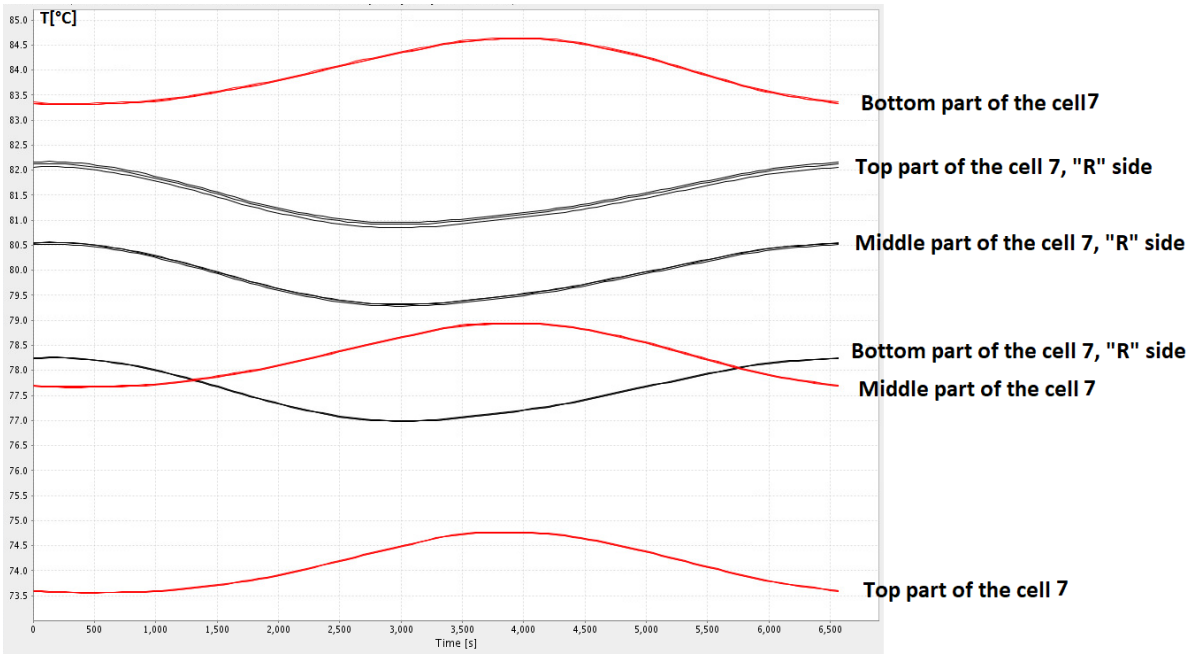

Figure 5.56: CASE 4A MIS-HOT: Temperature variation throughout the orbit of **cell 7 nodes** (black - ”R” side of the panel, red - the other side).

– **Case 4B MIS-OPR**

The temperature distribution over the front side of the panel can be seen in Fig. 5.57. When compared to the temperature gradients in *Case 4A MIS-HOT* it can be seen that with lower solar flux (SS in this case instead of WS in *Case 4A MIS-HOT*) and lower albedo (0.33 instead of 0.4) the maximum panel temperature decreased by ~16° (at the diode).

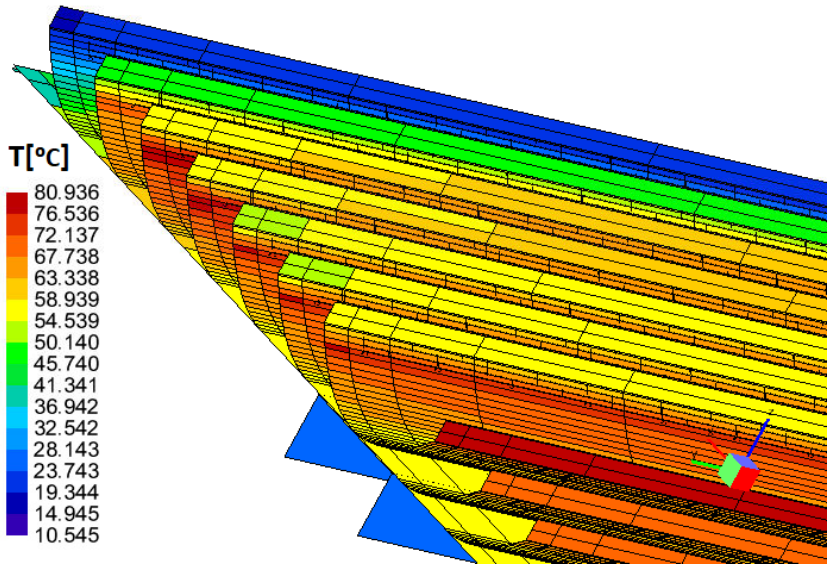

Figure 5.57: CASE 4B MIS-OPR: Temperature distribution over the front side of the panel, hottest location.

– **Case 4C MIS-HOT**
In this and next case the panel is tilted by 30°. Fig. 5.58 depicts temperature distribution over the front surface of the panel. It can be seen that with 30° misalignment angle the panel's highest temperature reaches 68.5°C (the solar cells). The cells reach the same temperature in case with no misalignment (with slightly lower albedo, solar flux and Earth temp. in *Case 3D OPR*), hence the misalignment has no effect on temperature, but rather on illumination pattern.

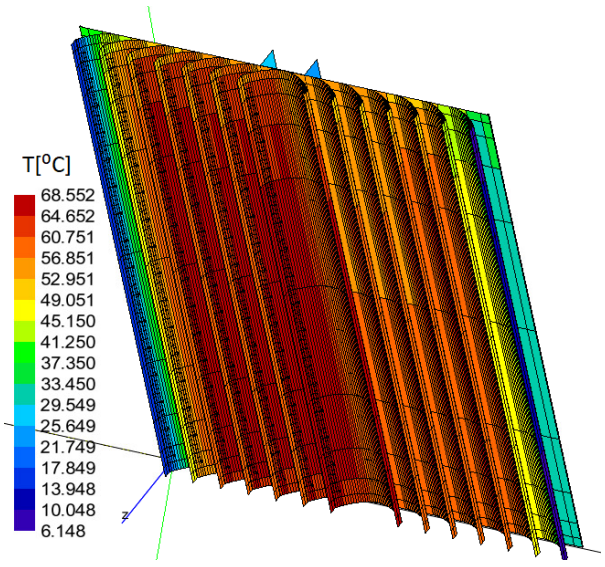

Figure 5.58: CASE 4C MIS-HOT: Temperature distribution over the front side of the panel under 30° misalignment.

Fig. 5.59 depicts temperature distribution of the middle nodes of all cells on concentrator 1 (middle of the panel). Due to the panel being tilted it was expected that the edge cells of each concentrator would experience less solar flux (and more on the opposite side of the concentrator) which would result in lower and higher temperatures. However, because there is a considerable amount of gap between the cell and the edge of the panel, the misalignment does not seem to affect the temperature of the cells. Between all cells it deviates (maximum) by 3°C which is insignificant.

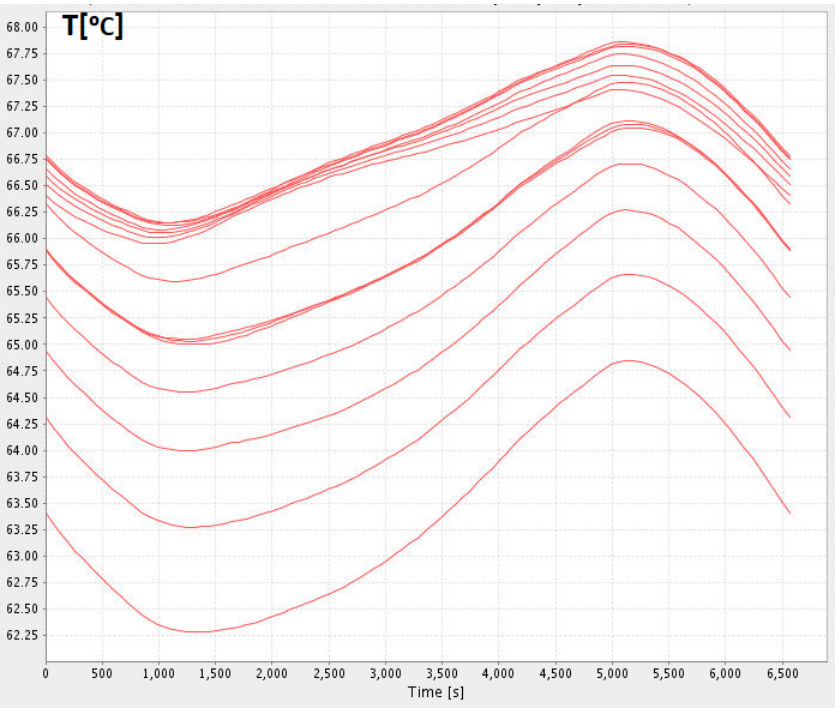

Figure 5.59: CASE 4C: Temperature variation of the middle nodes of all cells on concentrator 1 (middle of the panel).

– **Case 4D MIS-OPR**

In this case the temperature Fig. 5.60 and 5.43 are comparable to the ones in *Case 4C MIS-HOT* with the difference of some environmental parameters. The temperatures here are lower due to less solar illumination and lower albedo and planet temperature.

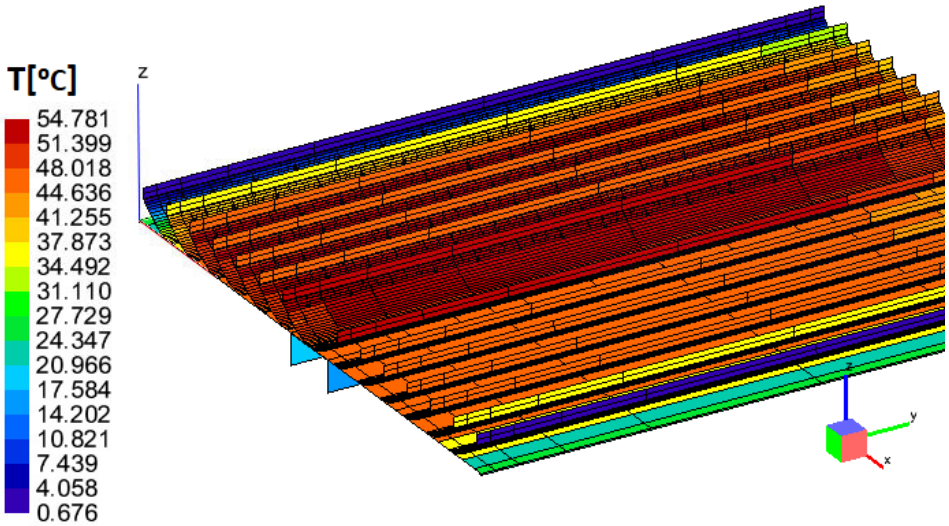

Figure 5.60: CASE 4D: Temperature distribution at the hottest location in orbit.

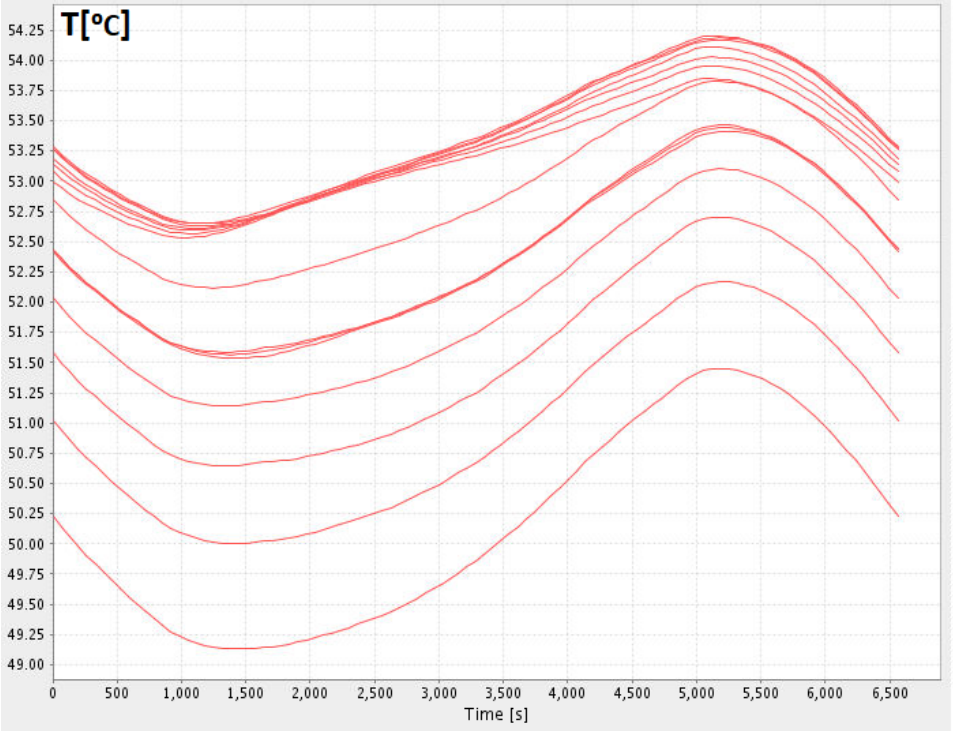

Figure 5.61: CASE 4D: Temperature variation of the middle nodes of all cells of concentrator 1.

5.4.2. Absorbed Flux

REST HEAT QR

As mentioned before, the rest heat source in this *ESATAN* model represents the amount of heat that is dissipated due to the energy conversion of the solar cells. Fig. 5.62 shows the QR changes over one orbit revolution. It is depicted for a single cell only (with 9 nodes, hence 9 curves), because the QR values and distribution is nearly the same for all cells on all concentrators. It mostly varies within each cell as the amount of incoming flux there varies due to imperfections in the geometrical reflection of the light from concentrators. It is, unfortunately not yet clear whether this is due to the nature of geometry or modelling imperfections. At the start of the orbit the panel is illuminated and solar cells produce electrical power (each node in the order of 0.15 - 0.21 $[W]$). During eclipse as expected QR is zero because there's no illumination, hence no heat dissipation until $\pm$4500 seconds when the panel leaves the eclipse again and begins to produce power. Note that Fig. 5.62 represents the radiative *Case 1D HOT* - the hottest case in orbit with solar cells turned ON.

Fig. 5.63 depicts the QR variation throughout the orbit for Radiative *Case 2A COLD*. When compared to the Fig. 5.62 it can be seen that no major differences occur despite the changes in albedo, solar flux, planet radiation and reflectivity parameters. The case in Fig. 5.63 has a lower albedo, lower planet radiation, lower incoming solar flux - which all lead to lower QR. However, the BOL property of the reflective coating has a higher value that at EOL (0.95 for BOL, 0.85 for EOL), which surpasses all above mentioned changes. Hence, as a result QR can be seen to not vary almost at all for both cases.

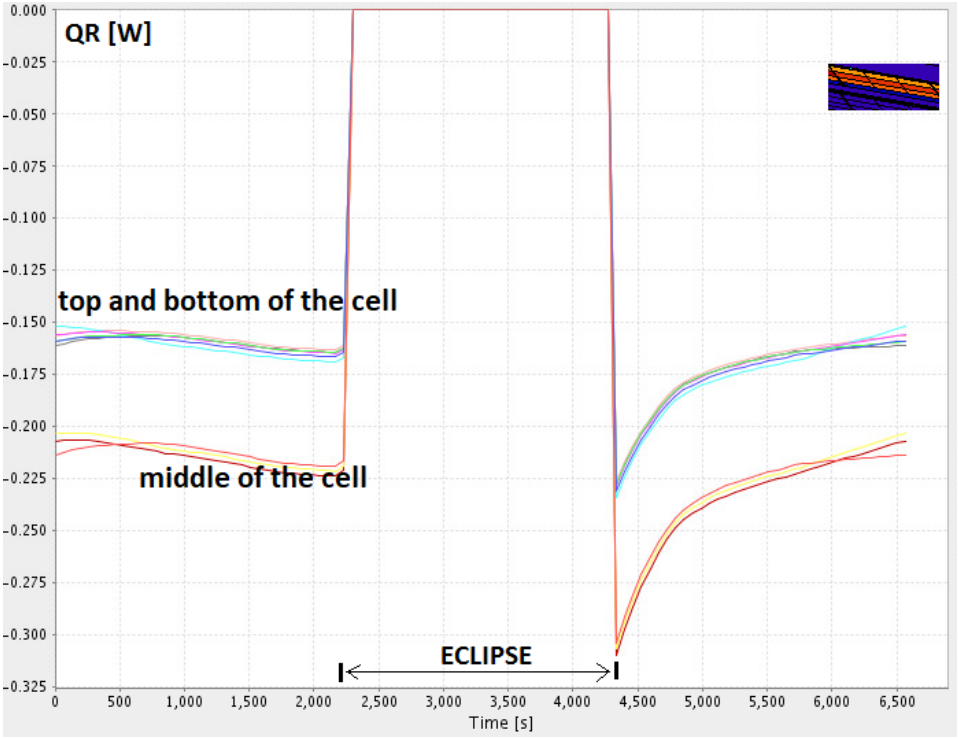

Figure 5.62: CASE 1D HOT: Amount of dissipated power as the rest heat (QR) throughout the orbit.

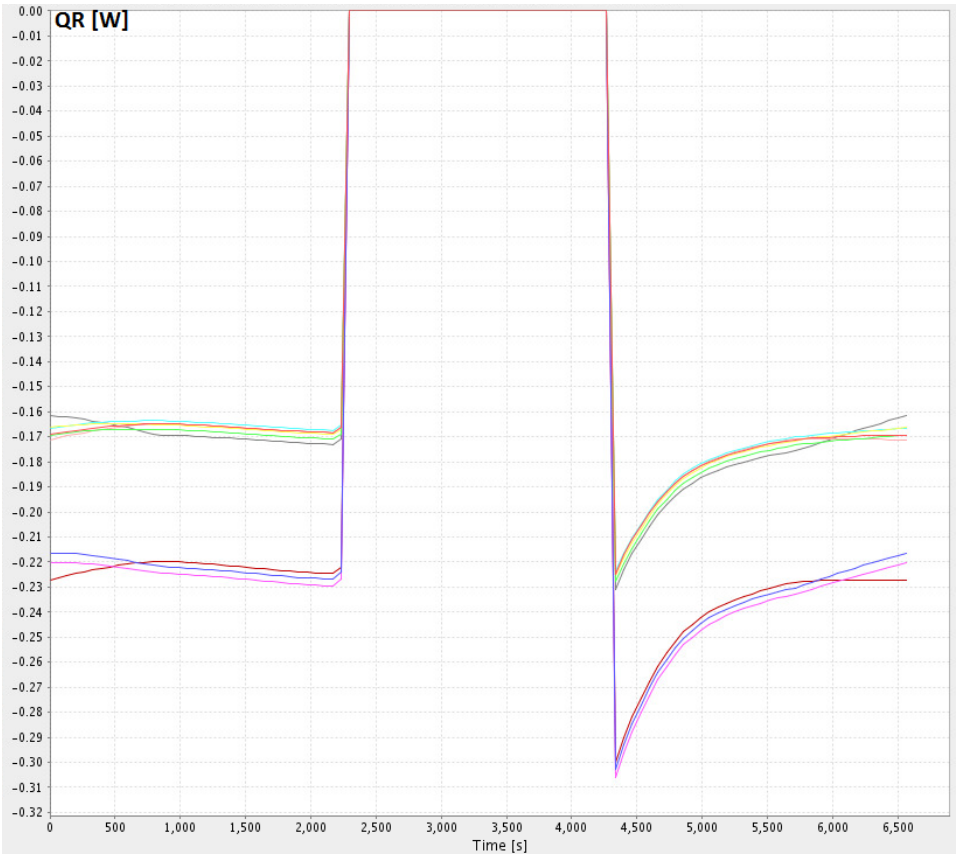

Figure 5.63: CASE 2A COLD: Amount of dissipated power as the rest heat (QR) throughout the orbit.

ALBEDO QA

Fig. 5.64 depicts the absorbed albedo energy by one of the solar cell nodes throughout one revolution around the Earth (without eclipse period). As can be seen, the albedo energy absorbed by the solar cell increases linearly until it peaks at 1500 seconds, after which it drops and again increases to another peak at 5000 seconds. The peaks (however low) happen to occur at when the S/C passes by the poles of the Earth, while the lowest drop occurs when the S/C is above the equator.

This behavior can be explained by the fact that the albedo at the poles is higher than at the equator due to snow and ice that reflect more solar light. The amount of absorbed albedo energy changes slightly from case to case due to variable solar intensity and concentrator coating reflectivity, but in general for orbits of 90° right ascension angle the two peaks and the sudden drop will all occur at the same time as in Fig. 5.64. For 0°C right ascension orbit (with eclipse) the absorbed albedo distribution is as shown in Fig 5.65 with similar peaks and zero during eclipse.

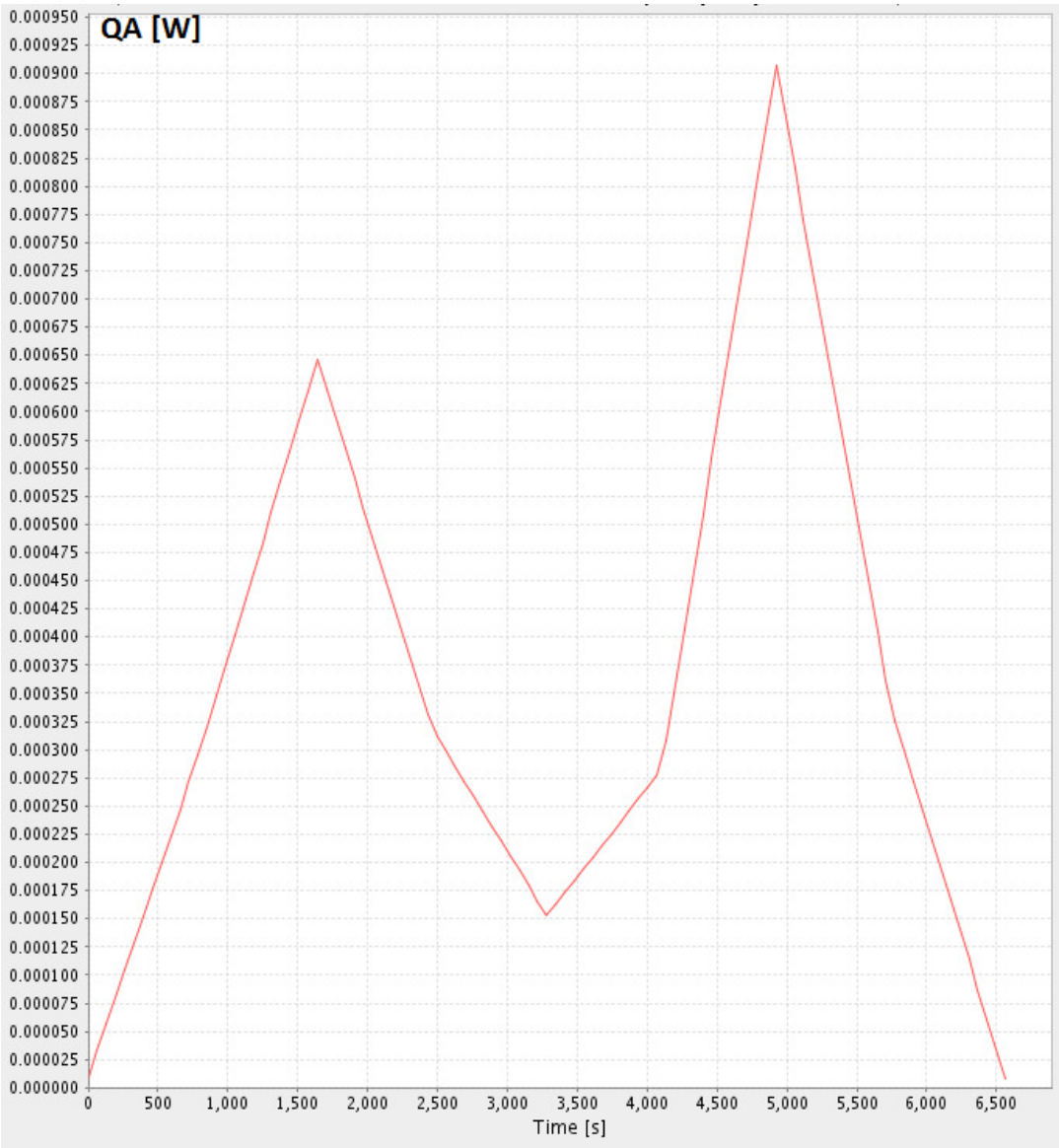

Figure 5.64: CASE 2B COLD: Amount of absorbed albedo energy by one of the cell nodes as a function of time in orbit (90° right ascension orbit).

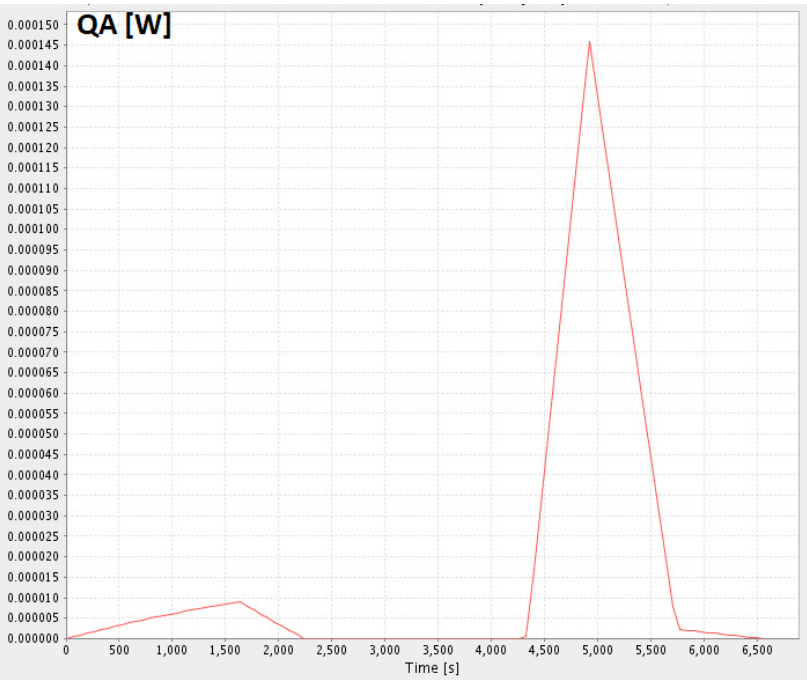

Figure 5.65: CASE 2A COLD: Amount of absorbed albedo energy by one of the cell nodes as a function of time in orbit (0° right ascension orbit)

COMBINED

– **Nominal pointing**

Fig. 5.67 and 5.66 depict the amount of solar and albedo flux absorbed by the cell nodes in *Cases 1D HOT and 3A OPR*. As can be seen for each cell the middle nodes receive more illumination than the bottom and the top nodes. Solar cell middle nodes receive (Fig. 5.67) $\pm$ 5800 W/m^2 while the top and bottom only $\pm$ 4300 - 5000 W/m^2. Uneven cell illumination might cause problems in power conversion, which is why it is advisable to do testing. Even more so, uneven illumination of the cells that are connected in series can cost in power production, since the total string current is defined by the lowest current in one of the cells.

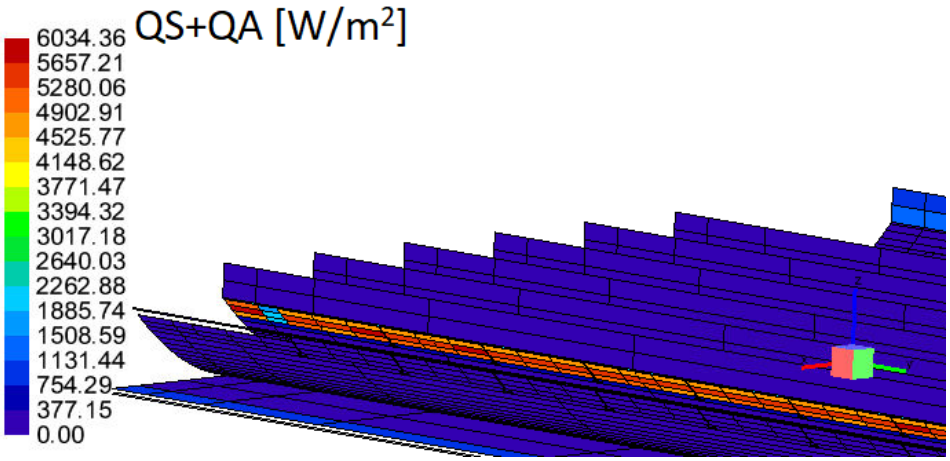

Figure 5.66: CASE 1D: Absorbed solar and albedo flux distribution over the cell nodes.

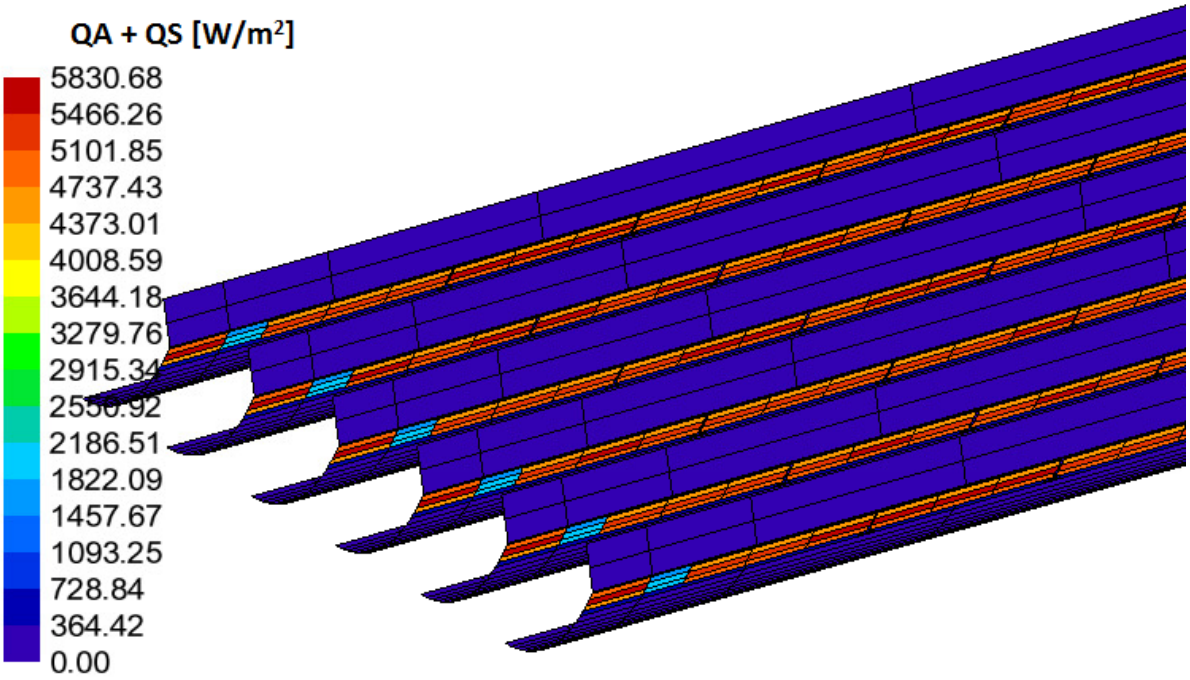

Figure 5.67: CASE 3A OPR: Absorbed solar and albedo flux distribution over the cell nodes. Note that the flux on the edge (in blue color) does not fall onto the solar cell, and, moreover, is an inaccurate calculation due to nodal mismatch at that location.

Figures 5.68 and 5.69 depict the solar, albedo and planetary absorbed amount of heat throughout the orbit by the cells. In Fig. 5.68 the absorbed heat by the edge and middle cells (cells 1, 7 and 15) middle nodes (node 8) of the concentrator 6 (at the panel edge) is plotted (3 lines). It can be seen that the amount of absorbed heat does not vary considerably with the cell location, by about 0.03 W which is a 4% error if the difference is ignored. Also it does not vary with concentrator location, which makes sense since the entire panel is receiving equal illumination everywhere. In Fig. 5.69 the absorbed heat by the middle cell (cell 7) of the concentrator 6 is plotted (9 nodes). From last few figures it can be seen that there is much more variation in the absorbed heat flux (and hence in power) within each cell (between the cell nodes), rather than between the different cells. It can be seen that the amount of energy absorbed by the middle cell nodes and the edge cell nodes is the same, with more energy fluctuations in the nodes of the middle cell.

This agrees with the conclusion drawn previously that there appears to be very little variation between the amount of absorbed heat between the different cells, and more variation within the cells themselves, however the temperature within the cells remains constant despite variation in the solar flux. Both figures show how little is the amount of QE and QA when compared to QS, and therefore do not influence the thermal behavior of the panel significantly.

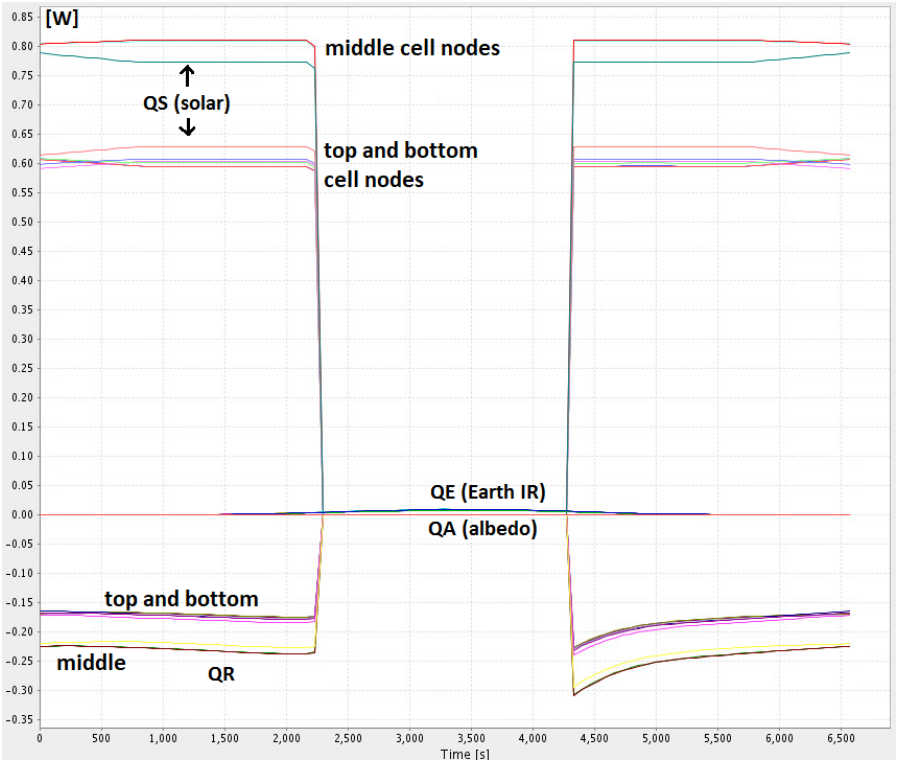

Figure 5.68: CASE 3A OPR: Absorbed solar, albedo and (dissipated) rest heat variation throughout the orbit of the **middle cell**, concentrator number 6 (0° right ascension angle).

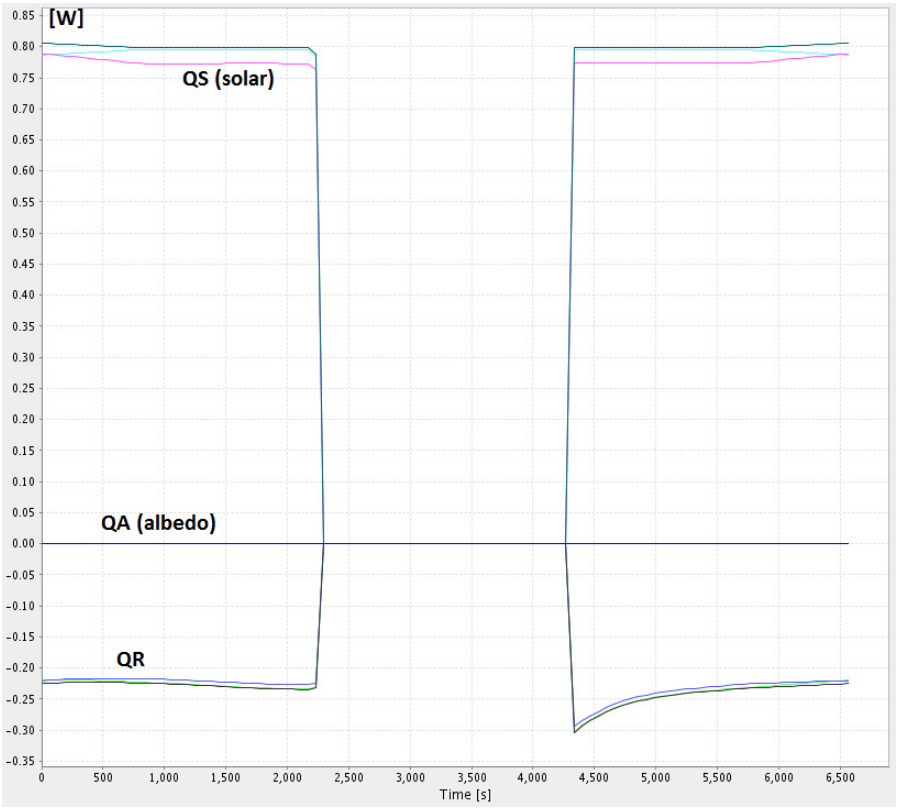

Figure 5.69: CASE 3A OPR: Absorbed solar, albedo and (dissipated) rest heat variation throughout the orbit of the **edge cell**, concentrator number 6 (0° right ascension angle).

To compare with Fig. 5.68, Fig. 5.70 depicts the absorbed solar and rest heat by the same cells for an orbit with no eclipse period. The amount of absorbed heat is exactly the same for both with the only difference in absence of eclipse period in Fig. 5.70.

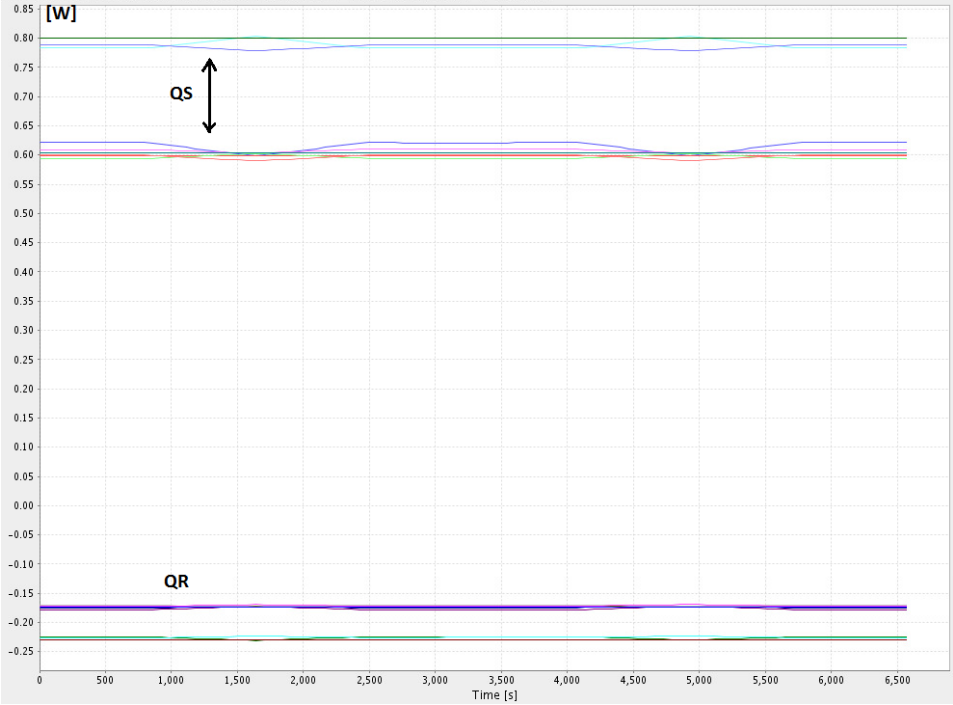

Figure 5.70: CASE 3B OPR: Absorbed solar and dissipated rest heat by the nodes of the **middle cell** of the concentrator number 1 (middle of the panel) (90° right ascension angle).

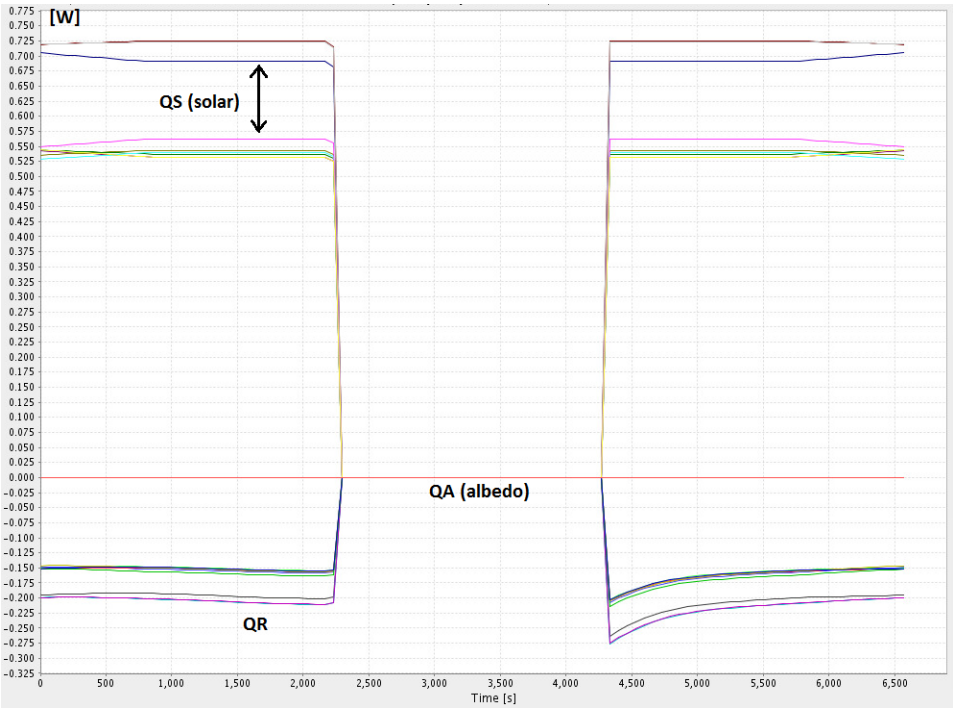

Figure 5.71: CASE 3C OPR: Absorbed amount of solar, albedo and (dissipated) rest heat by the nodes (9 nodes) of the **middle** cell of the concentrator 6 throughout the orbit (0° right ascension angle).

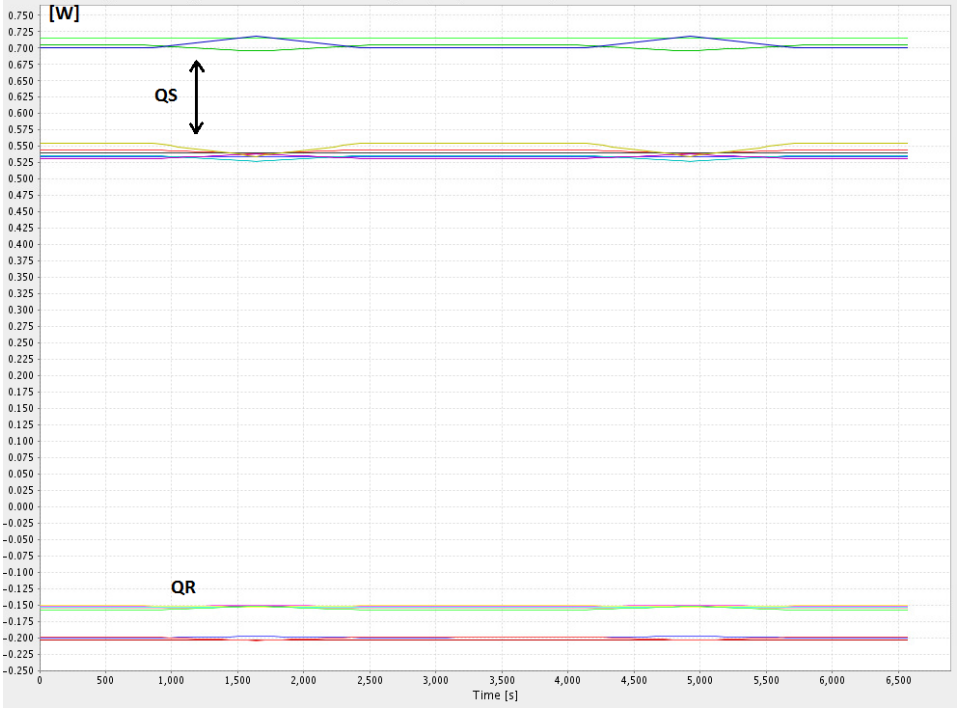

Figure 5.72: CASE 3D OPR: Absorbed amount of solar heat and dissipated rest heat by the nodes (9 nodes) of the **middle** cell of the concentrator 1 throughout the orbit (90° right ascension angle).

Figure 5.71 shows the amount of heat absorbed (and dissipated as QR) by the nodes of the **middle cell** of concentrator 6. When comparing to the results of *Case 3A OPR* the reduction in QS (from 0.8 W and 0.6 W to 0.7 W and 0.55 W) and QR absolute value can be seen. This is what happens as the concentrator coating reflectivity drops from 0.95 to 0.85. Less light is reflected onto the cell, which results in lower incoming flux, which leads to less power dissipation and less power absorption.

Fig. 5.72 depicts QS and QR by the nodes of the middle cell of the concentrator 1. Compared to the values obtained in **Case 3B OPR** it can be seen that the QS and QR are reduced similarly to the reduction of values in *Case 3C OPR* when compared to *Case 3A OPR*. The difference is due to varied coating reflectivity values (higher reflectvity (BOL) allows more light to be absorbed by the solar cell).

– **Misaligned cases**

Figures 5.73 and 5.74 depict the solar and albedo flux distribution by the cells located in the middle of the concentrator, close to the edge of the panel. On the ”R” side of the panel (Fig. 5.74) it can be seen that a lot of light falls onto the vertical radiator due to the misalignment, hence the lower part of the cell is receiving very little sunlight, nearly 5 times less than the middle and the upper parts of the cell. Fig. 5.73 shows that the opposite occurs on the other side of the panel: the lower part of the cell receives nearly 10 times more light than the upper cell part, and 3 times more light than the middle part. Comparing both sides to each other, the highest amount of flux received by the cell on ”R” side of the panel ($\sim$ 3.5 suns) is roughly two times less than the maximum received by the other panel side ($\sim$ 7 suns) which is an increase compared to the nominal pointing (4.5-5.5 suns as in Fig. 5.67). This means that the amount of power produced by both sides will most likely vary significantly. Electrically this means that the amount of current will differ on both sides of the panel which may affect amount of power produced.

Due to symmetry the amount of solar and albedo flux received and absorbed by concentrator 6 is the same as for other concentrators on the same side of the panel. Similarly, the amount absorbed on the other side of the panel is the same for all concentrators located on that side.

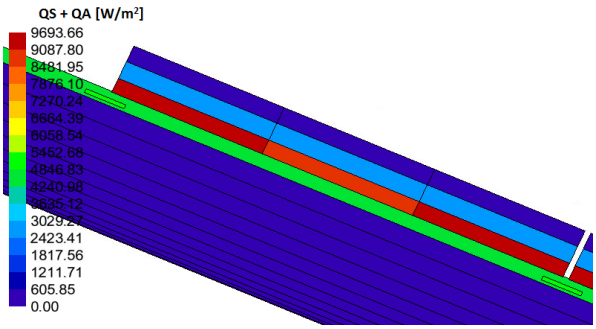

Figure 5.73: CASE 4A MIS-HOT: The distribution of absorbed **solar and albedo** flux by the solar cell number 7 (middle of the concentrator) of concentrator 6.

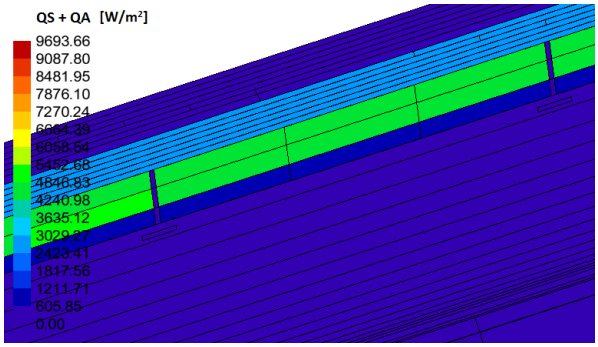

Figure 5.74: CASE 4A MIS-HOT: The distribution of absorbed **solar and albedo** flux by the solar cell number 7 (middle of the concentrator) of concentrator 6R ("R" side).

Having decreased the solar flux, albedo and planetary flux intensity Figures 5.75 and 5.76 of *Case 4B MIS-OPR* can be compared to those of *Case 4A MIS-HOT*. QS and QA from *HOT* to *Operational* conditions are reduced by roughly 13%.

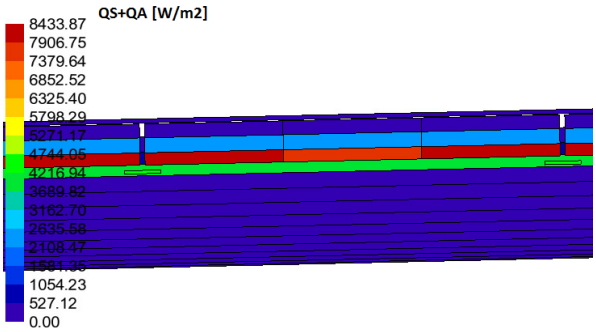

Figure 5.75: CASE 4B MIS-OPR: The distribution of the sum of absorbed **solar and albedo** flux by the solar cell number 7 (middle of the concentrator) of concentrator 6.

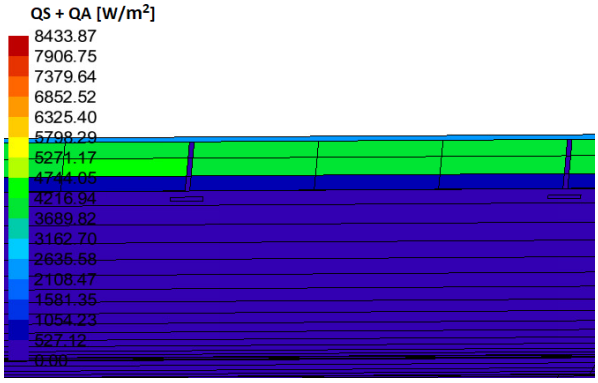

Figure 5.76: CASE 4B MIS-OPR: The distribution of absorbed **solar and albedo** flux by the solar cell number 7 (middle of the concentrator) of concentrator 6R ("R" side of the panel).

The sum of absorbed solar and albedo heat flux distribution over the panel under the 30° misalignment angle can be seen in Fig. 5.77 (with the last concentrator hidden). When compared to the amount of solar and albedo flux absorbed by the cells on the panel that is perfectly aligned (Fig. 5.67 of *Case 3A OPR*), the heat flux distribution is decreased by ~11%. However, the two compared cases are not identical in terms of input parameters, which is why 11% is an overestimation. However all parameters are the same as in *Case 1D HOT* (apart from orbit). Compared to Fig. 5.66 the absorbed flux is less most likely due to less albedo. It can be seen from Fig. 5.77 that despite the panel tilt of 30° the edge cell is fully illuminated. This might be due to the fact that the first edge cell is located 4 cm away from the edge.

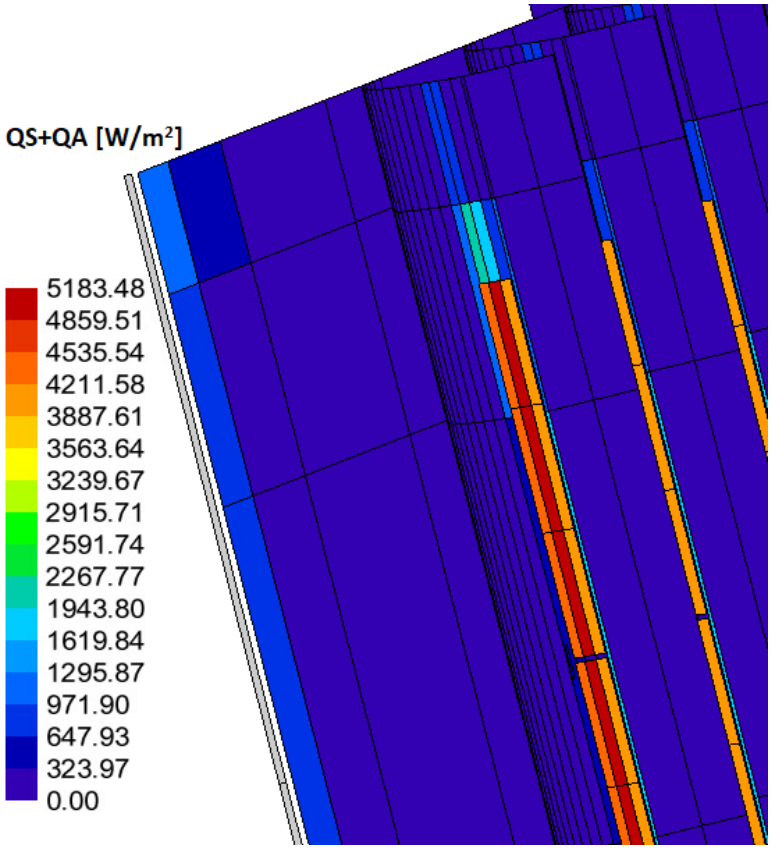

Figure 5.77: CASE 4C MIS-HOT: The distribution of absorbed **solar and albedo** flux by the edge cells of edge concentrators (top part - inclined towards the Sun).

5.4.3. Panel Tilt Effect on Electrical Power

The electrical power in Chapter 3 has been calculated for the case of the panel facing the Sun perfectly perpendicularly. However it may face the Sun in reality tilted around two different axis. As can be seen from Fig. 5.79 the misalignment of 30° around the x-axis causes very little variation in the absorbed solar flux, hence it is safe. However, a small tilt of 5° around the y-axis causes too much mismatch of the absorbed flux throughout the cell.

The absorbed flux results by the solar cells for cases with panel misalignment are summarized for each node of the cell in Fig. 5.78, 5.79 and 5.80 using the values depicted in Figures 5.67, 5.73, 5.74, 5.75 and 5.76.

CASE 3A OPR [W/m²]

4200	4200	4200
5500	5830	5500
4500	4500	4500

Figure 5.78: Absorbed flux values by the solar cell nodes in case of nominal pointing.

CASE 4C HOT, 30° tilt [W/m²]

3800	3800	3800
5200	5200	5200
4300	4300	4300

Figure 5.79: Absorbed flux values by the solar cell nodes under 30° tilt.

CASE 4A HOT, 5° tilt [W/m²]

1000	1000	1000
3500	3500	3500
9700	8500	9700

CASE 4A HOT, 5° tilt [W/m²]

5000	5000	5000
5000	5000	5000
1000	1000	1000

CASE 4B OPR, 5° tilt [W/m²]

900	900	900
3000	3000	3000
8433	8000	8433

CASE 4B OPR, 5° tilt [W/m²]

4500	4500	4500
4500	4500	4500
800	800	800

Figure 5.80: Absorbed flux values by the solar cells nodes at each half of the panel under 5° misalignment. Upper row: hot conditions, lower row: operational conditions.

It can be seen from the numbers above that the misalignment of 5° may cause some problems in generating optimum amount of electrical power, when compared to nominal pointing case and 30° misalignment case around another axis. In both cases the tilt induces extreme solar flux variation throughout the cell which may significantly affect the amount of power mainly due to the current that changes directly with the amount of illumination. It is unknown whether the cell would produce as much power as if calculated taking the average illumination into account, hence it is difficult to predict the outcome. However, the solar array drive mechanism (SADM) will be responsible for correcting the misalignment angle around the y-axis with precision of ≤1°. The flux mismatch will then be much lower, however not calculated in this project.

5.4.4. Summary of Radiative Cases

Table 5.27: Radiative cases - summarized results.

Case	**Cell OPR temp. [°C] (Max|Min, middle to edge)**	**Cell min. temp. (edge) [°C]**	**Panel temp. [°C] (Max|Min, middle to edge)**
1a Hot	122|100 to 110|85	-61	107|-60 to 80|-70
1a Hot ZERO ALBEDO	104|102 to 85|80	-61	87|-60 to 55|-68
1b Hot	100|97 to 85|78	78	85|84 to 55|50
1c Hot (rear illuminated)	105|-45 to 95|-50	NR	109|-45 to 100|-50
1d Hot	105|83 to 95|68	-62	95|-58 to 74|-68|
2a Cold	74|65 to 64|50	-69	65|-65 to 43|-74
2b Cold	61|60 to 50|45	45	51|50 to 28|25
2c Cold (rear illuminated)	83|78 to 75|70	-58	86|-60
3a OPR	83|66 to 73|52	-65	74|-62 to 54|-71
3b OPR	62|61 to 52|46	46	52|51 to 30|26
3c OPR	86|70 to 75|55	-65	77|-61 to 57|-71|
3d OPR	66|65 to 56|50	50	56|55 to 34|30
4a MIS-HOT	97|63 (diode)	63	71|70 to 40|35
4b MIS-OPR	81|50 (diode)	50	58|57 to 29|26
4c MIS-HOT	69|66 to 56|48	48	58|55 to 36|31
4d MIS-OPR	55|52 to 40|35	35	45|43 to 26|21

5.5. Additional Remarks/Assumptions

- For end-of-life configuration of the solar array the only property changed is the concentrator coating optical properties. Hence, it is assumed that the rest of the material properties do not change significantly with time.
- Wiring harness is not taken into account in thermal analysis because, as discussed with *Airbus* experts (N. v.d. Pas) a couple of very thin wires will not change the thermal behavior of the model significantly.
- In the middle of the panel (as can be seen in the electrical design drawings) there is a hole (4 cm diameter) to accommodate the hold down structure during the panel stowage phase. For the thermal analysis this was not modelled, as it was assumed to not have significant influence on the temperature distribution profile. However, since the structure will increase the heat capacitance the current analysis will likely show more extreme temperatures.
- In this thesis the PG conductivity is assumed to remain constant with temperature, and its value was taken at $\pm$100°C. As can be seen from Fig. 5.14, the conductivity decreases with temperature exponentially from 1350 W/mK at 100°C to $\pm$1200 W/mK at 220°C. Hence, the conductivity value at 120°C (hottest case) is very close to the one at 100°C. In operational cases (when panel reaches $\pm$ 70°C) the conductivity will be higher, and especially during the eclipse periods it will increase maximum up to $\pm$ 3000 W/mK (at 200 K). This means that the panel during eclipse will cool down more than currently calculated.

6

Cost Analysis

Developing the concentrator solar panel for space applications involves much more complexity and risks. Therefore, the only way to make this innovation successful is to make it an attractive option to clients, offering a cheaper energy solution per Watt than the conventional planar solar arrays. The initial requirement concerning the cost of the array states that the design should result in a minimum of 30-40% lower cost per Watt as compared to the planar solar array.

6.0.1. Cost of Conventional Solar Array

Conventional planar solar array in space nowadays provides electrical power to the S/C with an approximate rate of $\sim$ 1000 $Euro/W$ [3]. In terms of space a 1.2 m^2 planar solar panel with $\sim$270 solar cells (conventional dimension) can deliver $\sim$300 W (honeycomb panel benchmark from the Midterm Report [15]). This amounts to **250** W/m^2. The cost of a single wafer is 800 $Euro$ and it is split into two solar cells, hence the total cost of cells for the planar array is $\sim$ 108'000 $Euro$ or **360** $Euro/W$.

6.0.2. Cost of *ConCur* Solar Array

- **Solar Cells**

  The high efficiency triple junction Gallium Arsenide solar cells are produced in ingots and hence sold in round wafers of 9.6 cm diameter. Each wafer costs 800 $Euro$ (from discussion with Ir. R. v.d. Heijden at *Airbus*) and provides 4 rectangular cells of 15 x 80 mm dimensions. Hence, the cost of a single cell is 200 $Euro$. To generate required amount of power (300 W) the panel needs to consist of at least 168 solar cells, hence the number of wafers needed and the total cost of solar cells per wing are:

$$n_{wafers} = \frac{168}{4} = 42[\text{wafers}] \tag{6.1}$$

$$Cost_{cells} = 800 \cdot 42 = 33'600[\text{Euro}] \tag{6.2}$$

$$CostPerWatt = 33'600/300 = \mathbf{112\ [}Euro/W\mathbf{]} \tag{6.3}$$

$$CostPerSquareMeter = \frac{33'600}{1.11 \cdot 1.244} = \mathbf{24'333\ [}Euro/m^2\mathbf{]} \tag{6.4}$$

$$WattPerMeter = \frac{300}{1.11 \cdot 1.244} = \mathbf{217.3\ [}W/m^2\mathbf{]} \tag{6.5}$$

Comparing the costs of the electric power for planar array of 1 x 1.2 m to that of a concentrator array (in terms of cells) the latter is seen to be a cheaper option (nearly 3 times). Note that the amount includes the costs of raw material, molybdenum interconnects, cell laydown, coverglass and adhesive.

- **Substrate Panel and Concentrators**

In the Feasibility study by E. van den Abeele [13] the rough approximation of the costs was calculated based on the costs of raw material, bonding and coating costs, see Tab. 6.1. The panel parameters in the study [13] are not entirely identical to the ones here, hence the cost values are approximate.

Table 6.1: Updated cost estimation.

Cost of	**Amount**
Support panel dimensions	1.110 x 1.244 m
Solar cell dimensions	15 x 80 mm
Amount of concentrators	14
Amount of solar cells	168
Raw material CFRP (concentrators)	Eur 1'910.33
Bonding	Eur 1.800.00
Coating	Eur 1'273.55
Raw material support panel	Eur 7'695.00
Total cost of solar cells	**Eur 33'600.00**
***TOTAL (CONVENTIONAL PANEL, only cells)**	**Eur 108'000.00**
TOTAL (CONCUR PANEL) [14]	Eur 90'200.00
****TOTAL (CONVENTIONAL PANEL, assumed)**	Eur 300'000.00

* Based on the wafer cost; only cells without the honeycomb structure.
** Based on the 1000 $Euro/W$ cost estimation.

When comparing the cost of the solar cells alone it can be seen that for the same amount of power the *ConCur* solar array may save up to 60% of the cost required to get the same power from a planar solar array. In terms of full panel costs, *ConCur* is estimated to cost 2/3rds less than the conventional solar panel.

7

Conclusions and Recommendations

7.1. Conclusions

From the thermal results it was determined that the initial (baseline) design of the *ConCur* panel did not satisfy the thermal requirements in terms of heat conduction, leading to very high temperatures at the cell area where all the light was concentrated onto. Therefore, an alternative design was proposed offering much more efficient heat transfer and, hence better panel operating conditions. With the proposed conduction-enhancing methods the highest solar cell temperature in operation does not exceed 70°C, and with the cells off: 122°C, which lies within the cell operational limits of the solar cells used (*TJ GaAs 3G30C*). It has been determined that the initial size of the panel (1 x 1.2 m) was slightly too small for producing the required amount of power, hence it was slightly extended to 1.11 x 1.244 m. A concentrator solar panel of this size can carry 14 concentrators with a total of 168 solar cells providing 310 W of electrical power at EOL conditions with a geometric concentration ratio of 5.0. It will provide this amount of power throughout the orbit when placed in a 90° right ascension orbit, however in a 0° right ascension orbit it will experience eclipse 1/3rd of the entire lifetime, which limits the electrical power production. It was also determined that the panel under misalignment of 30° is capable of producing high amount of power.

The main purpose of developing *ConCur* solar panel design is to provide an innovative solution to lower the cost of the electrical power production in orbit. It has been calculated that *ConCur* indeed is capable of producing the same amount of power as the conventional planar solar array of the same size for a much less cost. A brief comparison of the conventional solar array and *ConCur* panel can be found in Tab. 7.1.

Table 7.1: Cost comparison of the planar array versus *ConCur*.

Parameter	**Unit**	**Planar Array**	***ConCur* Array**
Panel area	m^2	1 x 1.2	1.11 x 1.224
Number of cells	$-$	270	168
Amount of power	W	300	300
Total cost of cells	$Euro$	**108'000**	**33'600**
Cost per area	$Euro/m^2$	90'000	24'333
Power density (per panel area)	W/m^2	250	217.3
Total solar cell cost per watt	$Euro/W$	360	112
Total panel cost (cells+panel)	$Euro$	300'000.00	90'280.00

So far the concept has passed a feasibility study, structures and vibrations analytical testing and (in

this thesis) thermal and electrical detailed design development. In addition this report mentions numerous recommendations to executing the next necessary tasks towards a successful design.

7.2. Recommendations/Remarks

Setting aside tasks that were performed in this thesis, some initially planned analyses for this project were not executed due to the time constraint, hence they are added to the following list of recommendations for further concept development.

1. Test the solar cell performance under 5 Sun illumination (AM0 spectrum). Consider Auger recombination effect on the solar cell performance under concentration of 5 Suns.
2. Perform non-uniform cell illumination test to assess the non-homogeneity effects. Due to the concentration effect the cell will receive different amount of light throughout its surface area, and it is important to check whether that would cause any losses.
3. Test material properties versus time in orbit (CFRP and resin conductivity etc.).
4. The amount of radiation that was assumed in this thesis is most likely higher than that in reality (for extra safety factor), so the panel at BOL will produce most likely more power than calculated. The actual breadboard model testing in relevant environmental conditions will help to determine things more precisely.
5. Vertical radiator (made of PG) modeled in *ESATAN* as a shell - so zero thickness. This is not accurate, and if, for instance in the model it reaches 20°C, in reality it will be warmer (90° right ascension, *Case 1B HOT*).
6. If using flexprints (for wiring harness), account for space (they are 8 cm wide), and 200 μm thick (out of plane) (including adhesive).
7. Take care of the out-of-plane solar cell interconnects during the stowed phase, or use in-plane interconnects.
8. The amount of cells that can be shaded while still producing enough power depends on the MPPT operational limits. It should be looked into due to radiative cases when the panel is facing the Sun under an angle.
9. Use some adhesive over the busbars for protection during stowage (because aluminum/silver coating and CFRP are conductive), so use, for instance, adhesive *CV 1142* (from *ExoMars* mission).
10. In case it is decided to implement a U-beam at the rear of the panel, the wiring harness should be paid attention to, to account for mechanical clearance.
11. Perform thermal analysis of the panel in stowed configuration (during the launch).
12. The amount of solar cell degradation due to electrically charged particles (radiation) at EOL conditions was calculated in *SPENVIS* for planar solar array (hence with a higher view factor than for this panel) is most likely much lower in reality, because the cells are well-shaded due to low view factor. Hence the cells will most likely perform better in orbit (with less ageing effects) than calculated in this thesis.
13. Apart from implementing the thermal doubler (which introduces more complexity also) another good design alternative would be using aluminum panel substrate and concentrators (same material to prevent differential expansion), based on the thermal results. Although, there are certain drawbacks.
14. The absorbed solar flux tends to vary throughout the solar cell either due to the imperfections in geometry or modelling. This would be interesting to investigate further.

Bibliography

[1] A. D&S, *P6057405nl draft final: Solar panel with flexible optical elements,* Patent for ConCur solar array concentrator wing (2016).

[2] A. Gorbatenko, *Lierature study on thermal and electrical designs of a concentrator solar array,* Graduation thesis at Airbus, Literature Study (2017).

[3] H. Cruijssen, *Beetle: Concur concentrator solar array; some design aspects,* Lunch Session at Airbus Defence and Space (2016).

[4] O. Isabella, *Et4378 photovoltaic systems: Topologies of pv systems,* Delft University of Technology, the Netherlands (2016).

[5] M. Zeman, *Lecture 6: Basic semiconductor physics,* ET4376 Photovoltaic Basics (2015/2016).

[6] O. Isabella, *Et4378 photovoltaic systems: Pv systems components, modules,* Delft University of Technology, the Netherlands (2016).

[7] C. Consortium, *Cpv projects,* http://cpvconsortium.org/projects (2018).

[8] M. J. O'Neil *et al.*, *Ultra-light stretched fresnel lens solar concentrator for space power applications,* Presented at The International Symposium on Optical Science and Technology (2003).

[9] H. Cruijssen *et al.*, *Solar panel with flexible optical elements,* United States Patent Application Publication (2017).

[10] iridium.it, *The iridium system,* http://www.iridium.it/en/iridium.htm (2012).

[11] OneWeb, *Artist's concept of a oneweb satellite,* Spaceflight Now: OneWeb selects Airbus to build 900 Internet satellites (2015).

[12] T. Lorrier, *Panel structure design for solar concentrator array,* Graduation thesis at Airbus Defence and Space and Inholland University of Applied Sciences (2016).

[13] E. van den Abeele, *Feasibility of a concentrator solar array,* Graduation thesis (2016).

[14] S. Bakker, *Eindverslag: Concentrator solar array,* Leidse Instrimentmakers School (2018).

[15] A. Gorbatenko, *Midterm report: Thermal and electrical designs of a concentrator solar array,* Graduation thesis at Airbus, Midterm Report (2017).

[16] F. Corporation, *Fluor projects: Arco solar photovoltaic power plant - epc,* http://www.fluor.com/projects/arco-power-solar-renewable-epc (2017).

[17] J. Schaefer *et al.*, *Electrical degradation of the carrisa plains power plant,* 10th European Photovtaic Solar Energy Conference, Lisbon, Portugal (1991).

[18] R. J. M. Eskenazi, A. Jones, *Cellsaver qualification testing and contamination analysis,* Americal Institute of Aeronautics and Astronautics, Inc. (2003).

[19] K. Gantois *et al.*, *Proba 2: Mission and new technologies overview,* Verhaert Space, ESA/ESTEC, DLR/GSOC (2007).

[20] V. Ruelle *et al.*, *Low concentration solar array experiment on-board proba-2,* Centre Spatial de Liège, Galileo Avionica, European Space Agency (ESTEC) (2008).

[21] M. C. T. G. Stern, *Us patent: Lightweight solar concentrator cell array,* San Diego, California (1994).

[22] T. G. Stern and M. Piszczor, *A deep-space concentrator for inner and outer solar system missions,* IECEC 2002-20109 (2002).

[23] A. Susobhanan, *Is the sun a blackbody?* https://www.quora.com/Is-the-sun-a-blackbody (2015).

[24] NASA, *Solar and ultraviolet radiation testing,* Marshall Space Flight Center (2013).

[25] S. Makham *et al.*, *Modeling of solar cell degradation in space,* Solar Energy Materials and Solar Cells (2010).

[26] A. de Rooij, *Corrosion in space,* ESA, ESTEC (2007).

[27] K. de Groh *et al.*, *Environmental durability issues for solar power systems in low earth orbit,* 1995 International Solar Energy Conference (1995).

[28] G. Strobl, *From space to earth: Concentrator photovoltaics,* Azur Space Solar Power (2013).

[29] ESA, *Polyimide/fluorothermoplast insulated wires and cables, low frequency, 600v, -200 to +200,* European Space Components Coordination (2013).

[30] F. Dimroth and M. Steiner, *Am3 high efficiency multijunction cell technology for terrestrial concentrators and space photovoltaics,* 40th Photovoltaic Specialists Conference (2010).

[31] C. Honsberg and S. Bowden, *Types of recombination,* http://www.pveducation.org/ (2017).

[32] K. A. et al, *Investigation of the radiation hardness of gaas sensors in an electron beam: Energy band structure of si and gaas,* https://www.researchgate.net/figure/267702055_Energy-band-structure-of-Si-and-GaAs-5 (2012).

[33] I. Engines, *Esatan-tms release 2016 sp1: Esatan training,* UK (2016).

[34] H. S. Rauschenbach, *Solar cell array design handbook: The principles and technoloy of photovoltaic energy conversion,* TRW Defense and Space Systems Group (1980).

[35] B. Benthem and A. Maas, *Satellite thermal control,* Course AE4S20, Faculty of Aerospace Engineering, TU Delft and Airbus D&S Netherlands (2016).

[36] S. B. Materials, *The red book,* (2010).

[37] *Graphite and composites,* http://www-ferp.ucsd.edu/LIB/PROPS/PANOS/c.html (2010).

Stage onderzoek: **Aleksandra Gorbatenko** 01-11-2016 untill 01-09-2017 (planned)	AIRBUS DEFENCE & SPACE	Date: 12-09-2016

Directe ADSNL Begeleider:
Henk Cruijssen.
Alexander Maas

CC:
Sybren de Jong /
Sytze Kampen
Delft University

A

Thesis Assignment

Thermal design of panel substrate including concentrator reflectors for Concur™ SA wing

General

Within Dutch Space a novel solar array is prepared as a potential concept. The concept is based on a parabolic reflector concentrator type solar array. A patent (Concur™ Patent P6057405NL) is pending for this novel SA for small sats concept. The basic idea is to have a semi-rigid substrate, made of CFRP material, which is curved in the stowed condition. Once the hold down is released, the panel is straightened by releasing its elastic energy and springs back to a flat panel. Thereafter (of even simultaneously / TBC), the parabolic concentrator mirrors are erected. This provides the required concentration ratio. As such, cost saving can be obtained because less photo-voltaic cells are needed. A schematic view is shown below.

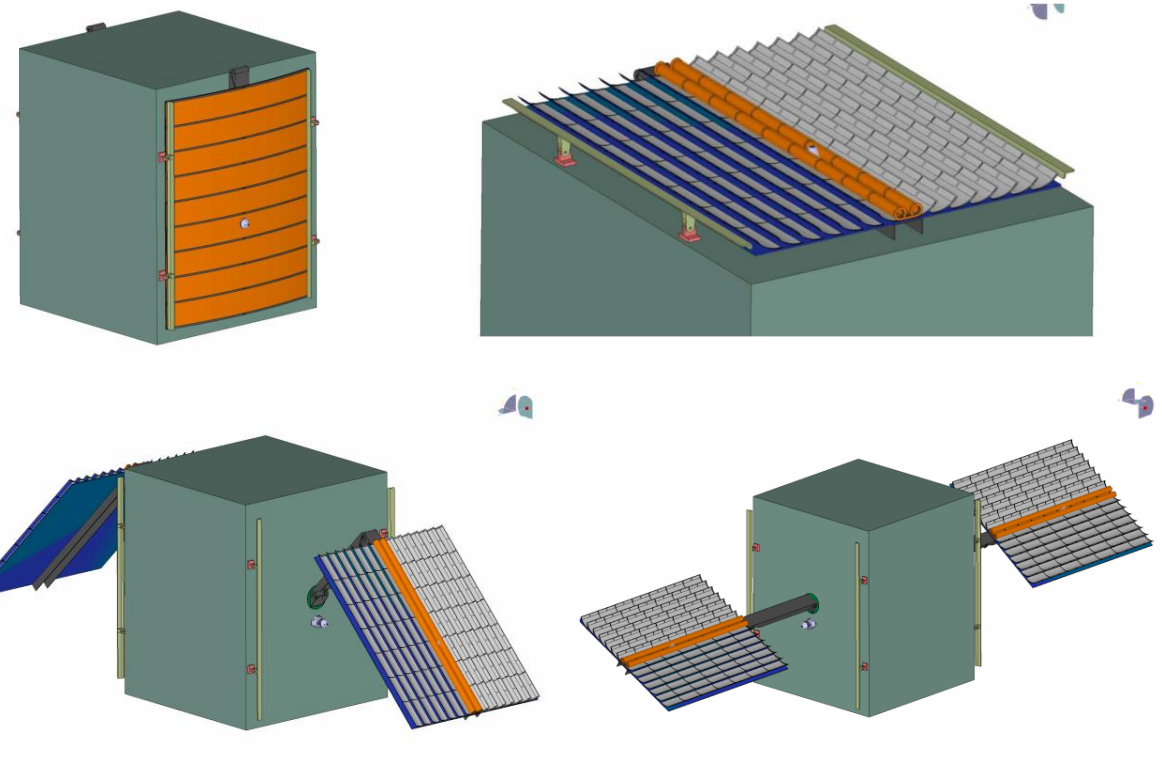

As there is an interface with the parabolic reflector, the structural connection of the reflector needs attention to release the protection foil for these reflectors in a controlled manner. Note, that the protection foil thereafter will have its own retraction function and its protection function (i.e. structural, thermal, wiring harness, photovoltaic cells etc.) and the parabolic reflectors with the PVA cells attached on the inside will rise, due to its own stored elastic energy (TBc)

Thesis Assignment

The assignment encompasses 5 thermal related topics.

1. Materials selection /degradation effects
2. Deployed wing thermal analyses including seasonal effects
3. Sensitivity for different LEO orbits (e.g. noon, morning, sun-synchronous)
4. Effect of different form of PVA cooling (if needed)
5. Stowed wing thermal analyses

Item 1: For the S/A concept some materials are fixed. However, there is still ample freedom of the materials which can be selected. Some materials are specifically needed for the structural behavior in the stowed or deployed configuration in order to meet the dynamic requirements. A selection of the most sensible materials is needed, meeting also the thermal requirements.

Item 2: As the thermal loadcase is considered important for the wing performance and the PVA efficiency. As the solar array requires accurate sun-tracking to make maximum use of concentrators, it may be expected that the sun rays are hitting the concentrator surface in a perpendicular mode by rotating the solar array with the SADM to a misalignment angle of maximum α<0.1 degree. (but disregarding the effects of seasonal variation). Seasonal effects shall be analyses to see how the sun will heat up the PVA. Conduction paths for adequate heat transfer and radiation to space shall be determined. In some cases the sun aspect angle β can result in a considerable offset. It is important to define these cases and establish if even thermal temperature distribution is attainable.

Item 3: As these S/C will be oriented in all kinds of orbits to achieve full coverage for internet etc, it is needed to establish if a double gimbal is needed to maintain safe temperature limits and optimum sun angles for maximum in-orbit power. Also, the shadow effects for different orbits will result in quite different performances of this type of concentrator solar array. The double gimbal mechanism may be located at the root or in between the deployment arm at the top hinge. A thermal optimum shall be presented. (not mechanism part; this is subject to other stage)

Item 4: In some S/A patents it is recognized that the thermal temperature of the PVA may become critical and will result in a degradation of performance. Hence, some design tricks are introduced such as thermal fins at the concentrator edge or at the backside of the concentrator. It shall be established if this does indeed provide the expected efficiency gain by keeping the PVA temperature low. In addition, effects of high conductive materials for the concentrator reflector (or bonding material to the support panel) shall be assessed. An optimum shall be presented for the various LEO cases.

Item 5: As the Concur™ S/A thermal design has now been established to achieve a sound thermal design for the in-orbit LEO cases, it shall be checked if for the stowed case also realistic thermal design temperatures are established. It shall be considered for only some worst case orbits in order to check if the material properties are not exceeded and if gradients are within acceptable limits to guarantee a sound release.

Stage onderzoek: **Aleksandra Gorbatenko** 01-11-2016 untill 01-09-2017 (planned)	AIRBUS DEFENCE & SPACE	Date: 12-09-2016

Step by Step Plan

1. Familiarization about SA concept in general and in detail to investigate and to understand the design to determine the thermal critical points.
2. Survey of existing documentation concerning thermal design for the panels, the reflective concentrators and the support beam / primary deployment beam. Include PVA aspects such as GA As cells and cell types which are specifically denoted to concentrators (i.e. elevated temperatures)
3. Generation of top-10 major thermal requirements for S/A panel concept. Define important parameters for evaluation.
4. Summary of viable thermal design concepts which could be used. Show some details about viable concepts with pro's / con's. Sufficient details to make later trade-off decisions.
5. Generation of max 3 viable thermal design concepts in ESATAN meeting the thermal constraints etc. Demonstrate via course sensitivity analyses the critical environments with adequate thermal design margin.
6. Define orbit and seasonal variation effects.
7. Show effects of double gimbal mechanism concerning thermal pointing and its associetd beneficial effects (if any)
8. Define selection / trade-off criteria for thermal panel design and make selection of preferred concept(s) or variations thereof, based on e.g. ESATAN calculations.
9. Determine effect on electrical performances. PVA = f (Temp) for some typical LEO orbits.
10. Define the preferred final thermal concept, and describe now how it will work efficiently to achieve the required thermal conditions.
11. Generation of a detailed thermal ESATAN model to demonstrate thermal improvements with a cooling fin concept in combination with high conductive fibres /resin and the working principles. Show gain in thermal performances (if any).
12. Define stowed model for some critical load cases during launch. Establish temeparture limits and gradients for safe release.
13. Generate final report with recommendations and justification files in Appendices.
14. Internal presentation at Airbus Defence & Space NL and subsequent presentation at Toulouse University

September 2016
Henk Cruijssen

AZURSPACE SOLAR POWER GMBH

B

Solar Cells

30% Triple Junction GaAs Solar Cell

Type: TJ Solar Cell 3G30C - Advanced

Best in Class EOL-Values!

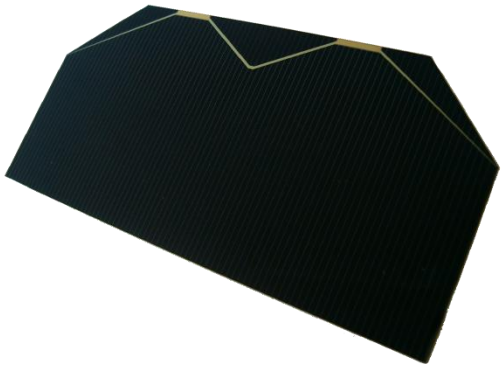

This cell type is a GaInP/GaAs/Ge on Ge substrate triple junction solar cell (efficiency class 30% advanced). The end-of-life version of the 3G30C solar cell offers best EOL-performance values and should be combined with an external bypass diode protection.

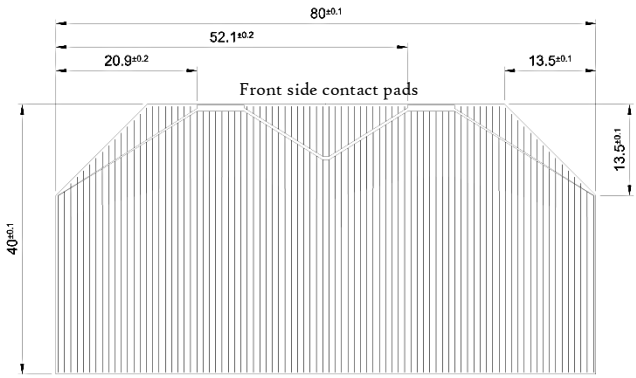

3G30C - Advanced

Space

30% Triple Junction GaAs Junction Solar Cell
Type: TJ Solar Cell 3G30C - Advanced

Design and Mechanical Data

Base Material	GaInP/GaAs/Ge on Ge substrate
AR-coating	TiO_x/Al_2O_3
Dimensions	40 x 80 mm ± 0.1 mm
Cell Area	30.18 cm^2
Average Weight	≤ 86 mg/cm^2
Thickness (without contacts)	150 ± 20 µm
Contact Metallization Thickness (Ag/Au)	4 – 10 µm
Grid Design	Grid system with 2 contact pads

Electrical Data

		BOL	2,5E14	5E14	1E15
Average Open Circuit V_{oc}	[mV]	2700	2616	2564	2522
Average Short Circuit I_{sc}	[mA]	520.2	518.5	514.0	501.9
Voltage at max. Power V_{mp}	[mV]	2411	2345	2290	2246
Current at max. Power I_{mp}	[mA]	504.4	503.2	500.6	486.6
Average Efficiency η_{bare} (1367 W/m^2)	[%]	29.5	28.6	27.8	26.5
Average Efficiency η_{bare} (1353 W/m^2)	[%]	29.8	28.9	28.1	26.8

Standard: CASOLBA 2005 (05-20MV1, etc); Spectrum: AMO WRC = 1367 W/m^2; T = 28 °C @fluence 1MeV [e/cm^2]

Acceptance Values

Voltage V_{op}	2350 mV
Min. average current $I_{op\ avg}$ @ V_{op}	505 mA
Min. individual current $I_{op\ min}$ @ V_{op}	475 mA

Temperature Gradients

			BOL	2,5E14	5E14	1E15
Open Circuit Voltage	$\Delta V_{oc}/\Delta T\uparrow$	[mV/°C]	- 6.2	- 6.5	- 6.6	- 6.7
Short Circuit Current	$\Delta I_{sc}/\Delta T\uparrow$	[mA/°C]	0.36	0.33	0.35	0.38
Voltage at max. Power	$\Delta V_{mp}/\Delta T\uparrow$	[mV/°C]	- 6.7	- 6.8	- 7.1	- 7.2
Current at max. Power	$\Delta I_{mp}/\Delta T\uparrow$	[mA/°C]	0.24	0.20	0.24	0.28

@fluence 1MeV [e/cm^2]

Threshold Values

Absorptivity	≤ 0.91 (with CMX 100 AR)
Pull Test	> 1.6 N at 45° welding test (with 12.5µm Ag stripes)
Status	Qualified

3G30C - Advanced

AZUR SPACE Solar Power GmbH
Theresienstr. 2
74072 Heilbronn
phone: +49 7131 67 2603
telefax: +49 7131 67 2727
e-mail: info@azurspace.com
website: www.azurspace.com

Certified Company

ISO 9001
ISO 14001
OHSAS 18001

Space

C

SPENVIS Degradation Data

Mission overview
Orbit around: Earth
Number of mission segments: 1
Mission start: 01/01/2011 00:00:00
Mission end: 31/12/2015 00:00:00
Mission duration: 1825.00 days (5.00 years)
Satellite axis: velocity vector

Mission segment 1:	
Orbit type:	general
Apogee:	1200.00 km
Perigee:	1200.00 km
Inclination:	90.00°
R. A. Ascending Node:	0.00°
Argument of Perigee:	0.00°
True Anomaly:	0.00°
Period:	1.82 hrs
Number of orbits:	52.72
Duration:	4.00 days
Orbit start:	01/01/2011 00:00: 0.0
Orbit end:	05/01/2011 00:00: 0.0
Segment end:	31/12/2015 00:00: 0.0
Segment length:	1825.00 days
Semi latus rectum:	7571.00 km
Semi major axis:	7571.00 km
Eccentricity:	0.00
Mean motion:	82.80 rad/day
Integration step:	0.50°
Time intervals	
60.0 s below 20000.0 km	
240.0 s between 20000.0 km and 80000.0 km	
3600.0 s above 80000.0 km	

Cell: AZUR 3G28
Electron/proton damage ratios: P_{max} = 1999.0 V_{oc} = 2669.0 I_{sc} = 857.0
Coverglass
material: SiO2 density: 2.32 (g/cm^3)

Summary of 1 MeV equivalent electron fluences (cm^{-2})												
Coverglass thickness			Total			Trapped electrons	Trapped protons			Solar protons		
g cm^{-2}	mils	micron	P_{max}	V_{oc}	I_{sc}	P_{max}, V_{oc}, I_{sc}	P_{max}	V_{oc}	I_{sc}	P_{max}	V_{oc}	I_{sc}
0.0000	0.0	0.00	4.222E+16	2.402E+16	4.392E+16	3.635E+12	3.718E+16	2.089E+16	3.887E+16	5.033E+15	3.121E+15	5.052E+15
0.0059	1.0	25.40	5.586E+14	5.542E+14	3.758E+14	3.154E+12	3.280E+14	3.262E+14	2.199E+14	2.274E+14	2.249E+14	1.527E+14
0.0177	3.0	76.20	2.669E+14	3.029E+14	1.517E+14	2.648E+12	1.562E+14	1.808E+14	8.595E+13	1.080E+14	1.195E+14	6.309E+13
0.0354	6.0	152.40	1.756E+14	2.142E+14	9.410E+13	2.189E+12	1.066E+14	1.341E+14	5.566E+13	6.677E+13	7.787E+13	3.626E+13
0.0707	12.0	304.80	1.222E+14	1.518E+14	6.013E+13	1.638E+12	8.051E+13	1.015E+14	3.822E+13	4.010E+13	4.860E+13	2.027E+13
0.1179	20.0	508.00	9.193E+13	1.169E+14	4.325E+13	1.212E+12	6.423E+13	8.268E+13	2.932E+13	2.649E+13	3.303E+13	1.272E+13
0.1768	30.0	762.00	7.591E+13	9.777E+13	3.507E+13	8.893E+11	5.535E+13	7.201E+13	2.490E+13	1.967E+13	2.488E+13	9.280E+12
0.3536	60.0	1524.00	5.434E+13	7.102E+13	2.434E+13	4.113E+11	4.298E+13	5.654E+13	1.891E+13	1.095E+13	1.406E+13	5.016E+12
User defined coverglass thickness												
0.0232	3.9	100.00	2.265E+14	2.644E+14	1.258E+14	2.457E+12	1.345E+14	1.608E+14	7.248E+13	8.944E+13	1.010E+14	5.077E+13

D

In-plane and Through Conduction Calculations and Values

Conduction Equations

Solar cell assembly (i - solar cell layers); Cxy $[W/K]$ and Cz $[W/m^2K]$:

$$Cxy_{SCA} = \sum Cxy_i = \sum k_i \cdot t_i = 0.0085(W/K) \tag{D.1}$$

$$Cz_{SCA} = \frac{1}{\sum \frac{1}{Cz_i}} = \frac{1}{\sum \frac{t_i}{k_i}} = 1440(W/m^2K) \tag{D.2}$$

Material Properties and Constants

Table D.1: Layer thickness, material properties and constants.

Layer	Parameter	Symbol	Value
Solar Cell Assembly (SCA):			
Coverglass	Thickness	t_{glass}	100 μm
	Conductivity	k_{glass}	2 W/mK
	Density	ρ_{glass}	2200 kg/m^3
	Heat capacity	C_P	736 J/kgK (at 21°C)
		$(dC_P/dT)_{LowTemp}$	2.8 J/kgK^2
		$(dC_P/dT)_{HighTemp}$	1.6 J/kgK^2
Adhesive DC93-500	Thickness	t_{adh}	20 μm
	Conductivity	$k_{adhesive}$	0.146 W/mK
	Density	$\rho_{adhesive}$	1100 kg/m^3
	Heat capacity	C_P	1029 J/kgK (at 21°C)
		$(dC_P/dT)_{LowTemp}$	4.0 J/kgK^2
		$(dC_P/dT)_{HighTemp}$	1.0 J/kgK^2
Germanium	Thickness	t_{cell}	140 μm
	Conductivity	$k_{germanium}$	58.58 W/mK
	Density	$\rho_{germanium}$	5325 kg/m^3
	Heat capacity	C_P	321 J/kgK (at 21°C)
		$(dC_P/dT)_{LowTemp}$	2.3 J/kgK^2
		$(dC_P/dT)_{HighTemp}$	0.2 J/kgK^2
Adhesive RTV 691	Thickness	t_{adh}	100 μm
	Conductivity	$k_{adhesive}$	0.4 W/mK
	Density	$\rho_{adhesive}$	1420 kg/m^3
	Heat capacity	C_P	1029 J/kgK (at 21°C)
		$(dC_P/dT)_{LowTemp}$	4.0 J/kgK^2
		$(dC_P/dT)_{HighTemp}$	1.0 J/kgK^2
Kapton	Thickness	t_{kapton}	51 μm
	Conductivity	k_{kapton}	0.2 W/mK
	Density	ρ_{kapton}	1420 kg/m^3
	Heat capacity	C_P	1029 J/kgK (at 21°C)
		$(dC_P/dT)_{LowTemp}$	3.9 J/kgK^2
		$(dC_P/dT)_{HighTemp}$	1.3 J/kgK^2
Concentrator:			
Ply #1 and #3 direction 0 deg.	Thickness	$t_{ply_1,3}$	0.06 mm
	Conductivity	k_x	47.5 W/mK
		k_y, z	1.3 W/mK
Ply #2 and #4 direction 90 deg.	Thickness	$t_{ply_2,4}$	0.06 mm
	Conductivity	k_x, z	1.3 W/mK
		k_y	47.5 W/mK
	Density	ρ_{CFRP}	1800 kg/m^3
	Heat capacity	C_P	916 J/kgK (at 21°C)
		$(dC_P/dT)_{LowTemp}$	3.0 J/kgK^2
		$(dC_P/dT)_{HighTemp}$	2.6 J/kgK^2
Panel substrate:			
Ply #1 - 25 (odd numbers) direction 0 deg.	Thickness	$t_{ply_1,3}$	0.06 mm
	Conductivity	k_x	47.5 W/mK
		k_y, z	1.3 W/mK
Ply #2 - 24 (even numbers) direction 90 deg.	Thickness	$t_{ply_2,4}$	0.06 mm
	Conductivity	k_x, z	1.3 W/mK
		k_y	47.5 W/mK
	Density	ρ_{CFRP}	1800 kg/m^3
	Heat capacity	C_P	916 J/kgK (at 21°C)
		$(dC_P/dT)_{LowTemp}$	3.0 J/kgK^2
		$(dC_P/dT)_{HighTemp}$	2.6 J/kgK^2
General Constants:	Stefan-Boltzmann's const.	σ	$5.67 \cdot 10^{-8}$ W/m^2K^4

E

Modelling Benchmarks: lessons learned

Lessons learned in **modelling**:

- (B1) The creation of the radiative case.
- (B1) The "Combine or cut" option explored.
- (B1) The transient and steady-state solution is set-up, and the gradual temperature change is visible.
- (B2) The modeling of conductive interfaces and contact zones between each two connecting surfaces: as fused or as a contact.
- (B2) Construction of a hollow cube using six equally-sized thin-walled square plates.
- (B2) Construction of a hollow cylinder using the "cylinder" option in *ESATAN* (available without the discs at its ends) and adding a disc at each end of it.
- (B2) Application of a *Total Area Heat Load* to the cube, as it is represented as one node.
- (B2) Application of initial and boundary temperature conditions to various shape objects.
- (B3) The generation of the conductive interfaces between the nodes by manual coding (to prevent the software from generating automatic unwanted conduction paths) in $Notepad++$.
- (B3) Implementing the orbital mission parameters in space and applying the desired model pointing parameters.
- (B3) Building up the assembly from sub-models.
- (B3) Nodal analysis and representation in *ThermNV* software.
- (B3) When running only the steady-state solution *ESATAN* considers the average flux over one orbit. The validity of results can be easily checked when comparing the heat flux of a radiative case to the heat flux in the steady-state solution.
- (B4) Creating a desired nodal mesh for better focusing on some particular areas of the structure.
- (B4) Learning the ways to combine several physically different layers into a single shell to still quite accurately represent the thermal behavior of the real structure.
- (B4) Estimating the conductance through several layers by means of theory, and applying the results in modeling.
- (B4) Implementing of the internal heat dissipation (due to solar cells in this case).

Lessons learned in **thermal analysis**:

- (B1) The difference of temperature levels for structures of the same geometry but different bulk material (middle plate versus upper plate): Aluminum versus CFRP.
- (B1) The temperature distribution over the upper plate: nodes become cooler as they encounter more shading from the middle plate.
- (B2) Temperature distribution in transient analysis, as a function strongly dependent on capacitance (thermal mass) of an object.
- (B2) Non-uniform heat distribution in transient analysis over the CFRP plate: orthotropic material.
- (B2) The thermal behavior of the structure including the heat load versus excluding it.
- (B2) The effect of optical coating on cube's temperature.
- (B3) Temperature variation throughout the orbit; the rate at which the structure heats up upon illumination and cools down when in eclipse.
- (B3) The edge effects and their influence on the temperature of the structure in orbit.
- (B3) The differences in steady-state versus transient temperature levels.
- (B3) The effect of the highly reflective coating on the thermal behavior of the structure and on flux (albedo and solar) distribution.
- (B3) The temperature variation due to heat flow towards the back side (heat sink).
- (B4) The typical temperature distribution curve throughout the orbit.
- (B4) Typical operating temperature range of the solar panel throughout the orbit cycle.
- (B4) The temperature gradient through the honeycomb core.
- (B4) The edge effects and their influence on the temperature of the structure in orbit.
- (B4) The way thermal design sets strict requirements to the thermal properties of an epoxy (T_{glass} for instance has to be higher than the highest achieved temperature on the panel).

F

Material Properties: Summary

Table F.1: Material properties [36].

Material	**Density** $[kg/m^3]$	**Specific Heat** $[J/kg \cdot K]$	**Conductivity** $[W/m \cdot K]$	**Operating temp.**	ϵ_{IR}	α_{SOLAR}	**Spectral/ diffuse** ρ_{SOLAR}	**Application/Remark**
AL 2024 T6	2700	900	121	>400°C	NR	NR	NR	
DC93-500	1080	1029	0.146	-65°C to +200°C	NR	NR	NR	Adhesive between the cover-glass and solar cells.
RTV 691	1420	1029	0.39	T_{glass} = -104°C	NR	NR	NR	Adhesive between the SCA and kapton.
CFRP M55J	1630	880 at 30°C, 1130 at 80°C, 1310 at 140°C	55.0 in fiber dir., 1.3 $W/m \cdot K$ in other two dir.	T_{max} = 150°C	0.85	0.9	0.1 diffuse	The bulk material for the panel substrate and concentrators.
CFRP KX 800			300 (in-plane)	T_{max} = 150°C				
Coverglass	2200	736	2.0	NR	-	-	-	Protective glass layer for solar cells and diodes.
FEP				-185°C to 150°C	0.4	0.09	0.91 specular	...
Invar	8.1		12	NR				Invar busbars. Has the lowest CTE among all metals and alloys in the range 20 - 230°C. Tt is ductile and easily weldable. It does not suffer from stress corrosion cracking.
Kapton	1420	1029	0.2	T_{glass} = 360°C	0.85	0.90	0.10 diffuse	Used between the cells and concentrator for electrical insulation.
Molybdenum	10300	254	142	NR	NR	NR	NR	Interconnects
OSR	NR	NR	NR	NR	0.665	0.084	0.916 specular	
Pyrolytic Graphite (PG)			1350 (in-plane), 10 W/mK out of plane	NR	NR	NR	NR	
Polished Al	NR	NR	NR	NR	0.05	0.05 (BOL), 0.15 (EOL)	0.85-0.95 specular	Used as a highly reflective coating over the concentrator front surface.
Solar Cells	5325	321	58.6	Max temp. 150°C	0.84	0.91	0.09 diffuse	

G

Electrical Calculations - Excel Sheet

		Corrected	Preliminary		
Remark	**Parameter**	**sun-sync orbit**		**Unit**	**Comment**
	Full cell width	15	15	mm	
	Full cell length	80	80	mm	
	Full cell area	1200	1200	mm2	
Requirement	Panel voltage	50	50	V	
Requirement	Panel current	6	6	A	
Contact	Area metallization	4	4	mm2	
	Number of met./cell	6	6	-	4 interconnects + 2 diodes
	Total met. area/cell	24	24	mm2	
	Effective Cell Area	1176	1176	mm2	11.76 cm2
	Packing Density	0.98	0.98	-	
	MAX temp (WS)	**67**	**110**	°C	WS
	MIN temp (SS)	**62**	**75**	°C	SS
EOL	Voc STC	2.616	2.616	V	2.5E14 degr.
EOL	Vmpp STC	2.345	2.345	V	2.5E14 degr.
EOL	Impp STC	0.196077932	0.196077932	A	2.5E14 degr.
EOL	dVoc/dT	-0.0065	-0.0065	V/°C	2.5E14 degr.
EOL	dIsc/dT	0.00033	0.00033	A/°C	2.5E14 degr.
EOL	dVmpp/dT	-0.0068	-0.0068	V/°C	2.5E14 degr.
EOL	dImpp/dT	0.0002	0.0002	A/°C	2.5E14 degr.
EOL	Isc STC	0.202039761	0.202039761	A	2.5E14 degr.
EOL	Lowest Voc/cell	2.3625	2.083	V	1 SUN, max temp
EOL	Lowest Voc/cell	2.403102329	2.130737488	V	5 SUNS
EOL	Lowest Vmpp/cell	2.0798	1.7874	V	1 SUN, max temp
EOL	Lowest Vmpp/cell	*2.1333*	*1.835137488*	V	5 SUNS
EOL	Lowest Impp/cell	0.202877932	0.205477932	A	1 SUN, min temp
EOL	Lowest Isc/cell	0.213259761	0.217549761	A	1 SUN, min temp
EOL	Cells in series	**23.43786622**	**27.24591499**	-	
	Geometric CR	5	5	-	
EOL	Reflectivity	0.85	0.85	-	
EOL	Corrected Lowest Isc	0.906353986	0.924586486	A	5 SUNS, min temp
EOL	Corrected Lowest Impp	*0.862231213*	*0.873281213*	A	5 SUNS, min temp
EOL	Strings in parallel	**6.958690327**	**6.870639048**	-	
BOL	Voc STC	2.7	-	V	
BOL	Vmpp STC	2.411	-	V	
BOL	Impp STC	0.196545527	-	A	
BOL	dVoc/dT	-0.0062	-	V/°C	
BOL	dIsc/dT	0.00036	-	A/°C	
BOL	dVmpp/dT	-0.0067	-	V/°C	
BOL	dImpp/dT	0.00024	-	A/°C	
BOL	Isc STC	0.202702187	-	A	
BOL	Lowest Voc/cell	2.4582	-	V	1 SUN, max temp
BOL	Lowest Voc/cell	2.499937844	-	V	5 SUNS
BOL	Lowest Vmpp/cell	2.1497	-	V	1 SUN, max temp
BOL	Lowest Vmpp/cell	*2.211870957*	-	V	5 SUNS
BOL	Lowest Impp/cell	0.204705527	-	A	1 SUN, min temp
BOL	Lowest Isc/cell	0.214942187	-	A	
BOL	Cells in series	**22.60529704**	-	-	
BOL	Reflectivity	0.95	-	-	
BOL	Corrected Lowest Isc	1.020975388	-	A	5 SUNS, min temp
BOL	Corrected Lowest Impp	*0.972351252*	-	A	5 SUNS, min temp
BOL	Strings in parallel	**6.170609628**	-	-	

Figure G.1: Electrical calculations; screenshot of the *MS Excel* sheet.

Concentrator:			Comment
Length	1300	mm	
Width	1110	mm	
Busbar	5	mm	
Number of busbars/conc	2	-	Minimum, on each side of the concentrator
String separation	20	mm	Additional 2 busbars+ 10 mm gap in between
Cells/concentrator	15	-	
Gap+busbar+string sep. space	24	mm	
Free space left	76	mm	38 mm on each side
Concentrators/panel	14	-	
Space left on each side	105	mm	Should be min 103.5
Gap between cells	1	mm	
Cells/panel	180	-	(Feasibility study: 192)
CHANGING PANEL SIZE			
Cells/panel	168	-	variable
Cells/concentrator	14	-	
Width	1110	mm	
Length	1224	mm	7.6 cm shorter
Free space left	76	mm	38 mm on each side
Number of busbars/conc	3	-	per concentrator
Gap+busbar+string sep. space	28	mm	
Cells in series	*24*	-	
Strings in parallel	*7*	-	

Figure G.2: Electrical calculations; screenshot of the *MS Excel* sheet.